2013

Altered Hemodynamic Control in the Skeletal Muscle Microcirculation in the Metabolic Syndrome: The Emergence of a new Attractor

Joshua Thomas Butcher
West Virginia University

Altered Hemodynamic Control in the Skeletal Muscle Microcirculation in the Metabolic Syndrome: The Emergence of a new Attractor

Joshua Thomas Butcher

Dissertation submitted to the School of Medicine at West Virginia University in partial

fulfillment of the requirements for the degree of:

Doctor of Philosophy in Cellular and Integrative Physiology

Jefferson C. Frisbee Ph.D. Mentor

Timothy Nurkiewicz Ph.D. Chair

Sarah Knox Ph.D.

Jeffrey Fedan Ph.D.

Gregory Dick Ph.D.

Shane Phillips Ph.D. External

Cellular and Integrative Physiology Program

Morgantown, West Virginia

2013

Key Words: peripheral vascular disease, metabolic syndrome, Zucker rat, thromboxane A_2, attractor

Abstract

Altered Hemodynamic Control in the Skeletal Muscle Microcirculation in the Metabolic Syndrome: The Emergence of a new Attractor

Joshua T. Butcher

Peripheral vascular disease is a pathological disease state whereby the peripheral vascular system becomes progressively limited in its ability to adequately perfuse extremities despite increases in metabolic demand. One of the primary risk factors for development of peripheral disease is the Metabolic Syndrome. It is the presentation of three simultaneous comorbidities, with obesity being the most common denominator in most metabolic syndrome patients, but also including a pro-inflammatory state, pro-oxidant state, pro-thrombotic state, increased blood pressure, atherogenic dyslipidemia, or insulin resistance. Currently, the population of the United States is approximately 75% overweight, obese, or extremely obese and the prevalence of obesity related consequences is rising, including but not limited to diabetes, cardiovascular disease, and peripheral vascular disease.

Our laboratory has demonstrated that a defining characteristic of metabolic syndrome is microvascular dysfunction. Increasing evidence has indicated that the mechanisms responsible for microvascular dysfunction in metabolic syndrome are oxidant stress-based alterations to arachidonic acid metabolism and increased sensitivity to adrenergic stimulation. However, it remains unclear if the altered microvascular reactivity that presents with metabolic syndrome plays a role in the perfusion: demand mismatch that accompanies and defines peripheral vascular disease. This dissertation seeks to understand the altered hemodynamic control found in metabolic syndrome. It set out to examine:

1. The effect of altered microvascular reactivity in metabolic syndrome on vascular tone and performance outcomes.

2. Identify the spatial and temporal alterations to perfusion distribution in metabolic syndrome.
3. Determine the effect of metabolic syndrome on erythrocyte distribution in the microvasculature and capillaries.

The results of these studies determined that a key contributor to the development, maintenance, and progression of peripheral vascular disease is microvascular dysfunction. This dysfunction increases the microvascular perfusion distribution by spatially distinct mechanisms, with adrenergic dysfunction dominating in larger microvessels and oxidant stress-based increases in thromboxane A_2 dominating in smaller microvessels. Additionally, metabolic syndrome blunts the temporal compensation that would serve to attenuate the increased perfusion distribution. Combined, the spatial and temporal impairments to microvasculature serve to alter erythrocyte distribution on a network level in skeletal muscle. These data shed light on how metabolic syndrome insidiously alters microvascular control of blood flow, leading to a perfusion: demand mismatch, and ultimately contributing to pathological disease states like peripheral vascular disease.

Dedication

To all the people who convinced me that giving up was never an option.

To Mom, Dad, Kiah, Justin, and Mark.

Acknowledgments

Much like my predecessor before me, I dislike this section. So many people to mention and thank, but I won't be able to remember where I parked my car in the garage this morning, so I'm certainly going to overlook someone and hurt their feelings. So I will start with an apology to those I neglect to mention.

I will start by thanking Kiah, my lovely and brilliant wife. This degree belongs to her as much as it does to me. She brought me here, she pushed me through, and she never stopped supporting me unconditionally. Although challenging, this graduate school adventure has been so much easier with a woman like her behind me. This degree most likely cost her far more than it ever cost me, and there is nothing I will ever be able to do to repay that debt. I pray the day never comes that you realize how completely unworthy I am of you. I have no doubt that without you, I wouldn't be here.

Special thanks to the Frisbee laboratory, past and present. Adam, you got me through a large chunk of my graduate school career. Thank you for the time you invested in me, both as a person and a scientist. It has taken me a long time to realize how utterly worthless I was when I worked with you. Sweet Jesus, I must have tortured you. And yet you never said anything, and you still take my phone calls. Your absence is still missed…..one could almost say the "passion" of research lessened with your graduation. Phoebe, thank you for always having an open door, and yes, you still scare me sometimes. Milinda, you were patient and always willing to help me, even long after it was your job. Shyla and Steve, thank you for all of your help and for putting up with me these last couple of months. I know it has been rough and for that, I am sorry. I will leave you with the same excellent advice Adam left me. "You have tremendous potential and, if you listen to Jeff, you'll go far. Keep in mind, most of the things that he says will make little to no sense at the time. Just roll with it." I guess the little one deserves mention. Paulina, you were a source of frequent amusement and often speechlessness. You handled the work load and my company on a daily basis with far more grace and aplomb than I expected. Well done and thank you. Please don't forget about research; you are quite exceptional at it. There is no doubt in my mind that you will be

successful at whatever you set your mind to and I wish you all the best. To Jefferson, I know there is a good chance you will never read this. A few years ago you asked me to trust you. You assured me that you would get me through, and that it would be worth it. You were right. Thank you for being my mentor, for pushing, pulling, and occasionally dragging me along. You made me a better scientist and a better person. There is really not much else I can say, not without being called a wus by your son, anyway. To Natty Cake, (there it is, printed forever) you are the man. While the title of "deviant uncle" still stings a little, I will miss you. And not just because I won't be able to reach the stuff on the top shelf.

To my Mom, Dad, Justin, Sara, Matt, Mark, my family, my friends, and frequent drinking buddies. Thank you for shaping me into what I am. Thank you for being there for me, both the good and the bad times. I hope I am not a complete disappointment. To each and every one of you who got me where I am today, thank you from the bottom of my heart.

Table of Contents

Abbreviations

4-Hydroxy-2,2,6,6-tetramethylpiperidine-1-^{15}N-oxyl	(TEMPOL)
17-octadecynoic acid	(17-ODYA)
Acetylcholine	(ACH)
Arachidonic acid	(AA)
Bod y Mass Index	(BMI)
Cyclooxygenase	(COX)
Lean Zucker Rat	(LZR)
Lipoxygenase	(LOX)
L-N^{G}-nitroarginine methyl ester	(LNAME)
Metabolic Syndrome	(MetSyn)
Nitric Oxide	(NO)
Nitric oxide synthase	(NOS)
Obese Zucker Rat	(OZR)
Peripheral Vascular Disease	(PVD)
Prostacyclin	(PGI_2)
Prostaglandin H_2	(PGH_2)
Thromboxane A_2	(TxA_2)

Introduction

Peripheral Vascular Disease

Peripheral vascular disease (PVD) is an insidious pathological disease state that deprives lower extremities and organs of adequate blood flow due to a narrowing of the supply arteries. Currently within the United States PVD afflicts between 8-13 million people, but is estimated to be significantly under diagnosed. PVD patients frequently present with intermittent claudication that occurs during low levels of exercise (walking, climbing stairs, etc.) but discontinues upon cessation of movement. Patients with a history of smoking, diabetes, increased blood pressure, obesity, physical inactivity, or high cholesterol greatly increase their risk of developing PVD, in addition to very high correlations with aging[1]. The interventions for PVD are focused upon alleviating the areas with restricted blood flow, and involve major life alterations to remove risk factors, exercise, drugs, angioplasty, stents, or bypass surgery. Once diagnosed PVD is largely irreversible barring surgery and possesses a high direct and indirect cost burden to society[2, 3]. It becomes clear when position statements are integrated from the American Heart Association (AHA), Centers for Disease Control (CDC), and American Diabetes Association (ADA) that one of the major contributing factors to the development of PVD is structural and functional alterations to vasculature[4, 5]. These alterations decrease the capacity of the peripheral vascular system to adequately regulate blood flow within the skeletal muscle. The impact of impaired regulation of blood flow becomes especially evident in the presence of increased metabolic demand. PVD results in an inability of the system to effectively

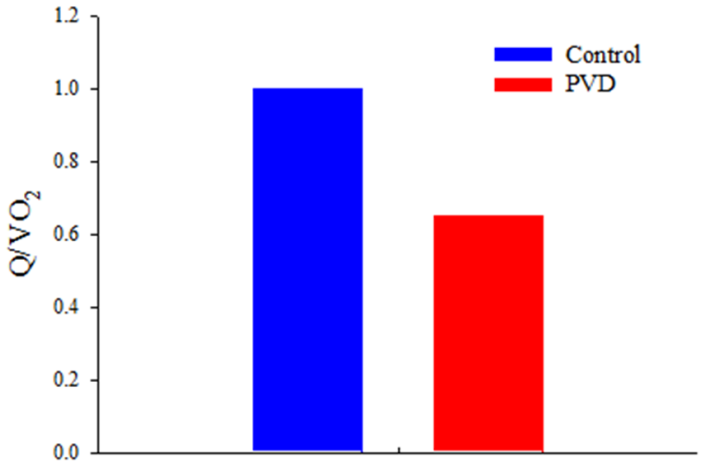

Figure 1: A schematic demonstrating the ratio of blood flow to VO_2 in health (blue) is matched (or 1). In PVD (red) the peripheral vascular system is unable to increase blood flow in response to increased VO_2, leading to a ration of < 1.

match blood flow with an increase in metabolic demand, which is illustrated in Figure 1. The functional outcome of PVD in humans is a progressive acceleration toward decreasing tolerance to exercise, ultimately leading to disability.

Classically, the perfusion: demand mismatch present in PVD has been characterized by structural alterations to larger conduit vasculature (e.g., atherosclerotic plaques and lesions)[6, 7]. However, there is a growing subset of human subjects that suffer from the symptoms of PVD, but do not exhibit the structural modifications to larger vasculature. These emerging observations suggest that the underlying perfusion: demand mismatch seen with development of PVD may be caused by alterations localized to the microvasculature. Given that structural abnormalities within the microcirculation generally focus on altered mechanics of the arteriolar wall (which we have demonstrated only impact perfusion at the highest levels of metabolic demand), or on the density of terminal arterioles and capillaries within the microvascular network (which also exert their influence primarily with elevated metabolic demand) the manifestations of PVD at low-moderate metabolic demand may reflect dysfunction within the regulation of and perfusion distribution in the resistance arterioles[8, 9]. Obviously, any alteration to normal processes of vascular reactivity within the resistance arterioles will exert a powerful effect on bulk blood flow and perfusion distribution and can result in local ischemia and impaired mass transport and exchange. This would likely be manifested by a variation in the distribution of erythrocytes in the distal microcirculation and capillary networks.

Purpose

The purpose of this dissertation is to investigate network control of blood flow to determine the extent to which Metabolic Syndrome-induced microvascular dysfunction alters hemodynamics within skeletal muscle. It will also endeavor to identify those relevant mechanisms within the microcirculation that serve as contributors to the negative functional outcomes associated with Metabolic Syndrome (MetSyn). The obese Zucker rat (OZR) is a model of MetSyn that possesses a recessive leptin receptor

mutation that leads to chronic hyperphagia. Subsequently, the OZR develops rapid onset obesity, insulin resistance, dyslipidemia, and moderate hypertension. As the OZR ages, it develops an increasingly severe myriad of vascular impairments, serves as an appropriate model of MetSyn and development of non-atherosclerotic peripheral vascular disease, and it mimics the leptin resistance induced hyperphagia observed within the human population. The hypothesis tested in this dissertation is that there is an altered intramuscular perfusion distribution throughout the skeletal muscle microcirculation in the MetSyn. Within each chapter of this dissertation is a sub-hypothesis that will address individual aspects of this hypothesis.

Chapter one hypothesized that oxidant stress-based increases in vascular thromboxane A_2 contribute to enhanced myogenic activation and blunted endothelial dependent dilation in both cerebral and skeletal muscle microvasculature in the OZR. It was designed to examine if vascular tone was affected when vessels integrated dilator stimuli and pressure induced constriction simultaneously and whether interventions targeting elevated oxidant stress or elevated TxA_2 production would be effective at restoring normal patterns of reactivity in the OZR. The data from Chapter 1 indicates that MetSyn induced microvascular dysfunction in the skeletal muscle is heavily dependent on altered arachidonic acid metabolism. In contrast, MetSyn induced cerebral microvascular dysfunction appears more dependent on nitric oxide bioavailability. The remainder of this dissertation will focus predominantly on skeletal muscle microvascular dysfunction.

Chapter two was designed to investigate constrained functional hyperemia in the skeletal muscle of the OZR. It was hypothesized that the increased resistance to skeletal muscle blood flow was due to a combined adrenergic constraint and endothelial dysfunction. These data would further support the relevant mechanisms identified in skeletal muscle in Chapter one, and direct the following two chapters to focus on high resolution microvascular dysfunction. Chapter three hypothesized that the increased perfusion heterogeneity observed at bifurcations in the OZR skeletal muscle microvasculature will result in severe impairments to distal arteriolar blood flow distribution. Further, it identified spatially distinct

mechanisms within the microvasculature contributing to the increased perfusion heterogeneity, with alpha adrenergic dysfunction dominating at the proximal microcirculation and oxidant stress based increases in TxA_2 dominating at the distal microcirculation. It would suggest to us that increased microvascular perfusion heterogeneity could be a major contributor to the poor muscle performance outcomes described in Chapter two.

Chapter four hypothesized that the natural compensation for the increased perfusion heterogeneity at bifurcations in the OZR would be temporal switching. Increased temporal switching would maintain skeletal muscle performance by serving as a compensatory mechanism to cope with the increased perfusion heterogeneity. Additionally, this study allowed for the generation of an attractor for peripheral vascular disease. Chapter 5 hypothesized that the result of the spatial and temporal impairments iterated across the microcirculatory network would be a negatively impacted erythrocyte distribution localized to microcirculation and gas exchange vessels. To briefly summarize the information found in the document below: The MetSyn alters spatial and temporal control of microvascular hemodynamics, specifically resulting in an altered perfusion distribution throughout the microvascular network, and serves to embed vascular impairments that contribute to the inability of the peripheral vascular system to adequately match blood flow with increases in metabolic demand.

Metabolic Syndrome

MetSyn is comprised of many comorbidities that significantly increase the risk for developing diabetes, stroke, cardiovascular disease (CVD), kidney disease, and PVD. The primary risk factors from the International Diabetes Federation (IDF), AHA, and CDC are summarized in Table 1[10]. An individual who is diagnosed with three of the primary risk factors meets the criteria for MetSyn. Other measureable factors considered are a pro-inflammatory state

Table 1: Risk Factors	Men	Women
Central Obesity (ethnicity dependent)	>40 inches	>35 inches
Triglycerides	>150mg/dL	>150mg/dL
HDL Cholesterol	<40mg/dL	<50mg/dL
Fasting plasma glucose	>100mg/dL	>100mg/dL
Blood pressure	>130/85	>130/85

(as measured by elevated high sensitivity C-reactive protein, elevated cytokines such as TNF-alpha or IL-6, or decreased adiponectin plasma levels) and a pro-thrombotic state (as measured by fibrinolytic factors like PAI-1 or clotting factors like fibrinogen). Other common contributors include aging, genetics, and an inactive lifestyle. MetSyn has received a steady increase in interest throughout popular culture as well as scientific research. This interest is mimicked as the incidence of MetSyn rises throughout the world, specifically developed countries[11].

It is generally associated that obesity is the condition that initiates the development of not only MetSyn, but also many of the relevant risk factors. There is no universally accepted definition of obesity, but the frequently referenced standard is body mass index (BMI). Table 2 illustrates the differences in BMI between the overweight, obese, and extremely obese classifications of individuals. The National Health and Nutrition Examination Surveys (NHANES), a representative sample of the United States, examined the prevalence of obese and overweight individuals by gender, age, and ethnicity from 1999-2010. The percentages of BMI within the adult population of the U.S. in 2010 are shown in Figure 2. It illustrates that two-thirds of the adult population is obese or overweight.

Table 2: Classification	BMI
Normal	18-25
Overweight	>25
Obese	>30
Extremely Obese	>40

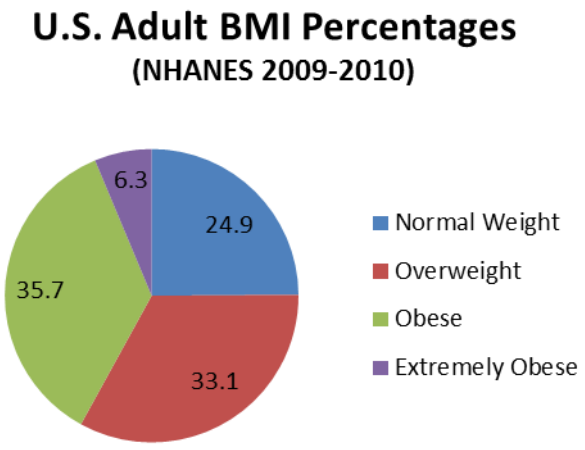

Figure 2: BMI within the U.S. adult population. Numbers are expressed as percentages of total population of normal, overweight, obese, and extremely obese individuals .

Data analyzed from the last five decades showed that although overweight individuals held fairly constant (≈34%), there was a significant increase in obese and extremely obese individuals (Figure 3)[12]. There has been a significant increase in obesity in the last decade in children age 2-19, ending with 17% of children in 2010 being considered overweight[13]. Obesity in adult men

significantly increased over the 10 year span, and in 2010 ≈35% were considered obese[14]. Obesity in adult women held constant across the ten years at ≈35%. A startling statistic was that obesity within the non-Hispanic black adults and Hispanic adults stood at ≈49% and ≈39% respectively, significantly higher than their Caucasian counterparts. Trends suggest that body weight is continuing to rise in children and men, while women have leveled off. The rate of obesity for children, adolescents, and adults has continued to rise. As of 2010, the combined percentages of overweight, obese, and extremely obese individuals for the U.S. adult population is just over 75%[15]. Of particular importance is that this trend of obesity appears to be occurring within a younger population, combined with the increasing life span of adults, it would suggest that an alarming amount of the population within the U.S. will have a significant risk for developing PVD, particularly at a much younger age. The obesity epidemic, MetSyn, and its associated risks for cardiovascular disease have only just begun, and this is further reinforced by the National Institutes of Health (NIH) 2011 Strategic Plan. It includes obesity research targeting the biological processes and factors that regulate and contribute to body weight control, as well as evaluate promising strategies and tools for obesity prevention and treatment.

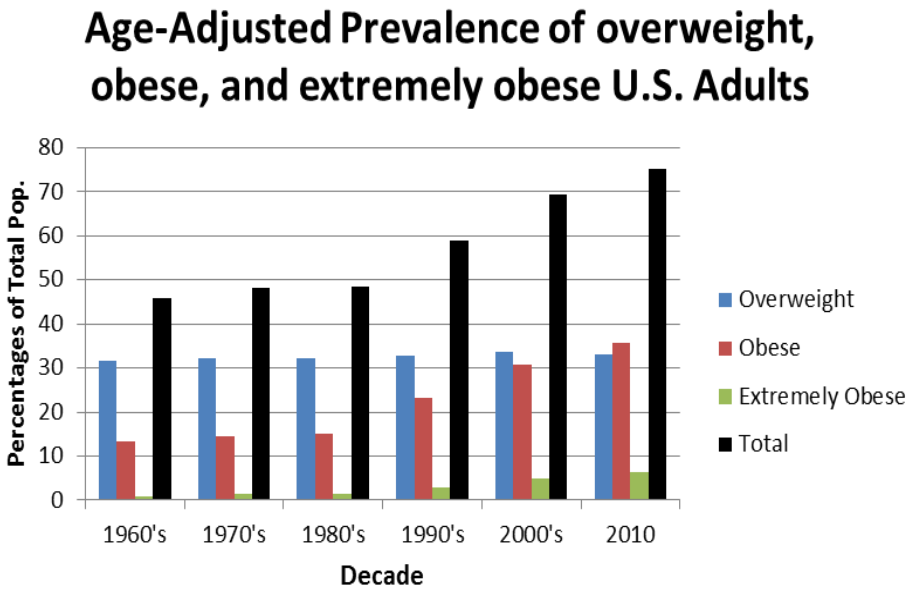

Figure 3: Age-adjusted prevalence of overweight, obese, and extremely obese adults within the U.S. population thru the 1960-2010.

MetSyn cumulatively increases risk for succumbing to a cardiovascular event. One of the many challenges that understanding MetSyn, and the pathologies it induces, is the broad variety of

comorbidities it can contain. While many individuals can be identified clinically as MetSyn patients, it is not a diagnostic tool. Physicians will target the specific indices of disease as they present. As such, public health professionals can identify many strong correlations for predicting further progression of MetSyn pathologies, but identifying causation is difficult. One concrete fact remains, the developed world as a whole is increasing in weight at a younger age and living longer. If this path is continues unabated, then an alarming amount of the American population will be significantly predisposed to many cardiovascular diseases and create an increased economic burden to society.

Vascular Impact of Development of Metabolic Syndrome

The multifaceted components of MetSyn have a varied impact upon the vasculature itself. This includes decreased endothelial function, increased thrombotic cardiovascular events, plaque destabilization, increased intima-media wall thickness, and increased vascular stiffness[16, 17]. It is becoming apparent that the risk factors involved in MetSyn act synergistically with each other to amplify alterations to vascular reactivity and structure. The combined outcome is an inability of the peripheral vascular system to adequately match perfusion with demand.

Vascular tone is the basal level of smooth muscle constriction that a blood vessel experiences at rest compared to its passive diameter and can vary depending on the tissue bed or organ that the blood vessel innervates. It is influenced by many factors, including the autonomic nervous system, vasoactive circulating factors, myogenic activation, shear stress, locally produced vasodilators/constrictors as well as tissue metabolic demand[18]. A vessel will integrate each of these influences and alter the blood flow accordingly. The microvasculature has a large impact on directing blood flow due to it being the primary site of resistance in the vasculature. The largest portion of resistance throughout the vasculature arises from arterioles (diameter ≈100 μm), the vessels located between the large conduit arteries and capillaries. The relationship between flow, pressure, and radius is described in equation 1 below:

$$Q \propto \frac{\Delta P}{R} \qquad \text{(Equation 1)}$$

where Q is flow, R is resistance, and ΔP is change in pressure. Resistance is defined by equation 2:

$$R \propto \frac{\eta L}{r4} \qquad \text{(Equation 2)}$$

where R is resistance, η is viscosity, and r^4 is radius to the fourth power. The combination of Equation 1 and 2 is known as Poiseuille's Law (Equation 3), and is used to approximate steady laminar flow of a Newtonian fluid through a tube of fixed length.

$$Q = \frac{\Delta P \pi r4}{8\eta L} \qquad \text{(Equation 3)}$$

In the vasculature, the viscosity of blood and the length of blood vessels can be considered constants, thus the primary director of blood flow is through altering the diameter of a vessel, and the influence diameter changes is magnified due to being raised to the fourth power. The microvasculature controls blood flow (and thus resistance) by altering the diameters of blood vessels. The above equation illustrates the importance of basal vascular tone, and in general how the microvasculature controls blood delivery by changing diameter. This dissertation has focused increased attention on the observation that the cumulative outcome of spatial and temporal alterations to the regulation of vascular tone in MetSyn results in the inability of skeletal muscle microvasculature to adequately match perfusion: demand, thus compromising tissue oxygenation. The imbalance in perfusion:demand matching results in

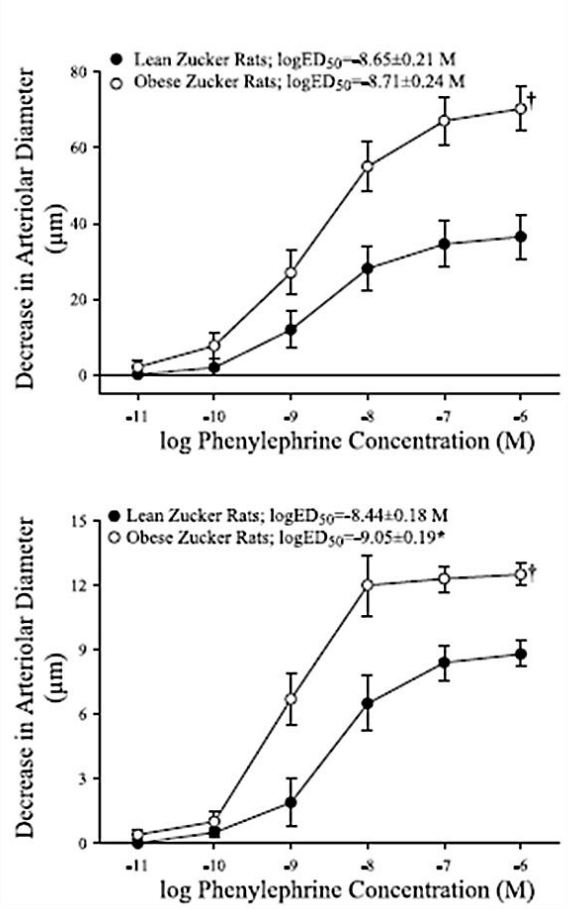

Figure 4: Constriction of isolated gracilis muscle resistance arterioles (top) and *in situ* cremaster muscle distal arterioles (bottom) from lean (LZR) and obese Zucker rats (OZR) in response to increasing concentrations of phenylephrine (a_1-adrenoreceptor agonist.

ischemia, compromised tissue function, and diminished tissue viability.

Myogenic activity is an intrinsic property of smooth muscle found within blood vessels and is part of autoregulaton within organ systems that seeks to maintain blood flow despite changes in perfusion pressure. Specifically, myogenic activity causes smooth muscle cells to contract when pressure is increased and relax when pressure is decreased. It has been identified as a potent regulator of vascular tone in several vascular beds, including splanchnic, renal, cardiac, and skeletal muscle, and as such is important in regulating basal peripheral vascular resistance. It is currently unclear whether the mechanisms for myogenic activation lie within a mechanical stimulus like a stretch receptor, ion channel, or cytoskeletal tension, but what is known is that it causes mobilization of calcium and that there is general agreement that voltage gated calcium channels play an important role[18, 19]. It has been demonstrated that the myogenic activity of blood vessels becomes especially relevant in vessels of a diameter lower than 100 μm and that it is endothelial independent, although certainly modulated by neural, humoral, and tissue factors[20, 21].

This dissertation will focus on the types of mechanisms by which MetSyn alters vascular tone including altered sympathetic activity, increased oxidant stress, and increased production of vascular thromboxane A_2. The first mechanism of altered vascular tone lies within the sympathetic nervous system. Although the alterations to sympathetic activity in MetSyn are not universally agreed upon, it is documented in animal models that sympathetic activity is increased in the presence of metabolic syndrome[22]. The sympathetic nervous system (SNS) is understood to innervate all of skeletal muscle vasculature but the primary effect of SNS stimulation appears to constrict the larger blood vessels. It potentially may be the result of lessening innervation in smaller vessels as smooth muscle lessens toward capillaries, or perhaps the greater influence of other factors, such as tissue metabolic rate[23]. The data from isolated skeletal muscle microvessels and the *in situ* cremaster preparation have shown an increase in constriction in the OZR to phenylephrine compared to the lean Zucker rat (LZR) (Figure 4). This constriction is not mimicked with other potent constrictors, such as angiotensin 2 (Ang 2) or endothelin[24].

The increased sensitivity to alpha adrenergic stimulation shows comparable results in an *in vivo* skeletal muscle artery preparation. This corresponds well with evidence within the human population that MetSyn increases muscle sympathetic nerve activity (MSNA), although the specific alterations to the pathway remain unclear[25]. SNS over-activity is frequently seen in individuals with hypertension, and it contributes significantly to the initiation, progression, and maintenance of the pathology. A recent study concluded that deregulation of the SNS is a powerful predictor of the development of MetSyn[26].

Another frequently described alteration to vascular tone within the confines of MetSyn is based on increases in oxidant stress. Reactive oxygen species (ROS) are highly reactive derivatives of oxygen metabolism that include the superoxide radical, hydroxyl radical, hydrogen peroxide, and include nitric oxide (NO) and the peroxynitrite radical. ROS are linked to many biochemical processes, including signaling, growth, and apoptosis. However, in MetSyn the balance of ROS and antioxidants is often upset, leading to a pro-inflammatory state within the body. In excess, the highly reactive oxidative products can lead to cellular damage. Research from the Frisbee laboratory, and others, has indicated that there is an increase in oxidative stress in the OZR, mirroring the human population of MetSyn[27]. Classically, this increase in oxidant stress is indicated to be responsible for the decrease in endothelium derived NO bioavailability. The powerful, yet transient, dilator is scavenged by ROS and is indicated to be responsible for a significant portion of the impaired dilator capacity of the OZR skeletal muscle arterioles.

Additionally, there is a growing body of evidence that suggests that the impact of oxidative stress is two-fold, as alterations to arachidonic acid (AA) metabolism increases the production of vascular TxA_2. Arachidonic acid is a membrane bound phospholipid found within most mammalian cells. It is freed from the membrane by the enzymes phospholipase A (PLA_2), phospholipase C, or phospholipase D. Once cleaved, the AA can diffuse into the cytoplasmic space and be metabolized. The three primary enzymatic pathways are through cyclooxygenase (COX), lipoxygenase (LOX), or cytochrome P450 (CYP450). The prostaglandins are derived via the COX pathway and are the focus of the subsequent research. Once AA

is metabolized into PGH_2 by COX, it can produce multiple vasoactive compounds that generally will be classified under two families, the prostacyclins and the thromboxanes (Figure 5).

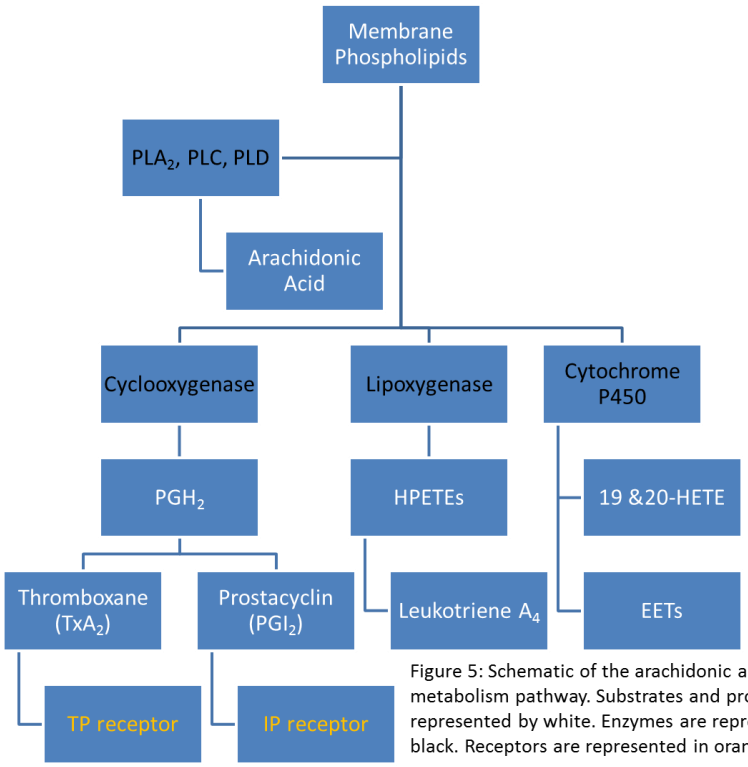

Figure 5: Schematic of the arachidonic acid metabolism pathway. Substrates and products are represented by white. Enzymes are represented in black. Receptors are represented in orange.

In health, a balance of constrictors and dilators will be produced, with a functional outcome on vascular tone being appropriate regulation of blood flow. Research has shown in mice with genetic dyslipidemia that AA induced dilation is blunted in skeletal muscle arterioles and that vascular TxA_2 end products are increased. However, treatment with an antioxidant or a TxA_2 receptor antagonist improved the altered reactivity and the antioxidant additionally improved the altered AA metabolism[28]. Additional research using the OZR, a model of metabolic syndrome, suggested that the impaired dilator response to reduced oxygen tension could be a result of not only a decrease in prostacyclin production, but also an increase in vascular TxA_2. This data suggests that the increase in oxidant stress goes beyond the inhibition of a vasodilator. By simultaneously scavenging NO and shifting AA metabolism from prostacyclin to TxA_2, the microvasculature predominantly experiences a greater tonic vasoconstrictor force as well as counteracting the effect of vasodilators.

Clinical Significance and Miscellaneous

The significance of this research has far reaching albeit indirect clinical implications. The most obvious is that treatment of PVD should not just address bulk blood flow impairments, which is classically what physicians address upon a diagnosis of PVD, but also microvascular dysfunction for real improvement to performance outcomes. The most difficult aspect of this, at the moment, would be proving microvascular dysfunction directly in human beings, given that the level of resolution for *in vivo* human blood flow is limited by technology. Additionally, while altered AA metabolism has long been suspected in many pathological states, and has long been a target for therapeutics, an effective target for the altered production of TxA_2 has not been demonstrated. Importantly, while the first chapter of this dissertation includes cerebral microvasculature but for the remainder focused on skeletal muscle microvasculature, the impact of altered cerebral blow flow on stroke, dementia, Alzheimer's, and other brain pathologies cannot be underestimated. One of the effective and frequently prescribed treatments for PVD is anticoagulants. Our experiments utilize a heparinized carotid catheter for the prevention of blood clots with the monitoring of mean arterial pressure. While this could potentially serve as a confounding variable in our experimental design, the concentration of heparin the animal is exposed to is well below the treatment limits. This is further verified by blood clotting during animal experimentation, of which no impairment is observed. It is worth noting that the vessels being studied in the *in vivo* and *in situ* studies have survived the progressive loss of microvessel density frequency observed in OZR of this age, and it is estimated that approximately 20-30% of vessels have undergone rarefaction.

Reference List

(1) **Ouriel K. Detection of peripheral arterial disease in primary care. *JAMA* 2001 September 19;286(11):1380-1.**

(2) **Mahoney EM, Wang K, Keo HH et al. Vascular hospitalization rates and costs in patients with peripheral artery disease in the United States. *Circ Cardiovasc Qual Outcomes* 2010 November;3(6):642-51.**

(3) **Ouriel K. Peripheral arterial disease. *Lancet* 2001 October 13;358(9289):1257-64.**

(4) **Allison MA, Ho E, Denenberg JO et al. Ethnic-specific prevalence of peripheral arterial disease in the United States. *Am J Prev Med* 2007 April;32(4):328-33.**

(5) **Lloyd-Jones D, Adams RJ, Brown TM et al. Heart disease and stroke statistics--2010 update: a report from the American Heart Association. *Circulation* 2010 February 23;121(7):e46-e215.**

(6) **Hamburg NM, Balady GJ. Exercise rehabilitation in peripheral artery disease: functional impact and mechanisms of benefits. *Circulation* 2011 January 4;123(1):87-97.**

(7) **Long J, Modrall JG, Parker BJ, Swann A, Welborn MB, III, Anthony T. Correlation between ankle-brachial index, symptoms, and health-related quality of life in patients with peripheral vascular disease. *J Vasc Surg* 2004 April;39(4):723-7.**

(8) **Frisbee JC, Goodwill AG, Butcher JT, Olfert IM. Divergence between arterial perfusion and fatigue resistance in skeletal muscle in the metabolic syndrome. *Exp Physiol* 2011 March;96(3):369-83.**

(9) **Goodwill AG, Frisbee SJ, Stapleton PA, James ME, Frisbee JC. Impact of chronic anticholesterol therapy on development of microvascular rarefaction in the metabolic syndrome. *Microcirculation* 2009 November;16(8):667-84.**

(10) **Alberti KG, Zimmet P, Shaw J. The metabolic syndrome--a new worldwide definition. *Lancet* 2005 September 24;366(9491):1059-62.**

(11) **Misra A, Khurana L. Obesity and the metabolic syndrome in developing countries. *J Clin Endocrinol Metab* 2008 November;93(11 Suppl 1):S9-30.**

(12) **Flegal KM, Carroll MD, Kit BK, Ogden CL. Prevalence of obesity and trends in the distribution of body mass index among US adults, 1999-2010. *JAMA* 2012 February 1;307(5):491-7.**

(13) **Cali AM, Caprio S. Obesity in children and adolescents. *J Clin Endocrinol Metab* 2008 November;93(11 Suppl 1):S31-S36.**

(14) **Ford ES, Mokdad AH. Epidemiology of obesity in the Western Hemisphere. *J Clin Endocrinol Metab* 2008 November;93(11 Suppl 1):S1-S8.**

(15) Ogden CL, Carroll MD, Curtin LR, McDowell MA, Tabak CJ, Flegal KM. Prevalence of overweight and obesity in the United States, 1999-2004. *JAMA* 2006 April 5;295(13):1549-55.

(16) Esposito K, Marfella R, Ciotola M et al. Effect of a mediterranean-style diet on endothelial dysfunction and markers of vascular inflammation in the metabolic syndrome: a randomized trial. *JAMA* 2004 September 22;292(12):1440-6.

(17) Scuteri A, Najjar SS, Muller DC et al. Metabolic syndrome amplifies the age-associated increases in vascular thickness and stiffness. *J Am Coll Cardiol* 2004 April 21;43(8):1388-95.

(18) Hill MA, Davis MJ, Meininger GA, Potocnik SJ, Murphy TV. Arteriolar myogenic signalling mechanisms: Implications for local vascular function. *Clin Hemorheol Microcirc* 2006;34(1-2):67-79.

(19) Hill MA, Zou H, Potocnik SJ, Meininger GA, Davis MJ. Invited review: arteriolar smooth muscle mechanotransduction: Ca(2+) signaling pathways underlying myogenic reactivity. *J Appl Physiol (1985)* 2001 August;91(2):973-83.

(20) Kuo L, Chilian WM, Davis MJ. Coronary arteriolar myogenic response is independent of endothelium. *Circ Res* 1990 March;66(3):860-6.

(21) Kuo L, Chilian WM, Davis MJ. Coronary arteriolar myogenic response is independent of endothelium. *Circ Res* 1990 March;66(3):860-6.

(22) Stepp DW, Frisbee JC. Augmented adrenergic vasoconstriction in hypertensive diabetic obese Zucker rats. *Am J Physiol Heart Circ Physiol* 2002 March;282(3):H816-H820.

(23) Saltzman D, DeLano FA, Schmid-Schonbein GW. The microvasculature in skeletal muscle. VI. Adrenergic innervation of arterioles in normotensive and spontaneously hypertensive rats. *Microvasc Res* 1992 November;44(3):263-73.

(24) Frisbee JC. Enhanced arteriolar alpha-adrenergic constriction impairs dilator responses and skeletal muscle perfusion in obese Zucker rats. *J Appl Physiol* 2004 August;97(2):764-72.

(25) Limberg JK, Morgan BJ, Sebranek JJ et al. Altered neurovascular control of the resting circulation in human metabolic syndrome. *J Physiol* 2012 December 1;590(Pt 23):6109-19.

(26) Licht CM, de Geus EJ, Penninx BW. Dysregulation of the autonomic nervous system predicts the development of the metabolic syndrome. *J Clin Endocrinol Metab* 2013 June;98(6):2484-93.

(27) Roberts CK, Sindhu KK. Oxidative stress and metabolic syndrome. *Life Sci* 2009 May 22;84(21-22):705-12.

(28) Goodwill AG, Stapleton PA, James ME, d'Audiffret AC, Frisbee JC. Increased arachidonic acid-induced thromboxane generation impairs skeletal muscle arteriolar dilation with genetic dyslipidemia. *Microcirculation* 2008 October;15(7):621-31.

Chapter 1

DIFFERENTIAL IMPACT OF DILATOR STIMULI ON INCREASED MYOGENIC ACTIVATION OF CEREBRAL AND SKELETAL MUSCLE RESISTANCE ARTERIOLES IN OBESE ZUCKER RATS

Joshua T. Butcher[1,2], Adam G. Goodwill[1,2], Shyla C. Stanley[1,2], and Jefferson C. Frisbee[1,2]

Department of Physiology and Pharmacology[1], and Center for Cardiovascular and Respiratory Sciences[2], West Virginia University HSC, Morgantown, WV

Running head: Metabolic syndrome and vascular reactivity

Address for Correspondence:

Jefferson C. Frisbee, Ph.D.
Center for Cardiovascular and Respiratory Sciences
Department of Physiology and Pharmacology
West Virginia University Health Sciences Center; 3152 HSN
1 Medical Center Drive
Morgantown, WV 26506
Phone: (304) 293-6527
Fax: (304) 293-5513
Email: jefrisbee@hsc.wvu.edu

ABSTRACT

Objective: To use the obese Zucker rat (OZR) model of the metabolic syndrome to determine the impact of dilator stimuli on myogenic activation (MA) of gracilis arterioles (GA) and middle cerebral arteries (MCA). We tested the hypothesis that increased oxidant stress and thromboxane A_2 (TxA_2) exacerbate MA, and prevent its blunting with dilator stimuli, in OZR. ***Methods:*** GA/MCA from OZR and lean Zucker rats (LZR) were pressurized *ex vivo*. MA was determined under control conditions and following challenge with acetylcholine, hypoxia and adenosine. Responses were also evaluated after pre-treatment with TEMPOL (antioxidant) and SQ-29548 (PGH_2/TxA_2 receptor antagonist). ***Results:*** MA was increased (and dilator responses decreased) in GA/MCA from OZR, dependent on the endothelium and ROS. In GA, the impact of ROS on MA and dilator effects was largely via TxA_2, while in MCA, this appeared was more dependent on NO bioavailability. Intrinsic responses of GA/MCA to carbacyclin, U46619, and NO donors were similar between strains. ***Conclusions:*** A developing ROS-based endothelial dysfunction in MCA and GA of OZR contributes to an enhanced MA of these vessels. While treatment of GA/MCA with TEMPOL attenuates MA in OZR, the mechanistic contributors to altered MA, distal to ROS, differ between the two resistance vessels.

Key Words: regulation of vascular tone, rodent models of metabolic syndrome, peripheral resistance, microcirculation

List of Abbreviations: Gracilis Arteriole (GA), Middle Cerebral Artery (MCA), Thromboxane A_2 (TxA_2), Reactive Oxygen Species (ROS)

INTRODUCTION

The metabolic syndrome, also referred to as insulin resistance syndrome or cardiometabolic syndrome, was fully articulated by Reaven in 1988 (25) but has since been more stringently defined with its continual increases in both incidence and prevalence (1, 4, 6, 7). According to the International Diabetes Federation (IDF), a clinical diagnosis of metabolic syndrome is made in patients that have central (abdominal) obesity, and two of the following co-morbidities: dyslipidemia, hypertension and impaired glycemic control (1). With these systemic pathologies, a companion pro-inflammatory and pro-thrombotic state is also commonly present (16, 20, 22). The most significant health outcome of these states is that they severely increase the risk for developing peripheral vascular disease (PVD) (4, 16, 20), a condition characterized by an inability of the vasculature to effectively match blood perfusion with local tissue/organ metabolic demand. As the regulation of vascular tone and the ability to effectively integrate multiple vasoactive processes is a critical component of blood flow regulation, alterations to the normal patterns of vascular reactivity could severely compromise perfusion:demand matching.

The obese Zucker rat (OZR: *fa/fa*) is an excellent model for the development of the metabolic syndrome and the associated negative vascular outcomes in humans. It possesses a recessive mutation leading to leptin receptor dysfunction (3, 29), causing a chronic hyperphagic state (17), which results in rapid-onset obesity. By 17 weeks of age, the OZR is severely obese, with the combined presentation of profound insulin resistance, dyslipidemia, and moderate hypertension (17, 26); a combination of pathologies that parallels metabolic syndrome in humans.

Full manifestation of the metabolic syndrome in OZR has been well documented to be associated with significant alterations to vascular reactivity (8, 15, 28). It has previously been shown that myogenic activation of both cerebral (24) and skeletal muscle (10) resistance vessels is enhanced, although there is no consistent understanding of the mechanistic underpinnings of this elevated responsiveness to intralumenal pressure. However, in *ex vivo* skeletal muscle and cerebral resistance arteries/arterioles from

OZR, there is an impaired response to multiple endothelium-dependent dilator stimuli (8, 9, 24, 28), and elevated levels of vascular oxidant stress can cause an increased production of the potent vasoconstrictor metabolite thromboxane A_2 (TxA_2; refs: 15, 21, 28). The extent to which impaired dilator responses and elevated production of constrictor metabolites can impact myogenic activation remains unclear.

Our previous work has suggested that the enhanced myogenic activation of skeletal muscle and cerebral resistance vessels in OZR may not reflect a common mechanistic basis (10, 24). Further, it is entirely unclear how myogenic activation in these critically important sites of vascular resistance integrates stimuli from intralumenal pressure and dilator influences to produce a change in diameter. As such, the general purpose of the present study is to determine the fundamental mechanisms of altered myogenic activation between these vascular beds, how this may be impacted by challenge with dilator stimuli, and if identified alterations are due to a consistent, system-wide effect. The general hypothesis is that oxidant stress-based increases in generation of vascular thromboxane A_2 will contribute to enhanced myogenic activation and blunted endothelium-dependent dilation in both cerebral and skeletal muscle resistance vessels.

MATERIALS AND METHODS

Animals: Male lean Zucker (LZR; n=32) and obese (OZR; n=35) rats (Harlan, Indianapolis, IN) of ~17 weeks age were used for all experiments. Animals were housed and fed standard chow and tap water *ad libitum* at the West Virginia University HSC and all protocols received prior approval from the Institutional Animal Care and Use Committee. Table 1 summarizes the baseline characteristics of animals used in the present study and clearly demonstrates the systemic pathologies associated with the metabolic syndrome. Following an overnight fast, all animals were anesthetized with pentobarbital sodium (50 mg/kg; i.p.) and received tracheal intubation to facilitate maintenance of a patent airway. All animals also received cannulation of both a carotid artery for blood pressure recording and a jugular vein for infusion of supplemental anesthetic (as needed) and the collection of blood samples. Venous blood

samples were analyzed for glucose (Freestyle Lite, Abbott, Alameda, CA), while the plasma components were analyzed for insulin concentrations (Millipore; Billerica, MA) as well as cholesterol/triglyceride levels (Wako Diagnostics; Richmond, VA), and nitrotyrosine (Oxis International; Foster City, CA). Unless otherwise noted, all drugs and chemicals were purchased from Sigma-Aldrich (St. Louis, MO, USA).

Preparation of Isolated Microvessels: After the initial surgery (above), a gracilis muscle resistance arteriole (GA) was surgically removed from the anesthetized animal and prepared for video microscopy, as described previously (5). Briefly, the arteriole was placed in a heated (37^{o}C) bath, doubly-cannulated with glass micropipettes and secured with silk suture. The vessel was then perfused and superfused with a physiological salt solution (PSS) equilibrated with 21% O_2, 5% CO_2, balance N_2. Immediately following removal of the GA from the animal, the rat was humanely euthanized and the brain was rapidly removed from the skull case, placed in chilled PSS (~4^{o}C), and the middle cerebral artery (MCA) was surgically removed from the base of the brain. The MCA was then doubly-cannulated and prepared in an identical manner as described for the GA. Both the MCA and the GA were allowed to equilibrate for at least 45 minutes at an intralumenal pressure of ~80% of the individual animal's mean arterial pressure (equilibration pressure). Vessel dimensions under control conditions and in response to imposed challenge were obtained under pressurized, zero flow conditions using video microscopy and an on-screen video-micrometer (5).

Changes in vessel diameter (myogenic activation) were measured following random changes in intralumenal pressure between 60 mmHg and 140 mmHg in 20 mmHg increments. After the initial assessment of myogenic responses, dilator reactivity was assessed at each level of intralumenal pressure following challenge with hypoxia (20 minutes), acetylcholine (10^{-6} M), and adenosine (10^{-6} M). For the purposes of the present study, hypoxia was defined as a change in PO_2 of the superfusate/perfusate PSS from ~135 mmHg [21% O_2, 5% CO_2, balance N_2 in the equilibration gas] to ~45 mmHg [0% O_2, 5% CO_2, balance N_2 in the equilibration gas]). These oxygen pressures have been previously validated with O_2 microelectrodes in the vessel chamber (19). Upon completion of data collection under untreated control

conditions (above), both MCA and GA were treated with either the antioxidant TEMPOL (10^{-4} M) or the PGH_2/TxA_2 receptor antagonist SQ-29548 (10^{-5}M) and at least 30 minutes was allowed for incubation. Following the incubation period, myogenic activation and dilator reactivity to the three stimuli at each level of intralumenal pressure was determined as described above. In an additional series of experiments, following the determination of responses under control conditions, the endothelium of both MCA and GA was denuded by passage of air boli through the vessel lumen (19) and the mechanical responses to intralumenal pressure and dilator stimuli were repeated.

A final series of experiments was performed to determine the responses of isolated GA and MCA from both LZR and OZR, at the equilibration pressures, in response to increasing concentrations of carbacyclin (10^{-12} – 10^{-8} M; a stable PGI_2 analog; Enzo Life Sciences, Farmingdale, NY), U46619 (10^{-12} – 10^{-8} M; a stable TxA_2 analog; Enzo Life Sciences, Farmingdale, NY), and sodium nitroprusside (10^{-10} – 10^{-6} M). These experiments were performed to determine if the development of the metabolic syndrome had a significant impact on the intrinsic responses of the GA or MCA in response to the major relevant vasoactive metabolites under interrogation in the present study.

Data and Statistical Analysis: All data are presented as mean±SE. Active tone of individual vessels at the equilibration pressure was calculated as $(\Delta D/D_{max})\bullet 100$, where ΔD is the diameter increase from rest in response to Ca^{2+}-free PSS, and D_{max} is the maximum diameter measured at the equilibration pressure in Ca^{2+}-free PSS. Curves describing myogenic activation under any of the imposed conditions were fit with linear regression equations: $y = \alpha_0 + \boldsymbol{\beta} x$; where y=vessel diameter (□m), x=intralumenal pressure (mmHg), α_0=y-intercept, and β=the slope of myogenic activation of the vessel. All other statistical analyses utilized Student's t-test or analysis of variance (ANOVA) with Student-Newman-Keuls test post-hoc. Statistical significance is represented by $p< 0.05$.

RESULTS

The baseline characteristics of LZR and OZR used in the present study are summarized in Table 1. At 17 weeks of age, OZR demonstrate significant increases in body mass, moderately elevated blood pressure, increased insulin resistance, and systemic oxidant stress. Table 2 summarizes the diameters of the vessels in this study from both LZR and OZR, at the equilibration pressures, under the different treatment groups in the present study. In GA, there were few differences between LZR and OZR, although the passive diameter of the vessel at the equilibration pressure was reduced in the obese animals. In contrast, MCAs manifested a significant increase in basal tone at the equilibration pressure, but exhibited no reduction in passive diameter.

Figure 1 summarizes myogenic activation of isolated GA (Panel A) and MCA (Panel B) from LZR and OZR in response to elevated intralumenal pressure. In both GA and MCA, the pressure-induced vasoconstriction was significantly elevated in vessels from OZR as compared to responses in LZR. The impact of endothelium denudation is presented in Panels C (for GA) and D (for MCA). Removal of the vascular endothelium abolished almost all of the differences in myogenic activation of either GA or MCA between LZR and OZR.

The impact of pre-treatment of vessels with the antioxidant TEMPOL or the PGH_2/TxA_2 receptor antagonist SQ-29548 on myogenic activation is presented in Figure 2. In GA from OZR, pretreatment with either TEMPOL (Panel A) or SQ-29548 (Panel B) significantly reduced the slope of the myogenic activation curve as compared to responses in untreated control conditions. In contrast, while TEMPOL exerted a similar effect on myogenic activation in MCA of OZR as compared to that in GA (Panel C), treatment with SQ-29548 did not significantly impact myogenic activation (Panel D). Combined treatment with both TEMPOL and SQ-29548 did not significantly reduce the slope of myogenic activation beyond that determined for either agent alone (data not shown).

The impact of hypoxia on myogenic activation of GA and MCA is summarized in Figure 3. In GA from LZR, imposition of hypoxia increased arteriolar diameter at the equilibration pressure and blunted

myogenic activation. In contrast, challenge with hypoxia had no significant impact on myogenic activation of GA from OZR (Panel A). Pre-treatment with either TEMPOL (Panel B) or SQ-29548 (Panel C) altered this response in GA from OZR, causing not only an increased diameter at the equilibration pressure, but also a significant reduction (i.e., less negative) in the □ □coefficient describing the pressure-induced constrictor response. Combined treatment with both TEMPOL and SQ-29548 did not result in any significant additive effect beyond that determined for either application alone (data not shown). The impact of hypoxia alone (Panel D) and hypoxia following pre-treatment with TEMPOL (Panel E) on myogenic activation of MCA were similar to that for GA from OZR. Hypoxia alone did not significantly impact the enhanced pressure-induced constriction from MCA in OZR, although pre-treatment with TEMPOL not only increased the vessel diameter at the equilibration pressure, it also blunted to slope of the myogenic activation curve to levels that were comparable to that in LZR. In contrast, pre-treatment with SQ-29548 did not significantly impact the relationship of myogenic activation and hypoxia in MCA from OZR (Panel F). As with GA, treatment of MCA with both TEMPOL and SQ-29548 did not alter the response as compared to the maximum improvement following single treatment (data not shown).

The impact of acetylcholine on myogenic activation of GA and MCA from LZR and OZR is presented in Figure 4. In GA from OZR, treatment with acetylcholine resulted in a modest dilation at the equilibration pressure, but did not significantly impact the slope of the myogenic activation curve (Panel A). While pre-treatment of GA from OZR with TEMPOL resulted in both an increased dilation at the equilibration pressure and a shifted slope coefficient for myogenic activation to levels that were not different from that in LZR (Panel B), treatment with SQ-29548 (Panel C) demonstrated no identifiable improvements to either the diameter at the equilibration pressure or the slope of myogenic activation. In MCA, acetylcholine increased the vessel diameter at the equilibration pressure in LZR, while also causing a significant shift in slope. In contrast, challenge with acetylcholine resulted in directionally similar, although less striking effect on myogenic activation of MCA from OZR (Panel D). Pre-treatment of

MCA from OZR with TEMPOL (+acetylcholine) reduced the severity of myogenic activation to a slope coefficient that was actually more positive than that determined under control conditions in LZR (Panel E). Treatment of MCA from OZR with SQ-29548 (Panel F) did not elicit a significant impact on myogenic activation following treatment with acetylcholine beyond that identified in for acetylcholine treatment alone (Panel D).

The mechanical responses of GA and MCA from LZR and OZR to increasing concentration of carbacyclin (Panel A), U46619 (Panel B) and sodium nitroprusside (Panel C) are summarized in Figure 5. For carbacyclin and sodium nitroprusside, dilator responses of GA and MCA in response to increasing concentrations of the agonist were brisk throughout the concentration range, with no significant differences between vessels from LZR and OZR. Similarly, constrictor responses to U46619, while brisk and extensive for both GA and MCA were not significantly different between LZR and OZR.

Figure 6 presents myogenic activation of GA and MCA from LZR and OZR in response to the presence of elevated adenosine (10^{-6}M). In both GA (Panel A) and MCA (Panel B), the presence of adenosine significantly increased vessel diameter at the respective equilibration pressures and blunted the severity of the enhanced myogenic activation.

DISCUSSION

Systemic PVD is an insidious disease that is characterized by an inability of the tissue/organ vasculature to adequately match local metabolic demand with perfusion. While there can be several contributors to this outcome, alterations to the control of vascular tone within resistance vessels represents a dominant factor. The OZR has proven to be an excellent model for the human progression to non-atherosclerotic PVD as the metabolic syndrome can alter vascular reactivity in the absence of plaque/lesion development (2). However, one of the challenges of studying any disease with a functional outcome on the regulation of blood flow and its intra-organ distribution is an understanding of how resistance arteries/arterioles integrate multiple inputs to produce an appropriate response. It has been established that OZR possess an enhanced myogenic activation in response to intralumenal pressure in both the skeletal muscle (10) and cerebral circulation (24). It has also been demonstrated that the chronic increase in vascular oxidant stress in OZR results in a shift in arachidonic acid metabolism, increasing production of vascular TxA_2 over levels determined in LZR (15). Further, it has been demonstrated that this this process can have a marked deleterious impact on intra-organ distribution of perfusion via alterations to the integrated regulation of vascular tone in skeletal muscle (11). From this, the question arises as to how vascular myogenic activation within the metabolic syndrome is impacted by changes in dilator stimuli and whether interventions targeting elevated oxidant stress or elevated TxA_2 production are effective at restoring normal patterns of reactivity between myogenic activation and interactions with dilator influences.

The initial observation from this study is that pressure-induced constriction is increased in both GA and MCA from OZR as compared to LZR, supporting previous observations (10, 24). Removal of the vascular endothelium largely abolished differences in myogenic activation between OZR and LZR, suggesting that the endothelium may represent the primary contributor to differences between the strains. Previous evidence using OZR (9, 10, 15, 28) and similar models (2) suggests that two endothelium-

dependent mechanisms, both of which stem from a chronically elevated vascular oxidant stress, may be responsible for the endothelial influence on myogenic activation: a reduction to vascular NO bioavailability via increased ROS scavenging and a shift in arachidonic acid metabolism toward production of the vasoconstrictor TxA_2. This interpretation is supported by data presented in Figure 2, where pre-treatment of GA or MCA of OZR with the TEMPOL shifted myogenic activation to levels that were comparable to those determined in LZR. However, while is it clear that ROS plays a role in myogenic activation of both GA and MCA, the role for TxA_2 is less consistent. In GA, pre-treatment with SQ-29548 resulted in a similar effect to that for TEMPOL, a restoration of pressure-induced constriction to levels in LZR. However, this treatment was largely without effect in MCA from OZR (Figure 2, Panel D). These data suggest that the contribution of ROS to increased myogenic activation may not be consistent across vascular beds; being more dependent on TxA_2 in skeletal muscle arterioles, and more dependent on NO bioavailability in the cerebral circulation.

To further explore the potential contribution of altered arachidonic acid metabolism to the main observations, the myogenic activation of *ex vivo* GA and MCA was evaluated under conditions of hypoxia. While other contributors to this response have been identified, including NO (8, 13, 24) and metabolites produced from cytochrome P450 □-hydroxlases and epoxygenases (8, 12, 13), in both GA and MCA, this has been demonstrated to be a dilator response that is largely-dependent on the production of PGI_2 from arachidonic acid (15, 19, 21). As shown in Figure 3, imposition of hypoxia alone had only mild effects on myogenic activation in either GA or MCA from OZR. This was not surprising, as hypoxic dilation of resistance vessels is impaired in OZR, in large measure due to a reduction in mediator bioavailability and an increased production of TxA_2 (8, 15, 24). However, when pre-treated with TEMPOL, the impact of hypoxia became much more pronounced, significantly blunting the slope of myogenic activation in vessels from OZR. This observation clearly suggests that the increased vascular oxidant stress is contributing to not just the enhanced myogenic activation of GA and MCA, but also to the inability of hypoxia to blunt the enhanced pressure-induced constriction in vessels from OZR. An

intriguing disparity exists when this is extended to the potential role for TxA_2, as pre-treatment with SQ-29548 resulted in an identical outcome as that for TEMPOL pre-treatment in GA from OZR (Figure 3, Panel C), while having a very limited effect in MCA (Figure 3, Panel F). These data clearly suggest that the impact of ROS on myogenic activation in GA from OZR, and the relative inability of hypoxia to blunt the pressure-induced constriction in these vessels, may be mediated predominantly through the production and actions of TxA_2. In contrast, while the effects of ROS and the impact of hypoxia on myogenic activation of MCA from OZR are qualitatively similar in MCA, the contribution of TxA_2 to this process may be considerably lower.

Pursuant to this, we switched to a mechanistically different dilator, acetylcholine, which is largely NO-dependent in the rat vasculature (27). While the impact of acetylcholine on myogenic activation of GA and MCA from OZR was comparable to that for hypoxia, and pre-treatment with TEMPOL increased the impact of the stimulus on myogenic activation of both GA and MCA, pre-treatment with SQ-29548 had no identifiable impact on myogenic activation of either vessel (+ acetylcholine; Figure 4, Panels C and F). Based on previous data regarding the mechanistic pathways for acetylcholine and the results presented above, these data provide additional support for the concept of a divergence in ROS-dependent contributors to the enhanced myogenic activation of GA and MCA from OZR.

One question that arises from the results of the present study is the intrinsic sensitivity of GA and MCA from LZR and OZR in response to PGI_2 (carbacyclin), TxA_2 (U46619) and nitric oxide, and whether this changes with the evolution of the metabolic syndrome. However, the data presented in Figure 5 indicate that vascular responsiveness to these three metabolites remains robust and does not demonstrate any consistent alteration in this model. As such, it is plausible at this time to ascribe differences in vascular responses to myogenic stimulation and dilator influences as an issue of mediator bioavailability, rather than one of vascular responsiveness.

Used as a proxy variable for elevated metabolic demand, the impact of elevated adenosine (10^{-6} M) on myogenic activation of GA and MCA from OZR reveals an intriguing relationship. In skeletal muscle arteriole of OZR, elevated adenosine attenuated the severity of the pressure-induced vasoconstriction, resulting in a response that was similar to that determined in GA from LZR. One would predict that this would be an appropriate response of the resistance vasculature in response to elevated metabolic demand – a shift in the overall setting of myogenic activation, such that flow regulation can still be maintained, although at a lower overall resistance. However, given that this 'adenosine-treated' response remains blunted below that in GA from LZR treated with adenosine, altered myogenic activation in GA of OZR may still represent a contributor to reduced bulk perfusion and altered perfusion distribution with elevated metabolic demand (14). In contrast, application of adenosine to MCA resulted in a very comparable blunting of myogenic activation in vessels from both LZR and OZR. Speculatively, these observations suggest that the ability of local metabolic demand in the brain may be more able to override the increased pressure-induced constriction in the cerebral resistance vessels of OZR than in the skeletal muscle microcirculation. However, the extent to which this may serve as a protective mechanism under conditions of cerebral ischemia or hypoxia in OZR, where stroke severity may be enhanced (22) remains unknown at this time.

PERSPECTIVES

With the development of the metabolic syndrome in this model, an increased pressure-induced constriction of resistance vessels develops in both the skeletal muscle and cerebral circulation. While the genesis of this increased myogenic activation for both vessels appears to lie within an elevation in vascular oxidant stress, the increased response in skeletal muscle vessels appears to reflect an increased contribution from the production of TxA_2, while responses in the cerebral circulation appear to reflect a loss of dilator metabolite bioavailability. Importantly, the ability of local metabolic demand to override myogenic activation appears to still be present in both tissues, and may be fully intact in the brain. While this may reflect a protective mechanism in the brain versus skeletal muscle, further interrogation into the

functional impact of these differences on organ perfusion as well as therapeutic interventions against the increased myogenic activation should keep this in mind.

Acknowledgements

This study was supported by grants from the National Institutes of Health (NIH T32 HL 90610, RR 2865AR and IDeA P20 GM 103434), the American Heart Association (AHA EIA 0740129N). The authors also wish to express their gratitude for the expert technical assistance from Ms. Milinda James from the Department of Physiology and Pharmacology at West Virginia University.

LITERATURE CITED

1. Alberti KG, Zimmet P, Shaw J. Metabolic syndrome--a new world-wide definition. A Consensus Statement from the International Diabetes Federation. Diabet Med 23: 469-480, 2006.
2. Amy RM, Dolphin PJ, Pederson RA, Russell JC. Atherogenesis in two strains of obese rats: The fatty Zucker and LA/N-corpulent. Atherosclerosis 69: 199-209, 1998.
3. Bray GA. The Zucker-fatty rat: a review. Fed Proc 36: 148-153, 1977.
4. Bray GA, Bellanger T. Epidemiology, trends, and morbidities of obesity and the metabolic syndrome. Endocrine 29: 109-117, 2006.
5. Butcher JT, Goodwill AG, Frisbee JC. The ex vivo isolated skeletal microvessel preparation for investigation of vascular reactivity. J Vis Exp 28: 2012.
6. Eckel, RH, Grundy SM, Zimmet PZ. The metabolic syndrome. Lancet 365: 1415-1428, 2005.
7. Ervin RB. Prevalence of metabolic syndrome among adults 20 years of age and over, by sex, age, race and ethnicity, and body mass index: United States, 2003-2006. Natl Health Stat Report 13: 1-7, 2009.
8. Frisbee JC. Impaired dilation of skeletal muscle microvessels to reduced oxygen tension in diabetic obese Zucker rats. Am J Physiol Heart Circ Physiol 281: H1568-H1574, 2001.

9. Frisbee JC. Reduced nitric oxide bioavailability contributes to skeletal muscle microvessel rarefaction in the metabolic syndrome. Am J Physiol Regul Integr Comp Physiol 289: R307-R316, 2005.

10. Frisbee JC, Maier KG, Stepp, DW. Oxidant stress-induced increase in myogenic activation of skeletal muscle resistance arteries in obese Zucker rats. Am J Physiol Heart Circ Physiol 283: H2160-H2168, 2002.

11. Frisbee JC, Hollander, JM, Brock RW, Yu HG, Boegehold MA. Integration of skeletal muscle resistance arteriolar reactivity for perfusion responses in the metabolic syndrome. Am J Physiol Regul Integr Comp Physiol 296: R1771-R1782, 2009.

12. Frisbee JC, Krishna UM, Falck JR, Lombard JH. Role of prostanoids and 20-HETE in mediating oxygen-induced constriction of skeletal muscle resistance arteries. Microvascular Research 62: 271-283, 2001.

13. Frisbee JC, Maier KG, Falck JR, Roman RJ, Lombard JH. Integration of hypoxic dilation signaling pathways for skeletal muscle resistance arteries. Am J Phys Reg Int and Comp Physiology 283: R309-R319, 2002.

14. Frisbee JC, Goodwill AG, Butcher JT, Olfert IM. Divergence between arterial perfusion and fatigue resistance in skeletal muscle in the metabolic syndrome. Exp Physiol. 96:369-383, 2011.

15. Goodwill AG, James ME, Frisbee JC. Increased vascular thromboxane generation impairs dilation of skeletal muscle arterioles of obese Zucker rats with reduced oxygen tension. Am J Physiol Heart Circ Physiol 295: H1523-H1528, 2008.

16. Gorter PM, Olijoek JK, Van Der GY, Algra A, Rabelink TJ, Visseren FL. Prevalence of the metabolic syndrome in patients with coronary heart disease, cerebrovascular disease, peripheral arterial disease or abdominal aortic aneurysm. Atherosclerosis 173: 363-369, 2004.

17. Kurtz TW, Morris RC, Pershadsingh HA. The Zucker fatty rat as a genetic model of obesity and hypertension. Hypertension 13: 896-901, 1989.

18. Lenda DM, Sauls BA, Boegehold MA. Reactive oxygen species may contribute to reduced endothelium-dependent dilation in rats fed high salt. Am J Phys Heart and Circulatory Physiology 279: H7-H14, 2000.

19. Lombard JH, Liu Y, Fredricks KT, Bizub DM, Roman RJ, Rusch NJ. Electrical and mechanical responses of rat middle cerebral arteries to reduced PO_2 and prostacyclin. Am J Phys Heart and Circ Phys 276: H509-H516, 1999.

20. Lusis AJ, Attie AD, Reue K. Metabolic syndrome: from epidemiology to systems biology. Nat Rev Genet 9: 819-830, 2008.

21. Messina EJ, Sun D, Koller A, Wolin MS, Kaley G. Increases in Oxygen Tension Evoke Arteriolar Constriction by Inhibiting Endothelial Prostaglandin Synthesis. Microvascular Research 48: 151-160, 1994.

22. Miranda PJ, Defronzo RA, Califf RM, Guyton JR. Metabolic syndrome: definition, pathophysiology, and mechanisms. Am Heart J 149: 33-45, 2005.

23. Osmond JM, Mintz JD, Dalton B, Stepp DW. Obesity increases blood pressure, cerebral vascular remodeling and severity of stroke in the Zucker rat. Hypertension. 53:381-386, 2009.

24. Phillips SA, Sylvester FA, Frisbee JC. Oxidant stress and constrictor reactivity impair cerebral artery dilation in obese Zucker rats. Am J Physiol Regul Integr Comp Physiol 288: R523-R530, 2005.

25. Reaven GM. Banting lecture 1988. Role of insulin resistance in human disease. Diabetes 37: 1595-1607, 1988.

26. Stepp DW, Frisbee JC. Augmented adrenergic vasoconstriction in hypertensive diabetic obese Zucker rats. Am J Physiol Heart Circ Physiol 282: H816-H820, 2002.

27. Ungvari Z, Sun D, Huang A, Kaley G, Koller A. Role of endothelial [Ca2+] in activation of eNOS in pressurized arterioles by agonists and wall shear stress. Am J Physiol Heart Circ Physiol. 281:H606-H612, 2001.

28. Xiang L, Naik JS, Hodnett BL, Hester RL. Altered arachidonic acid metabolism impairs functional vasodilation in metabolic syndrome. Am J Physiol Regul Integr Comp Physiol. 290:R134-R138, 2006.

29. Zucker LM, Antoniades HN. Insulin and obesity in the Zucker genetically obese rat "fatty". Endocrinology 90: 1320-1330, 1972.

Table 1. Baseline characteristics of 17 week-old LZR and OZR used in the present study. * $p<0.05$ versus LZR.

	LZR (n=30)	**OZR (n=34)**
Mass (g)	344±11	669±12*
MAP (mmHg)	106±6	126±5*
$[Glucose]_{plasma}$ (mg/dl)	105±11	181±10*
$[Insulin]_{plasma}$ (ng/ml)	1.4±0.2	8.5±1.2*
$[Nitrotyrosine]_{plasma}$ (ng/ml)	15±5	45±8*

Table 2. Inner diameter (at the equilibration pressure) of gracilis arterioles (GA) and middle cerebral arteries (MCA) of LZR and OZR used in the present study. Data in parentheses represents % active tone. * $p<0.05$ versus LZR.

	Gracilis Arteriole		**Middle Cerebral Artery**	
	LZR	**OZR**	**LZR**	**OZR**
Control	104±5 (44±4%)	96±5 (43±3%)	121±4 (43±4%)	105±5 (46±4%)*
-Endothelium	101±4	100±5	118±5	114±4
+Hypoxia	118±4	100±5	138±4	115±5*
+SQ-29548	107±4	102±4	120±5	109±4
+TEMPOL	104±5	105±4	116±5	113±5
+Acetylcholine	115±5	101±5	133±5	112±4
+Adenosine	118±4	109±5	129±4	119±5
Ca^{2+}-free PSS (Passive)	184±5	169±5*	204±4	194±5

FIGURE LEGENDS

Figure 1: Data describing myogenic activation of isolated gracilis muscle arterioles (Panels A and C; n=5 for both) and middle cerebral arteries (Panels B and D; n=5-6 for both) from LZR and OZR in response to increased intralumenal pressure. Data, presented as mean±SE, are presented for vessels under control conditions (Panels A and B) and following removal of the endothelium (Panels C and D). Slope (□) coefficients describing the curve of myogenic activation are presented in the inset legend. * $p<0.05$ vs. LZR-Control; † $p<0.05$ vs.OZR-Control.

Figure 2: Data describing myogenic activation of isolated gracilis muscle arterioles (Panels A and B; n=5-7 for both) and middle cerebral arteries (Panels C and D; n=6 for both) from LZR and OZR in response to increased intralumenal pressure. Data, presented as mean±SE, are presented for vessels under control conditions and following pre-treatment of the vessels with either TEMPOL (10^{-4}M) or the PGH_2/TxA_2 receptor antagonist SQ-29548 (10^{-5}M). Slope (□) coefficients describing the curve of myogenic activation are presented in the inset legend. * $p<0.05$ vs. LZR-Control; † $p<0.05$ vs.OZR-Control.

Figure 3: Data describing myogenic activation of isolated gracilis muscle arterioles (Panels A-C; n=5-6 for all) and middle cerebral arteries (Panels D-F; n=5 for all) from LZR and OZR in response to increased intralumenal pressure. Data, presented as mean±SE, are presented for vessels under control conditions, following imposition of hypoxia and following pre-treatment of the hypoxic vessels with either TEMPOL (10^{-4}M) or the PGH_2/TxA_2 receptor antagonist SQ-29548 (10^{-5}M). Slope (□) coefficients describing the curve of myogenic activation are presented in the inset legend. * $p<0.05$ vs. LZR-Control; † $p<0.05$ vs.OZR-Control; ‡ $p<0.05$ vs. OZR-Hypoxia.

Figure 4: Data describing myogenic activation of isolated gracilis muscle arterioles (Panels A-C; n=5 for all) and middle cerebral arteries (Panels D-F; n=5-6 for all) from LZR and OZR in response to increased intralumenal pressure. Data, presented as mean±SE, are presented for vessels under control conditions,

following challenge with acetylcholine (10^{-6} M) and following pre-treatment of the acetylcholine-challenged vessels with either TEMPOL (10^{-4}M) or the PGH_2/TxA_2 receptor antagonist SQ-29548 (10^{-5}M). Slope (□) coefficients describing the curve of myogenic activation are presented in the inset legend. * $p<0.05$ vs. LZR-Control; † $p<0.05$ vs.OZR-Control; ‡ $p<0.05$ vs. OZR-Hypoxia.

Figure 5: Data describing the mechanical responses of isolated gracilis muscle arterioles and middle cerebral arteries from LZR and OZR in response to increased concentrations of carbacyclin (Panel A; n=5 for all), U46619 (Panel B; n=5 for all) and sodium nitroprusside (Panel C; n=5 for all). Data, presented as mean±SE, are presented for vessels under control conditions, at their equilibrium pressure. There were no significant differences in the mechanical responses of GA or MCA between LZR and OZR for the three agonists.

Figure 6: Data describing myogenic activation of isolated gracilis muscle arterioles (Panel A; n=5) and middle cerebral arteries (Panel B; n=5) from LZR and OZR in response to increased intralumenal pressure. Data, presented as mean±SE, are presented for vessels under control conditions and following challenge with adenosine (10^{-6} M). * $p<0.05$ vs. LZR-Control; † $p<0.05$ vs.OZR-Control.

Figures:

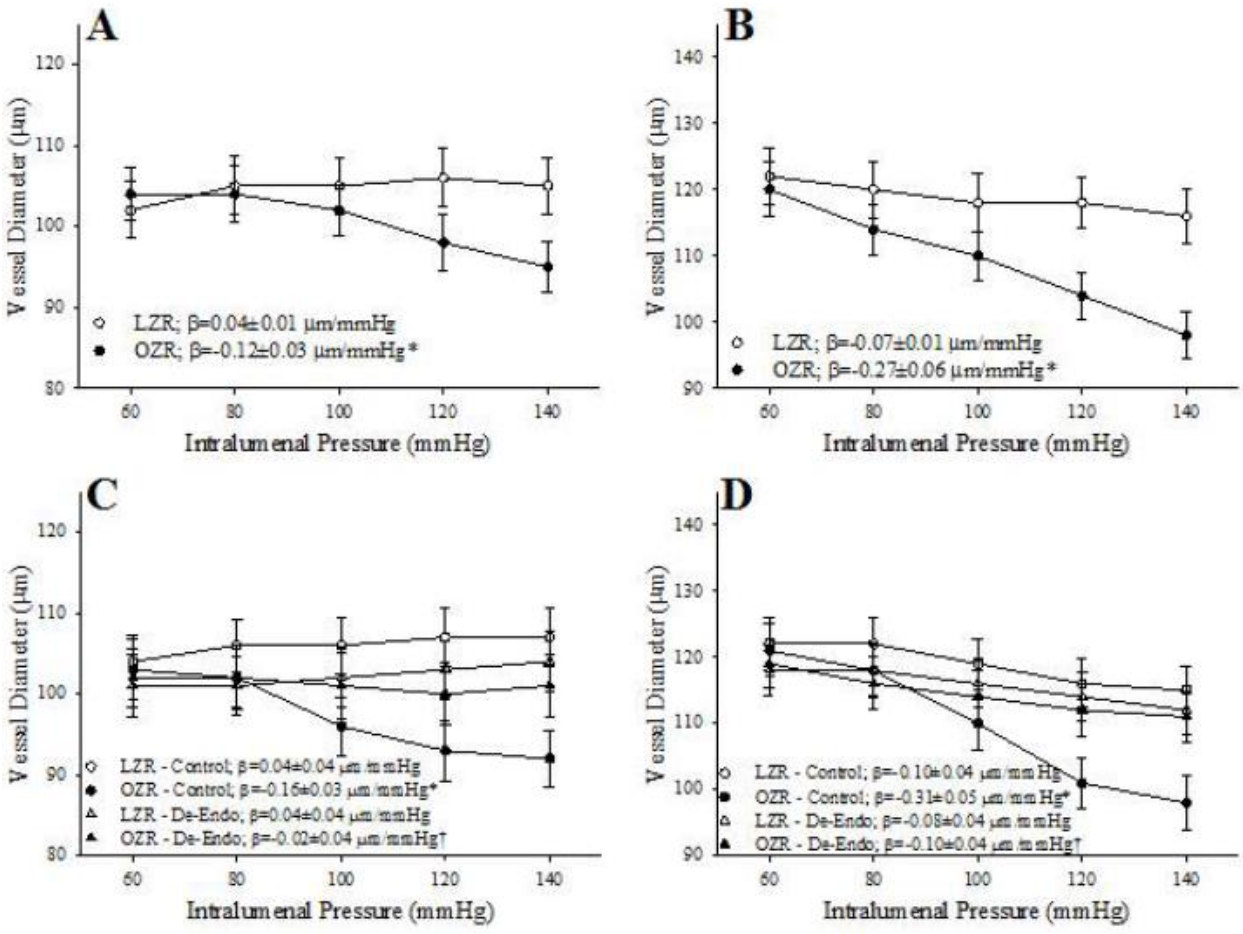

Figure 1
Butcher et al.

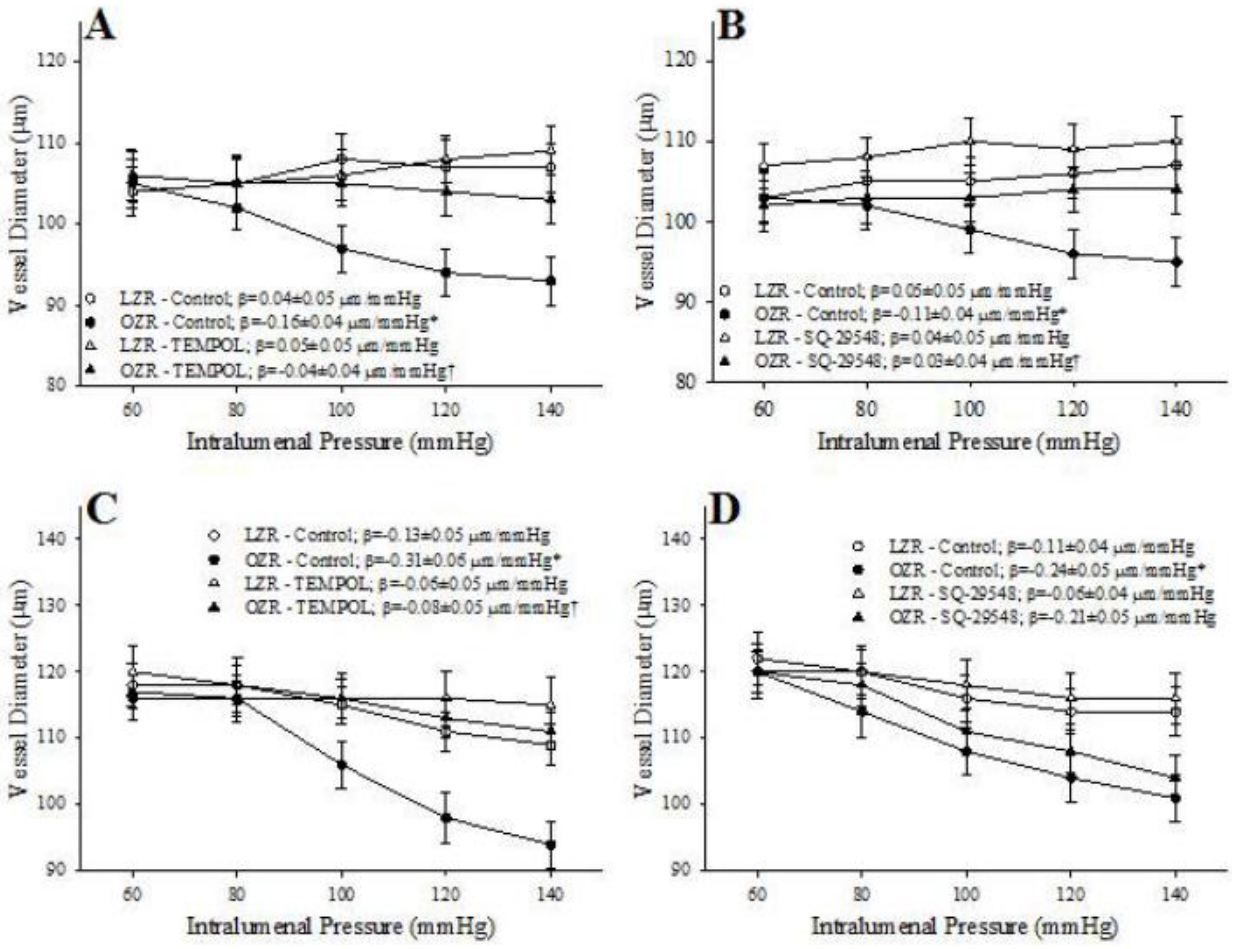

Figure 2
Butcher et al.

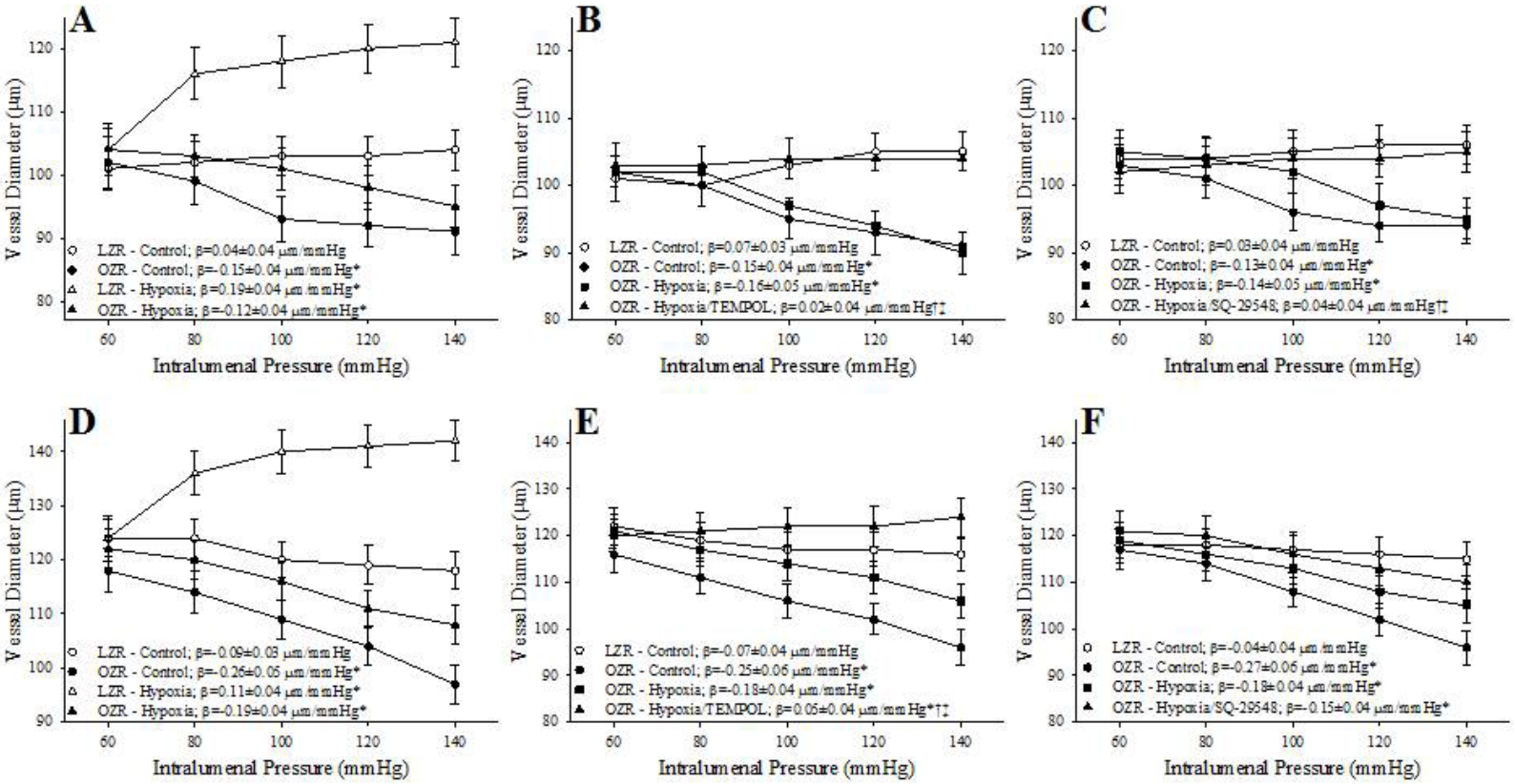

Figure 3
Butcher et al.

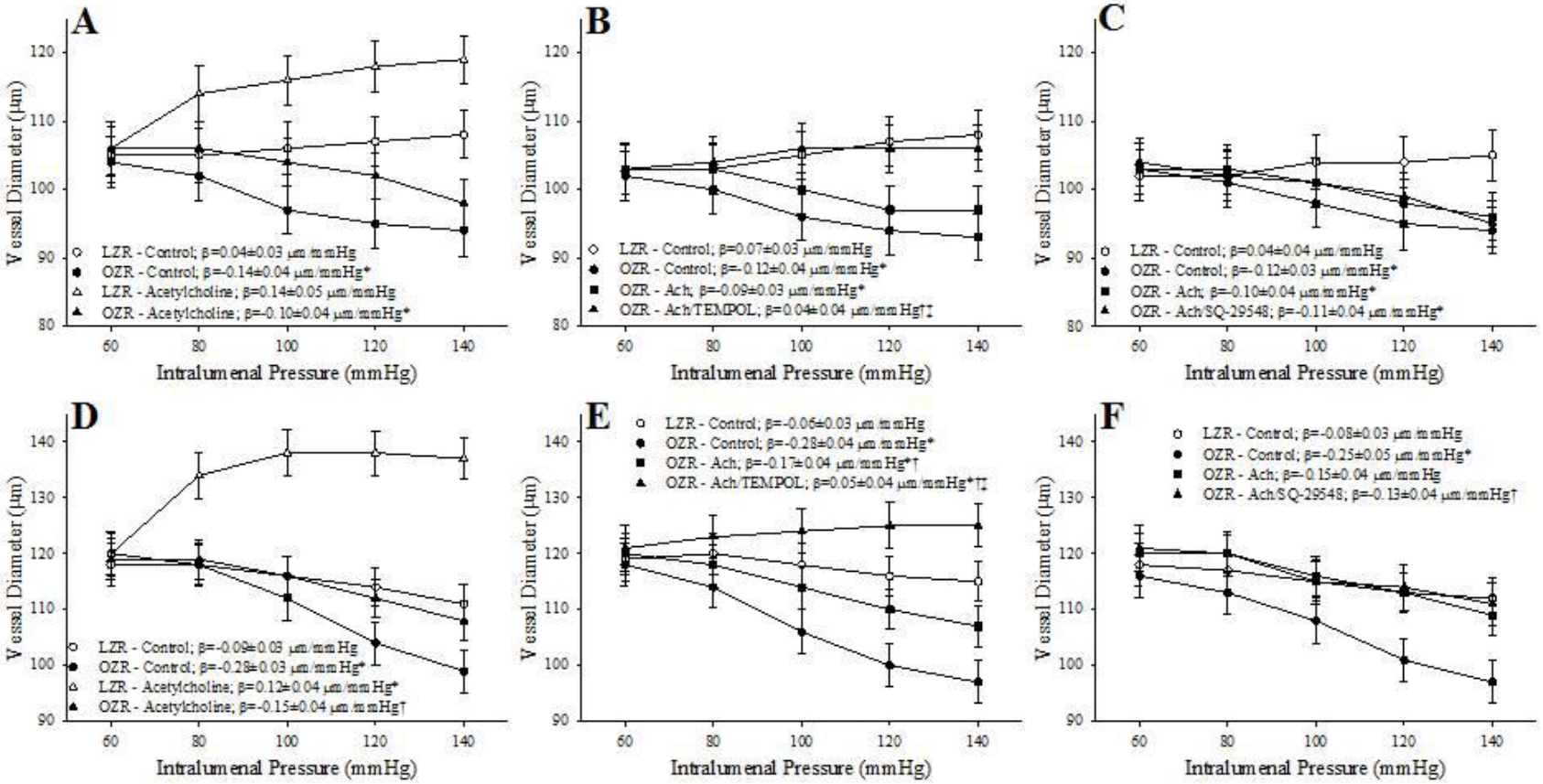

Figure 4
Butcher et al.

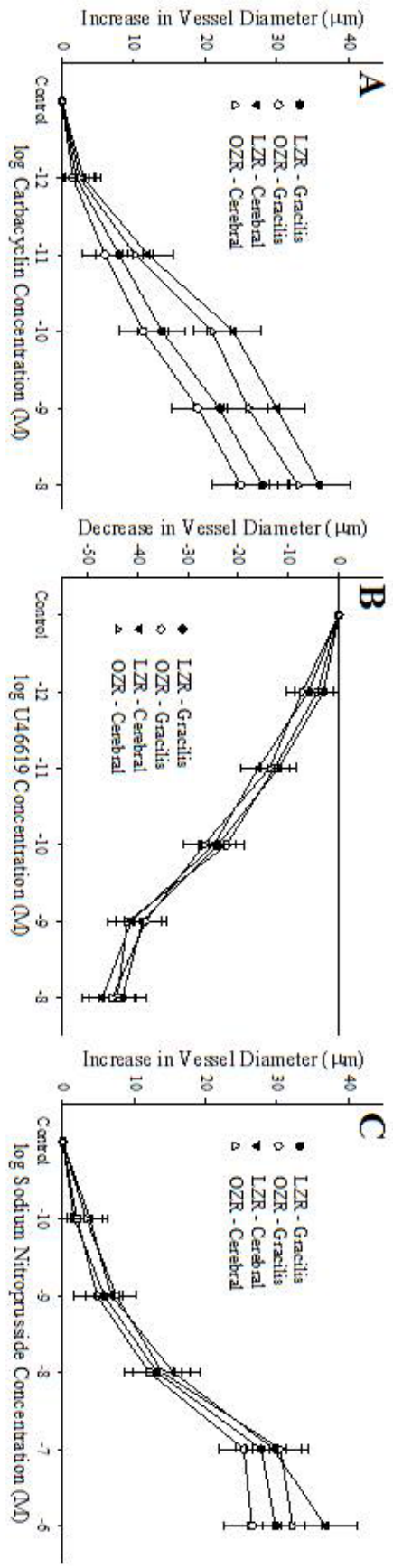

Figure 5
Butcher et al.

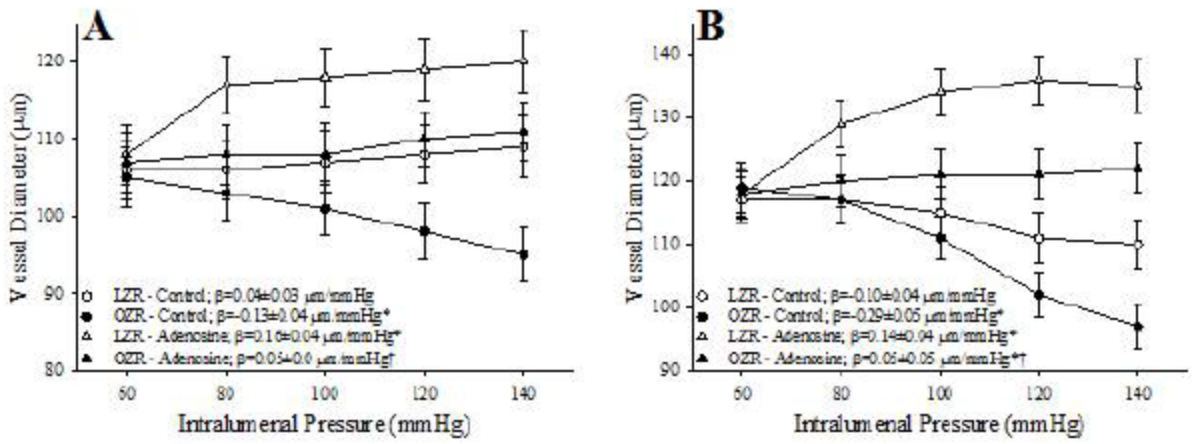

Figure 6
Butcher et al.

Conceptual Framework:

The first chapter of this dissertation is entitled "Differential Impact of Dilator Stimuli on Increased Myogenic activation of Cerebral and Skeletal Muscle Resistance Arterioles in Obese Zucker Rats". This paper is part of the foundational work that illustrates the potent impact of MetSyn on vascular tone. Myogenic activation is a dominant factor controlling vascular tone because it is part of the intrinsic vascular control within vessels that maintains a constant blood supply despite changes in perfusion pressure. It has been previously shown that myogenic activation is increased in vascular beds in the OZR compared to the LZR, although the mechanism for this increase had not been elucidated. This paper sought to examine if the increase in oxidant stress and/or altered AA metabolism were appropriate interventions to treat the increased myogenic activation and how this will integrate with other dilator stimuli. The data confirmed the increased myogenic activation seen previously in the OZR in both skeletal muscle and cerebral vasculature, and that the changes in myogenic activation appear to largely be endothelial dependent. It also revealed that the impact of ROS was primarily through the action of TxA_2. In the isolated microvessel preparation the skeletal muscle gracilis arteriole showed a restoration of myogenic activation with treatment of TEMPOL, a ROS scavenger, and a similar response to SQ-29548, a TxA_2 receptor antagonist. Further experiments integrating dilator conditions (hypoxia, acetylcholine, and adenosine) with myogenic activation revealed an attenuated dilator response compared to the LZR. In skeletal muscle, a large portion of the impaired dilator response is oxidant stress-induced as well as mediated through the production and action of TxA_2. A key part of these data showed that the increased myogenic activation seen in the OZR was capable of blunting the adenosine response. Adenosine is often used as a mimic for an increase in metabolic demand, and this indicates that increased myogenic activation contributes to altered vascular responses even during increased levels of metabolic demand. This chapter lays the groundwork for suggesting that the microvasculature in the OZR is compromised in its ability to integrate vasoactive compounds and adequately regulate blood flow.

Chapter 2

DIVERGENCE BETWEEN ARTERIAL PERFUSION AND FATIGUE RESISTANCE IN SKELETAL MUSCLE IN THE METABOLIC SYNDROME

Jefferson C. Frisbee[1], Adam G. Goodwill[1], Joshua T. Butcher[1], and I. Mark Olfert[2]

Department of Physiology and Pharmacology[1] and Division of Exercise Physiology[2] and Center for Cardiovascular and Respiratory Sciences, West Virginia University HSC, Morgantown, WV

Address for Correspondence:

Jefferson C. Frisbee, Ph.D.

Center for Cardiovascular and Respiratory Sciences

Department of Physiology and Pharmacology

West Virginia University Health Sciences Center; 3152 HSN

1 Medical Center Drive

Morgantown, WV 26506

Phone: (304) 293-6527

Fax: (304) 293-5513

Email: jfrisbee@hsc.wvu.edu

ABSTRACT

The metabolic syndrome is associated with elevated peripheral vascular disease risk, characterized by mismatched blood flow delivery/distribution and local metabolism. The obese Zucker rat (OZR) model of the metabolic syndrome exhibits myriad vascular impairments, although their integrated impact on functional hyperemia remains unclear. In this study, arterial pressor responses and skeletal muscle perfusion were assessed in lean Zucker rats (LZR) and OZR during adrenergic stimulation (phenylephrine), challenge with thromboxane (U46619) and endothelium-dependent dilation (methacholine). OZR were hypertensive versus LZR, but this was abolished by adrenoreceptor blockade (phentolamine); pressor responses to U46619 were similar between strains and were abolished by blockade with the PGH_2/TxA_2 receptor antagonist, SQ-29548. Depressor reactivity to methacholine was impaired in OZR, but was improved by antioxidant treatment (TEMPOL). Across levels of metabolic demand, blood flow to *in situ* gastrocnemius muscle was restrained by adrenergic constriction in OZR, although this diminished with increased demand. O_2 extraction, reduced in OZR vs. LZR across levels of metabolic demand, was improved by TEMPOL or SQ-29548; treatment with phentolamine did not impact extraction and neither TEMPOL nor SQ-29548 improved muscle blood flow in OZR. While VO_2 and muscle performance were consistently reduced in OZR vs. LZR, treatment with all three agents improved outcomes, while treatment with individual agents was less effective. These results suggest that contributions of vascular dysfunction to perfusion, VO_2 and muscle performance are spatially distinct, with adrenergic constriction impacting proximal resistance and endothelial dysfunction impacting distal microvessel-tissue exchange. Further, these data suggest that increasing skeletal muscle blood flow in OZR is not sufficient to improve performance, unless distal perfusion inhomogeneities are rectified.

Key Words: rodent models of obesity; skeletal muscle blood flow regulation; models of peripheral vascular disease; blood flow heterogeneity; vascular dysfunction

INTRODUCTION

One of the hallmark characteristics in the development of the metabolic syndrome, with its constituent systemic pathologies of obesity, insulin resistance/type II diabetes mellitus, atherogenic dyslipidemia and hypertension, is the substantially increased risk for the progressive evolution of peripheral vascular disease (Cannon, 2008; Ford and Mokdad, 2008; Jones 2008; Obunai *et al.* 2007). While this can possess atherosclerotic or non-atherosclerotic elements in its constitution (with distinct etiological characteristics and outcomes), one of the defining elements of peripheral vascular disease (PVD) is an evolving inability to effectively match tissue perfusion with local metabolic demand, an observation routinely demonstrated in both humans and in multiple animal models of the metabolic syndrome (Baron, 2002; He *et al.* 1995; Nicholson *et al.* 1992; Ruiter *et al.* 2010; Wolfram *et al.* 2001). While this has been identified across numerous organs/tissues, we have demonstrated reduced bulk blood flow to *in situ* gastrocnemius muscle of the obese Zucker rat (OZR) across ranges of demand from rest to near maximum metabolic intensity (Frisbee *et al.* 2009; Frisbee 2005; 2004; 2003).

In OZR, a model of the metabolic syndrome which derives its genesis through chronic hyperphagia as a result of a severe receptor-based leptin resistance (Guerre-Millo, 1997; Williams *et al.* 2001), the basic contributing mechanisms underlying the compromised perfusion and hyperemic responses may include: 1) enhanced adrenergic constrictor reactivity and signaling of skeletal muscle arterioles (Frisbee, 2004; Naik *et al.* 2006; Stepp and Frisbee, 2002), 2) a widespread impairment to arteriolar dilator reactivity, primarily centered around compromised endothelial function (Bouvet *et al.* 2007; Frisbee *et al.* 2009; Goodwill *et al.* 2008; Katakam *et al.* 2009; Lu *et al.* 2010), and 3) structural remodeling of the microvasculature (Bovet *et al.* 2007; Goodwill *et al.* 2009; Lu *et al.* 2010; Stepp *et al.* 2004), including a reduced wall distensibility of the resistance arterioles (predominantly contributing to an elevated vascular resistance) and a rarefaction of the distal microvasculature (predominantly contributing to impairments to mass transport and exchange in the microenvironments). With these

elements in place, a progressive deterioration in tissue perfusion develops which can, and ultimately does, negatively impact the ability of the skeletal muscle to resist fatigue (Frisbee, 2006; 2004).

However, recent data suggests that a more complex relationship than has been previously understood may exist with regard to the linkages between skeletal muscle perfusion and fatigue resistance within the metabolic syndrome. Specifically, we have recently provided initial evidence that multiple pathways which derange the normal patterns of skeletal muscle arteriolar reactivity integrate to impair not only vascular dilation in a metabolic demand-dependent fashion, but also that these can contribute to perfusion heterogeneity at microvascular bifurcations which could represent a significant contributor to the compromised ability of microvascular networks to match perfusion to local metabolic demand (Frisbee *et al.* 2009).

As a result of these recent observations, there is an immediate need for a more accurate understanding of the relationships between the perfusion to, and the performance of, skeletal muscle within the setting of the metabolic syndrome. Given that the metabolic syndrome represents a condition which strongly predisposes individuals to an elevated risk of PVD, which can be defined as a condition wherein the perfusion:metabolic demand matching can be substantially impaired, the translational importance of the thorough understanding of how perfusion and muscle performance are intertwined in this pathological setting is imperative. The purpose of this study is to thoroughly evaluate functional outcomes (performance) in skeletal muscle and to provide a framework for future interrogation into the detailed relationships between vascular function, perfusion and skeletal muscle performance outcomes. This study was designed to provide a rigorous test of the hypothesis that functional hyperemia is constrained within skeletal muscle of OZR owing to the combined impact of adrenergic constraint and endothelial dysfunction, each of which acts to either inappropriately increase, or prevent reductions in, the resistance to skeletal muscle blood flow over a range of imposed metabolic demand.

MATERIALS AND METHODS

Animals: 15-17 week old male lean Zucker rats (LZR) and OZR fed standard chow and tap water *ad libitum* were used for all experiments. Data describing the baseline characteristics of LZR and OZR in the present study are presented in Table 1. At this age range, OZR were significantly heavier than age-matched LZR and also demonstrated fasting (overnight) hyperglycemia, hyperinsulinemia, elevated plasma triglyceride levels and moderate hypertension. Rats were housed in animal care facility at either the Medical College of Wisconsin or at the West Virginia University Health Sciences Center, and all protocols received prior IACUC approval. Rats were anesthetized with injections of sodium pentobarbital (50 $mg \bullet kg^{-1}$ i.p.), and received tracheal intubation to facilitate maintenance of a patent airway. In all rats a carotid artery and an external jugular vein were cannulated for determination of arterial pressure and for intravenous infusion of additional substances as necessary (e.g., anesthetic, heparin, etc.).

Preparation of In Situ Blood-Perfused Skeletal Muscle: In all LZR and OZR, the left gastrocnemius muscle was isolated *in situ* (Frisbee, 2003). Briefly, the left leg received a medial incision from the calcaneus to the femoral triangle, and all muscles, vessels and connective tissue overlaying gastrocnemius muscle were removed, thus exposing the gastrocnemius muscle, its vascular supply, and the sciatic nerve. The nerve was isolated and utilized for initiating muscle contraction via a stimulating electrode attached to an electrical stimulator (Grass SD9). Branches from the femoral artery that did not perfuse the gastrocnemius muscle directly were ligated or cauterized, depending on size and location. A microcirculation flow probe (Transonic) was placed around the femoral artery, immediately distal to its origin from the iliac artery, in order to measure blood flow to the gastrocnemius muscle. As a final step, a 24 gauge angiocatheter was inserted into the femoral vein to allow for sampling of venous blood from the contracting muscle. The entire preparation was covered in PSS-soaked gauze and plastic film to minimize evaporative water loss and was placed under a lamp to maintain temperature at 37°C. At this time, heparin (500 U/kg) was infused via the jugular vein to prevent blood coagulation.

Section One: Arterial Pressor and Hindlimb Perfusion Responses: Following the complete surgical preparation of the rats, it was necessary to validate the effectiveness of the experimental conditions that were

to be utilized for the subsequent interrogations of skeletal muscle perfusion and fatigue resistance relationships. For these procedures, rats received an intravenous infusion of the α_1/α_2 adrenoreceptor antagonist phentolamine (10 mg/kg; followed by 30 minutes of equilibration), the superoxide dismutase mimetic 4-hydroxy-2,2,6,6-tetramethylpiperidine-N-oxyl (TEMPOL; 50 mg/kg; followed by 45 minutes of equilibration), or the PGH_2/TxA_2 receptor antagonist SQ-29548 (10 mg/kg; followed by 30 minutes of equilibration) in order to remove the influences of adrenergic tone, vascular oxidant stress and influence of vascular sources of TxA_2 from the system, respectively. Following treatment of the individual rats with phentolamine, TEMPOL or SQ-29548, each animal was challenged with an intravenous infusion of the α-adrenoreceptor agonist phenylephrine (10 μg/kg), the endothelium-dependent nitric oxide donor methacholine (10 μg/kg) or the TxA_2 mimetic U46619 (10 μg/kg). Alterations in mean arterial pressure and femoral artery perfusion were monitored following agonist infusion in order to determine peak responses and the time to restoration of baseline (pre-treatment) conditions. All infused intravenous doses of drugs were corrected for differences in circulating blood volume between LZR and OZR at this age (Frisbee, 2006; Schreihofer *et al.* 2005).

Section Two: Responses of Contracting In Situ Skeletal Muscle: Following validation of the actions of phentolamine, TEMPOL or SQ-29548 and restoration of baseline conditions, the gastrocnemius muscle was stimulated to perform (via the sciatic nerve) bouts of isometric twitch contractions (1, 3, or 5 Hz, 0.4 ms duration, 5V) for 3 minutes followed by 15 minutes of self-perfused recovery, with arterial pressure and femoral artery blood flow continuously monitored. Data were collected under control conditions and following treatment of the rats with phentolamine, TEMPOL or SQ-29548, as described above.

Data Calculations: In specific experiments, 200 μl blood samples were drawn from the carotid artery cannula and femoral vein angiocatheter immediately prior to and following completion of, the muscle contraction periods. Samples were stored on ice until they were processed for blood gas pressures, percent oxygen saturation and hemoglobin concentration using a Corning Rapidlab 248 blood gas analyzer. Muscle perfusion, arterial pressure, and bulk blood flow through the femoral artery were monitored for one minute

prior to muscle contractions and throughout the contraction period using a Biopac MP150 with Acqknowledge data acquisition software at a 50Hz sampling frequency. Muscle perfusion and performance data after three minutes of contraction were normalized to gastrocnemius mass, which was not different between LZR (2.18±0.09 g) and OZR (2.06±0.10 g). Oxygen content within the blood samples was determined using the following standard equation:

$$C_xO_2 = (1.39 \times [Hb] \times \%SatO_2) + (0.003 \times P_xO_2) \quad \text{Eq. 1}$$

Where C_xO_2 and P_xO_2 represent the total content (ml/dL) or partial pressure of oxygen (mmHg), respectively, of arterial or venous blood (denoted simply as 'x'). [*Hb*] represents hemoglobin concentration within the blood sample (g/dL); $\%O_2$Sat represents the percentage oxygen saturation of the hemoglobin and 1.39 and 0.003 represent constants describing the amounts of bound and dissolved oxygen in blood. Oxygen uptake across the gastrocnemius muscle was calculated using the Fick equation:

$$\dot{V}O_2 = \dot{Q} \times (CaO_2 - CvO_2)$$

Eq. 2

where $\dot{V}O_2$ represents oxygen uptake by the gastrocnemius muscle, $\dot{Q}$ represents femoral artery blood flow (ml/g/min), and CaO_2 and CvO_2 represent arterial and venous oxygen content, respectively. Perfusion resistance across gastrocnemius muscle was calculated as the quotient of mean arterial pressure and muscle blood flow. Muscle O_2 conductance (DmO_2) was calculated using Fick's law of diffusion as a simple model of O_2 flux to the working muscle,

$$\dot{V}O_2 = DmO_2\ (P\bar{c}O_2 - PmitoO_2)$$

Eq. 3

where DmO_2 is the diffusing capacity of O_2 at the muscle (ml/min/mmHg/mg muscle), $P\bar{c}O_2$ is the mean capillary PO_2 (mmHg), and $PmitoO_2$ is average mitochondrial PO_2 (mmHg) (Kurdak *et al.* 1996; Roca *et al.* 1989). Estimation of $P\bar{c}O_2$ is based on a numerical (Bohr) integration procedure that uses a single parameter for tissue diffusing capacity-to-muscle blood flow ratio (DO_2/QT), which is assumed to be constant along the capillary, where DO_2/QT is varied iteratively until the calculated end-capillary PO_2 matches the measured venous PO_2 to within 0.1 mmHg (Kurdak *et al.* 1996; Roca *et al.* 1989). Mean capillary PO_2 ($P\bar{c}O_2$) is then a time-weighted average of all computed PO_2 values along the capillary based on the initial measured arterial and venous PO_2 values. Explicit assumptions in making the DmO_2 calculation are that, 1) mitochondrial PO_2 is negligibly small (i.e. $PmitoO_2$=0 mmHg) at maximal or near maximal exercise, and that 2) the only explanation of O_2 remaining in the femoral venous blood is diffusion limitation of O_2 efflux from the muscle microcirculation (Wagner, 1992). Accordingly, perfusional or diffusional shunts are considered negligible, and we only calculate DmO_2 for data obtained at maximal or near maximal exercise (i.e. electrical stimulation at 5 Hz). For all calculations we used hemoglobin of 15 gm/dL and p50 of 26.8 mmHg.

Statistical Analyses: Statistically significant differences in determined results were assessed using either Student's *t*-test or analysis of variance (ANOVA), with Student-Newman-Keul's post-hoc test as needed. In all cases, $p<0.05$ was taken to reflect statistical significance. All data are presented as mean±SE.

RESULTS

Data describing the animals under investigation in the current study are summarized in Table 1. At 15-17 weeks of age, OZR were dramatically heavier than LZR, and demonstrated a significant impairment to glycemic control, dyslipidemia, and chronic elevations in vascular oxidant stress.

Figure 1 summarizes the impact of challenge of LZR and OZR with phenylephrine (with and without pre-treatment with phentolamine) on arterial pressure (Panel A), femoral artery blood flow (Panel B) and vascular resistance (Panel C) in LZR and OZR. In response to intravenous infusion of the adrenoreceptor

agonist, mean arterial pressure was significantly increased in both strains, although the magnitude of this increase was similar between LZR (67±9 mmHg) and OZR (72±12 mmHg). Pre-treatment of animals with phentolamine reduced arterial pressure in both strains to a similar level and abolished pressor responses to infused phenylephrine (Panel A). Femoral artery blood flow in OZR was not significantly different as compared to LZR under control conditions, and challenge with phenylephrine infusion resulted in a mild, but variable, reduction in blood flow in both strains (Panel B). Following treatment with phentolamine, femoral artery blood flow was mildly elevated to similar levels between LZR and OZR, and infusion of phenylephrine was without effect. Vascular resistance, elevated in OZR versus LZR under control conditions, increased significantly in both strains following infusion of phenylephrine (Panel C), although this response was enhanced in OZR [347±42 mmHg/(ml/g/min)] as compared to LZR [187±30 mmHg/(ml/g/min)]. Treatment of rats with phentolamine lowered resistance in both strains to a similar level, and blocked the overwhelming majority of the phenylephrine-induced increases in vascular resistance.

The impact of challenging the animal with the TxA_2 analog U46619 and the effectiveness of blockade of the PGH_2/TxA_2 receptors with SQ-29548 is summarized in Figure 2. Infusion of U46619 increased arterial pressure in both strains, although the magnitude of this effect was very similar between LZR and OZR (Panel A). While blockade of PGH_2/TxA_2 receptors had no discernible impact on arterial pressure, it abolished the pressor response to U46619 in both strains. Infusion of U46619 (either with or without pre-treatment with SQ-29548) had no impact on bulk blood flow through the femoral artery in either LZR or OZR (Panel B). Treatment of rats with U46619 resulted in a similar, significant increase in vascular resistance in both strains, and this response was abolished by pre-treatment with SQ-29548 (Panel C).

Figure 3 presents data describing the impact of both infusion of methacholine and the effects of pre-treatment with TEMPOL on arterial pressure (Panel A), femoral artery blood flow (Panel B) and vascular resistance across the gastrocnemius muscle (Panel C) in LZR and OZR. In LZR, challenge with methacholine caused a rapid, significant depressor response that was unaffected by pre-treatment with TEMPOL. In contrast, infusion of methacholine in OZR did not significantly reduce arterial pressure, while

pre-treatment of rats with TEMPOL improved the depressor response (Panel A). In preliminary studies, treatment of either LZR or OZR with the nitric oxide synthase inhibitor L-NAME (100 mg/kg) prevented the depressor effects of methacholine under any condition (ΔMAP from control in LZR+L-NAME=-3.5±3.6 mmHg; (ΔMAP from control in OZR+L-NAME=+1.4±4.1 mmHg). In LZR, infusion of methacholine resulted in an increased femoral artery blood flow, a response not identified in OZR. This effect was not altered in LZR following pre-treatment with TEMPOL, although it was increased in OZR to the point of reaching statistical significance (Panel B). Similarly, methacholine infusion resulted in a decreased vascular resistance in LZR only (with or without TEMPOL treatment), while methacholine-induced reductions in resistance in OZR were identified following pre-treatment with TEMPOL (Panel C).

The hemodynamic characteristics within gastrocnemius muscle of OZR and LZR under resting conditions in the present study are summarized in Figure 4. The decreased femoral artery blood flow in OZR as compared to LZR at rest was eliminated following treatment with phentolamine, although treatment with either TEMPOL or SQ-29548 was without effect (Panel A). Incorporating arterial pressure, the elevation in vascular resistance across the gastrocnemius in OZR was corrected following infusion of phentolamine, while treatment with TEMPOL or SQ-29548 provided no discernible benefit (Panel B). Under resting conditions, the extraction of oxygen from arterial to venous blood was significantly reduced in OZR versus LZR and, in contrast to the previous panels, only treatment with TEMPOL or SQ-29548 increased extraction, while adrenoreceptor blockade was without effect (Panel C). Integrating blood flow and extraction, oxygen uptake at the gastrocnemius muscle was reduced in OZR versus LZR, and only combined treatment of OZR with all three agents (phentolamine, TEMPOL and SQ-29548) resulted in a significant improvement to muscle VO_2. In preliminary experiments, treatment of LZR with phentolamine, TEMPOL and/or SQ-29548 failed to elicit a consistent and/or significant change in the above parameters (data not shown).

In response to 1Hz twitch contractions (Figure 5), the general patterns of the measured outcomes in the present study were not strikingly different than that presented in Figure 4. Femoral artery blood flow (Panel A) was reduced and vascular resistance (Panel B) was elevated in OZR versus LZR, and these

alterations were corrected by pre-treatment with phentolamine (TEMPOL and SQ-29548 having no consistent measureable impact). In contrast, the reduction in oxygen extraction in OZR versus LZR (Panel C) was only ameliorated following treatment with either TEMPOL or SQ-29548, with only a trivial benefit provided by treatment with phentolamine. However, the recovery in VO_2 in contracting gastrocnemius of OZR to levels determined in LZR was only realized following treatment of the animal with all three agents (Panel D). Muscle fatigue resistance mirrored the patterns in VO_2, with a reduced tension development after three minutes of contraction in OZR as compared to LZR, and a significant improvement in contractile performance only occurring following combined treatment of OZR with phentolamine, TEMPOL and SQ-29548 (Panel E).

Figure 6 summarizes hemodynamic responses in gastrocnemius muscle of LZR and OZR in response to three minutes of contraction at 3Hz. While femoral blood flow was lower (Panel A) and vascular resistance was higher (Panel B) in OZR versus LZR, the ability of phentolamine to restore these values was less robust than at lower levels of metabolic demand, with neither TEMPOL nor SQ-29548 exerting a discernible impact on these outcomes. In contrast, both TEMPOL and SQ-29548 improved oxygen extraction (Panel C) and VO_2 (Panel D) across gastrocnemius muscle of OZR, while phentolamine exerted only minimal benefits. Phentolamine was unable to improve skeletal muscle fatigue resistance in OZR at 3Hz, while both TEMPOL and SQ-29548 did result in a mild improvement to performance, and combined treatment with all three agents resulted in the greatest improvement in the ability of the gastrocnemius muscle to maintain developed tension (Panel E).

Data describing the perfusion responses of *in situ* gastrocnemius muscle of OZR and LZR in response to 5Hz contraction are summarized in Figure 7. These data appear present a different conceptual framework, as no employed intervention was able to improve femoral artery blood flow in OZR above that identified under control conditions (Panel A), and this was paralleled by measures of vascular resistance, which were very consistent across OZR groups, regardless of intervention (Panel B). However, treatment with TEMPOL or SQ-29548 improved oxygen extraction (Panel C) to levels similar

to that in LZR, and VO_2 as well (Panel D), although this improvement was constrained by the limits on normalized muscle O_2 conductance (Panel E). Finally, while treatment of OZR with phentolamine was without effect on muscle fatigue resistance at 5Hz, and both TEMPOL and SQ-29548 resulted in mild improvements, combined therapy with all agents significantly improved muscle performance in OZR over that determined under control conditions (Panel F). In preliminary experiments, treatment of LZR with phentolamine, TEMPOL and/or SQ-29548 failed to elicit a consistent and/or significant change in the above parameters across levels of metabolic demand (data not shown).

The robust correlative relationships between skeletal muscle O_2 conductance and muscle performance at 5Hz contraction for LZR and OZR under the conditions of the present study are shown in Figure 8. DmO_2 was a strong correlate of muscle fatigue resistance across LZR and OZR, with an r-squared value explaining nearly 60% of the variability in the data.

DISCUSSION

One of the most vexing challenges to public health and the quality of life of afflicted individuals is the insidious progression of peripheral vascular disease (PVD), with its characteristic impairment to blood flow delivery and the accelerated development of fatigue in those muscles experiencing an increased metabolic demand (Baron, 2002; Hudlicka and Brown, 2009; Nicholson *et al.* 1992; Ruiter *et al.* 2010; Wolfram *et al.* 2001). The OZR, with its inherent development of obesity, insulin resistance, moderate hypertension and hyperlipidemia represents an excellent model of non-atherosclerotic PVD risk, and while there have been numerous studies describing alterations to vascular reactivity, microvascular network structure and microvessel wall mechanics in OZR, the ability to extend these observations to an integrated system for the regulation of blood flow has been far more limited. While several studies have indicated that functional dilation (Xiang *et al.* 2008; 2006) or hyperemia (Frisbee, 2004; 2003) are impaired in skeletal muscle of OZR as compared to LZR, these remain superficially described, and results

from recent study suggests that the integration across vascular structure/function relationships, the regulation of perfusion, functional hyperemia and skeletal muscle fatigue resistance may be more complicated than has previously been appreciated (Frisbee *et al.* 2009).

The initial observations from the first section of this study demonstrate that the increased resistance across the skeletal muscle microcirculation of OZR is multi-factorial in nature. While the adrenergic component to this elevated resistance can be effectively removed with α_1/α_2 adrenoreceptor blockade (Figure 1), this is clearly a more complicated process, and one that appears to involve alterations to endothelial function. While data in Figure 2 suggest that vascular responses to TxA_2 are not altered in OZR, supporting earlier observations (Goodwill *et al.* 2008), previous studies provided compelling evidence that vascular production of TxA_2, elevated in OZR (Xiang *et al.* 2008; 2006), can compromise functional dilation and hyperemic responses within the distal microcirculation (where contribution to overall resistance is lower; Greene *et al.* 1989) (Frisbee *et al.* 2009; Xiang *et al.* 2008; 2006). Additionally, the muted response to the endothelium-dependent agonist methacholine in OZR was partially ameliorated by pre-treatment with the antioxidant TEMPOL (and was consistently abolished by the nitric oxide synthase inhibitor L-NAME), clearly indicating the impairments to nitric oxide bioavailability through oxidant scavenging, an especially compelling issue for several reasons. Not only does elevated systemic oxidant stress in OZR have the capacity to severely compromise nitric oxide bioavailability, it also has the capacity to alter arachidonic acid metabolism leading toward the increased generation of TxA_2 (Goodwill *et al.* 2008; Zou, 2007; Zou *et al.* 2004). While these can obviously have immediate impacts on vascular tone regulation themselves, alterations in NO and TxA_2 bioavailability in the microcirculation of OZR have also been demonstrated to contribute to significant changes to the patterns and severity of adrenergic constriction (Stepp and Frisbee, 2002), myogenic activation (Frisbee *et al.*2002), and the integration of these parameters for the determination of net vascular tone (Frisbee *et al.* 2009).

The second portion of this study focused on relationships between vascular function, blood flow and muscle fatigue resistance in OZR under control conditions and in response to the imposed interventions of phentolamine, TEMPOL and SQ-29548. As compared to LZR, OZR exhibited a blunted functional hyperemia and an elevated vascular resistance across gastrocnemius muscle across the continuum of metabolic demand. Interestingly, this was also accompanied by a reduction in oxygen extraction and a compromised VO_2 in OZR, which, not surprisingly, was strongly predictive of an impaired muscle performance. This is a particularly intriguing outcome for multiple reasons. The gastrocnemius muscle was driven to contract via electrical stimulation of the sciatic nerve, and not only were the stimulation parameters identical between strains, but gastrocnemius mass was also very similar, which should have minimized differences between metabolic demand and muscle performance between the two strains. Further, at this age, daily physical activity is very similar between LZR and OZR (Stepp *et al.* 2004), fiber type profiles are similar (Adachi *et al.* 2007; Pujol e*t al.* 1993), and the maximum developed tension was nearly identical between the two strains (Table 1). As such, results from these experiments strongly suggest that impairments to muscle performance in OZR at this age appear to reflect an altered behavior within blood delivery/distribution in the microcirculation (i.e. O_2 flux across the working muscle), rather than overt dysfunction within skeletal muscle myocyte and motor unit recruitment patterns. However, it must be emphasized that these conclusions are relevant for OZR at this age only, as previous studies have clearly demonstrated significant, although variable, alterations to contractile and metabolic functions of skeletal muscle myocytes in OZR afflicted with the metabolic syndrome with increasing age (Campion *et al.* 1987; Farkas *et al.* 1994; He *et al.* 1995).

At the lower end of this continuum of metabolic demand, blood flow to gastrocnemius muscle of OZR was restrained by increased adrenergic tone, as infusion of phentolamine abolished the elevated vascular resistance (Figures 4 and 5). However, adrenergic constraint appeared to play little role in terms of the poor oxygen extraction and VO_2, as these were unaffected by phentolamine infusion. In contrast, the endothelial dysfunction in OZR was not a significant contributor to perfusion resistance across the

gastrocnemius muscle, as neither TEMPOL nor SQ-29548 altered femoral artery blood flow. What was most compelling was that TEMPOL and SQ-29548 improved oxygen extraction across the gastrocnemius of OZR as compared to LZR, although VO_2 remained low owing to the lack of an impact on blood flow. These relationships were also evident in the gastrocnemius of OZR working at 3 Hz contractions (Figure 6), wherein the influence of phentolamine, while decreased with elevated metabolic demand, was primarily via reduced blood flow resistance while TEMPOL and SQ-29548 improved oxygen extraction, and the combined influence of all three agents improving VO_2 and muscle performance to the greatest extent. The condition at 5 Hz (Figure 7) contractions was somewhat different owing to the structural remodeling of the microvessel wall and networks to impose an upper 'ceiling' on bulk blood flow to the muscle in OZR (Frisbee, 2005). As such, phentolamine was without effect on resistance in OZR, although its restrictive effect was diminishing with increased contraction frequency owing to metabolic sympatholysis (Frisbee, 2004). However, TEMPOL and SQ-29548 retained their ability to improve oxygen extraction and conductance such that an optimal muscle VO_2 under these conditions in OZR was realized. Not surprisingly, regardless of metabolic demand, optimization of bulk blood flow, muscle oxygen conductance in OZR, specifically following treatment with all three pharmacological agents, was associated with the greatest improvement to gastrocnemius muscle fatigue resistance.

Taken together, the results of the present study have three significant and novel implications. The first of these is the altering blood flow alone cannot restore skeletal muscle performance within the OZR model of PVD. This observation is in some contrast to the accepted interpretations of PVD, wherein a consistent assumption is that improving blood flow to active tissue, and certainly in proportion to the continuum of metabolic demand (i.e. O_2 uptake), would improve functional outcomes. That an intervention which enhanced functional hyperemia was ineffective at improving muscle oxygen conductance and performance emphasizes the complexity of the processes affecting the diffusional conductance of oxygen that is central to the poor outcomes identified in OZR and the strong relationship determined between muscle O_2 conductance and the fatigue response (Figure 8).

Importantly, treatment of OZR with TEMPOL or SQ-29548 improved oxygen flux across the microcirculation of the gastrocnemius muscle with minimal impact on aggregate vascular resistance. This observation suggests that the beneficial impact of improving endothelial function with regard to enhancing the integrated outcome of muscle performance may be the result of optimizing hemodynamic behavior in the distal microcirculation (where localized mass transport and exchange phenomena are most relevant) than in the proximal microcirculation (where the regulation of perfusion resistance is most relevant). This observation is be supported by the muscle performance data in the present study, wherein neither phentolamine nor TEMPOL/SQ-29548 alone improved muscle performance, while only combined treatment with all three agents reduced fatigue development. This apparent spatial distinction of the major contributors to poor perfusion and muscle performance outcomes, with the beneficial impacts of adrenoreceptor blockade being primarily relevant in the proximal microcirculation and those for improved endothelial dysfunction being primarily relevant in the distal microcirculation represents the second major implication and novel observation of the results present study.

The concept involving the spatial relevance of interventions suggests the third major implication of the present study. The results of the previous study indicated that one of the hallmark characteristics of the distal microcirculation within *in situ* cremaster muscle of OZR was that perfusion distribution at microvascular bifurcations was more heterogeneous than in LZR, with potential contributors to this derangement being elevated oxidant stress and increased TxA_2 production (Frisbee *et al.* 2009). Speculatively, this may be the underlying physiological/hemodynamic mechanism for the impact of TEMPOL/SQ-29548 on improving oxygen flux in contracting muscle of OZR in the present study. If development of PVD in OZR is characterized by an increasing perfusion heterogeneity at microvascular bifurcations, resulting in a poor pattern of oxygen extraction across the muscle through an increasing propensity for ‘high flow pathways’ with lower extraction and ‘low flow pathways’ which become flow-limited, this could compromise net oxygen extraction and be reflective of a generalized impairment to mass transport and exchange across the skeletal muscle microcirculation. Indeed, this process is akin to

matching of ventilation and perfusion in the lung, which is known to be an important determinant in transfer of O_2 (i.e. O_2 conductance) from alveolar gas into blood. Further interrogation of the contributing physiological, biochemical and molecular signaling mechanisms, their spatio-temporal distribution, their interactions, and the potential for ameliorative intervention appears to be well justified.

While the results of this study provide for a compelling framework for the interrogation of the relationships between perfusion and fatigue in skeletal muscle under conditions of the metabolic syndrome, one inherent limitation that should be acknowledged is the preparation itself. The combination of a barbiturate anesthetic, which can inhibit reflex sympathetic excitation as a result of the muscle contraction, clearly has the potential to impact the results of study in an unpredictable manner. Further, the potential for electrical activation of sympathetic postganglionic fibers and group IV afferents as a result of the current applied to the sciatic nerve cannot fully be discounted. Given these inherent limitations to the preparation, further effort into the verification and potential application of a decerebrate preparation without the necessity of anesthesia where the skeletal muscles in question can be activated via direct stimulation of ventral roots may be warranted.

ACKNOWLEDGEMENTS

This study was supported by grants from the National Institutes of Health (NIH DK R01 64668; RR2865AR) and the American Heart Association (AHA SDG 0330194N and EIA 0740129N to JCF and BGIA 3630002 to IMO). The authors also wish to express their gratitude for the expert technical assistance of Mr. Tianjian Huang from the Department of Physiology at the Medical College of Wisconsin, Ms. Milinda James from the Department of Physiology and Pharmacology and Ms. Sarah Olenich from the Division of Exercise Physiology at West Virginia University and for support provided through the Translational Research Facility in the Center for Cardiovascular and Respiratory Sciences at the West Virginia University HSC. The authors express their gratitude to Dr. Peter D. Wagner from the University of California at San Diego Medical Center for his helpful insights and suggestions regarding the determination of oxygen conductance.

LITERATURE CITED

1. Adachi T, Kikuchi N, Yasuda K, Anahara R, Gu N, Matsunaga T, Yamamura T, Mori C, Tsujimoto G, Tsuda K, Ishihara A. (2007). Fibre type distribution and gene expression levels of both succinate dehydrogenase and peroxisome proliferator-activated receptor-gamma coactivator-1alpha of fibres in the soleus muscle of Zucker diabetic fatty rats. Exp Physiol. 92(2):449-55.

2. Baron AD. (2002). Insulin resistance and vascular function. J Diabetes Complications. 16(1):92-102.

3. Bouvet C, Belin de Chantemèle E, Guihot AL, Vessières E, Bocquet A, Dumont O, Jardel A, Loufrani L, Moreau P, Henrion D. (2007). Flow-induced remodeling in resistance arteries from obese Zucker rats is associated with endothelial dysfunction. Hypertension. 50(1):248-54.

4. Campion DR, Shapira JF, Allen CE, Hausman GJ, Martin RJ. (1987). Metabolic characteristics of skeletal muscle from lean and obese Zucker rats. Growth. 51(4):397-410.

5. Cannon CP. (2008). Mixed dyslipidemia, metabolic syndrome, diabetes mellitus, and cardiovascular disease: clinical implications. Am J Cardiol. 102(12A):5L-9L.

6. Farkas GA, Gosselin LE, Zhan WZ, Schlenker EH, Sieck GC. (1994). Histochemical and mechanical properties of diaphragm muscle in morbidly obese Zucker rats. J Appl Physiol. 77(5):2250-9.

7. Ford ES, Mokdad AH. (2008). Epidemiology of obesity in the Western Hemisphere. J Clin Endocrinol Metab. 93: (11 Suppl 1):S1-S8.

8. Frisbee JC, Hollander JM, Brock RW, Yu HG, Boegehold MA. (2009). Integration of skeletal muscle resistance arteriolar reactivity for perfusion responses in the metabolic syndrome. Am J Physiol Regul Integr Comp Physiol. 296(6):R1771-82.

9. Frisbee JC. (2005). Reduced nitric oxide bioavailability contributes to skeletal muscle microvessel rarefaction in the metabolic syndrome. Am J Physiol Regul Integr Comp Physiol. 289(2):R307-R316.

10. Frisbee JC. (2006). Impaired hemorrhage tolerance in the obese Zucker rat model of metabolic syndrome. J Appl Physiol. 100(2):465-73.

11. Frisbee JC. (2004). Enhanced arteriolar alpha-adrenergic constriction impairs dilator responses and skeletal muscle perfusion in obese Zucker rats. J Appl Physiol. 97(2):764-72.

12. Frisbee JC. (2003). Impaired skeletal muscle perfusion in obese Zucker rats. Am J Physiol Regul Integr Comp Physiol. 285(5):R1124-34.

13. Frisbee JC, Maier KG, Stepp DW. (2002). Oxidant stress-induced increase in myogenic activation of skeletal muscle resistance arteries in obese Zucker rats. Am J Physiol Heart Circ Physiol. 283(6):H2160-8.

14. Goodwill AG, Frisbee SJ, Stapleton PA, James ME, Frisbee JC. (2009). Impact of chronic anticholesterol therapy on development of microvascular rarefaction in the metabolic syndrome. Microcirculation. 16(8):667-84.

15. Goodwill AG, James ME, Frisbee JC. (2008). Increased vascular thromboxane generation impairs dilation of skeletal muscle arterioles of obese Zucker rats with reduced oxygen tension. Am J Physiol Heart Circ Physiol. 295(4):H1522-8.

16. Greene AS, Tonellato PJ, Lui J, Lombard JH, Cowley AW Jr. (1989). Microvascular rarefaction and tissue vascular resistance in hypertension. Am J Physiol. 256(1 Pt 2):H126-31.

17. Guerre-Millo M. (1997). Regulation of ob gene and overexpression in obesity. Biomed Pharmacother. 51(8):318-323.

18. He D, Bolstad G, Brubakk A, Medbø JI. (1995). Muscle fibre type and dimension in genetically obese and lean Zucker rats. Acta Physiol Scand. 155(1):1-7.

19. Hudlicka O, Brown MD. (2009). Adaptation of skeletal muscle microvasculature to increased or decreased blood flow: role of shear stress, nitric oxide and vascular endothelial growth factor. J Vasc Res.46(5):504-12.

20. Jones PH. (2008). Expert perspective: reducing cardiovascular risk in metabolic syndrome and type 2 diabetes mellitus beyond low-density lipoprotein cholesterol lowering. Am J Cardiol. 102(12A):41L-47L.

21. Katakam PV, Domoki F, Snipes JA, Busija AR, Jarajapu YP, Busija DW. (2009). Impaired mitochondria-dependent vasodilation in cerebral arteries of Zucker obese rats with insulin resistance. Am J Physiol Regul Integr Comp Physiol. 296(2):R289-98.

22. Kurdak SS, Grassi B, Wagner PD, Hogan MC. (1996). Blood flow distribution in working in situ canine muscle during blood flow reduction. J Appl Physiol. 80(6):1978-83.

23. Lu X, Guo X, Karathanasis SK, Zimmerman KM, Onyia JE, Peterson RG, Kassab GS. (2010). Rosiglitazone reverses endothelial dysfunction but not remodeling of femoral artery in Zucker diabetic fatty rats. Cardiovasc Diabetol. 19;9:19.

24. Obunai K, Jani S, Dangas GD. (2007). Cardiovascular morbidity and mortality of the metabolic syndrome. Med Clin North Am. 91(6):1169-84.

25. Naik JS, Xiang L, Hester RL. (2006). Enhanced role for RhoA-associated kinase in adrenergic-mediated vasoconstriction in gracilis arteries from obese Zucker rats. Am J Physiol Regul Integr Comp Physiol. 290(1):R154-61.

26. Nicholson CD, Angersbach D, Wilke R. (1992). The effect of physical training on rat calf muscle, oxygen tension, blood flow, metabolism and function in an animal model of chronic occlusive peripheral vascular disease. Int J Sports Med. 13(1):60-4.

27. Pujol A, Lefaucheur L, Ecolan P, Picon L, Penicaud L. (1993). Fiber type composition and enzyme activities of muscles in two models of obese rats. Comp Biochem Physiol B. 106(2):269-72.

28. Roca J, Hogan MC, Story D, Bebout DE, Haab P, Gonzalez R, Ueno O, Wagner PD. (1989). Evidence for tissue diffusion limitation of VO2max in normal humans. J Appl Physiol. 67(1):291-9.

29. Ruiter MS, van Golde JM, Schaper NC, Stehouwer CD, Huijberts MS. (2010). Diabetes impairs arteriogenesis in the peripheral circulation: review of molecular mechanisms. Clin Sci (Lond). 119(6):225-38.

30. Schreihofer AM, Hair CD, Stepp DW. (2005). Reduced plasma volume and mesenteric vascular reactivity in obese Zucker rats. Am J Physiol Regul Integr Comp Physiol. 288(1):R253-61.

31. Stepp DW, Pollock DM, Frisbee JC. (2004). Low-flow vascular remodeling in the metabolic syndrome X. Am J Physiol Heart Circ Physiol. 286(3):H964-70.

32. Stepp DW, Frisbee JC. (2002). Augmented adrenergic vasoconstriction in hypertensive diabetic obese Zucker rats. Am J Physiol Heart Circ Physiol. 282(3):H816-20.

33. Xiang L, Dearman J, Abram SR, Carter C, Hester RL. (2008). Insulin resistance and impaired functional vasodilation in obese Zucker rats. Am J Physiol Heart Circ Physiol. 294(4):H1658-66.

34. Xiang L, Naik JS, Hodnett BL, Hester RL. (2006). Altered arachidonic acid metabolism impairs functional vasodilation in metabolic syndrome. Am J Physiol Regul Integr Comp Physiol. 290(1):R134-8.

35. Wagner PD. (1992). Gas exchange and peripheral diffusion limitation. Med Sci Sports Exerc. 24(1):54-8.

36. Williams G, Bing C, Cai XJ, Harrold JA, King PJ, Liu XH. (2001). The hypothalamus and the control of energy homeostasis: different circuits, different purposes. Physiol Behav. 74(4-5):683-701.

37. Wolfram RM, Budinsky AC, Sinzinger H. (2001). Assessment of peripheral arterial vascular disease with radionuclide techniques. Semin Nucl Med. 31(2):129-42.

38. Zou MH. (2007). Peroxynitrite and protein tyrosine nitration of prostacyclin synthase. Prostaglandins Other Lipid Mediat. 82(1-4):119-127.

39. Zou MH, Cohen R, Ullrich V. (2004). Peroxynitrite and vascular endothelial dysfunction in diabetes mellitus. Endothelium. 11(2):89-97.

Table 1. Baseline characteristics of 15-17 week-old LZR and OZR used in the present study. * $p<0.05$ versus LZR.

	LZR	**OZR**
Mass (g)	366±8	684±11*
MAP (mmHg)	101±5	124±6*
$[Glucose]_{plasma}$ (mg/dl)	111±10	184±14*
$[Insulin]_{plasma}$ (ng/ml)	2.0±0.4	9.4±1.1*
$[Cholesterol]_{plasma}$ (mg/dl)	78±9	138±12*
$[Triglycerides]_{plasma}$ (mg/dl)	84±11	348±19*
$[Nitrotyrosine]_{plasma}$ (ng/ml)	14±4	48±8*
Maximum Tension Development (g/g)	384±28	369±27

Table 2. Arterial and femoral venous blood oxygen content values (ml O_2/dL blood) from LZR and OZR under the conditions of the present study. Data are presented under resting conditions and across levels of increasing metabolic demand.

	Rest		**1Hz**		**3Hz**		**5Hz**	
	C_aO_2	**C_vO_2**	**C_aO_2**	**C_vO_2**	**C_aO_2**	**C_vO_2**	**C_aO_2**	**C_vO_2**
LZR	20.8±1.1	14.2±1.1	20.7±1.1	12.1±0.8	20.7±1.1	11.0±1.2	20.6±1.1	7.4±0.9
OZR	21.0±0.9	15.9±1.0	20.6±1.0	13.9±1.4	20.6±1.1	13.2±1.6	20.8±1.1	9.9±1.4
OZR+Phentolamine	20.7±0.9	15.2±0.9	20.1±0.9	14.1±1.2	19.9±1.1	13.1±0.9	20.7±1.2	10.1±1.6
OZR+TEMPOL	20.7±1.0	14.3±1.0	20.6±1.0	11.8±1.5	20.8±1.0	10.8±1.3	20.2±1.2	6.9±1.5
OZR+SQ-29548	20.9±0.8	13.9±1.0	19.9±1.4	12.0±1.2	20.8±1.2	10.9±1.6	19.9±1.1	7.1±1.2
OZR+All	20.7±0.9	14.1±1.1	20.4±0.9	12.0±1.1	20.6±1.1	9.8±1.5	20.5±1.3	6.7±1.5

FIGURE LEGENDS

Figure 1. Arterial pressor responses and gastrocnemius muscle perfusion in LZR and OZR following intravenous infusion of the adrenoreceptor agonist phenylephrine (10 □g/kg) under control conditions and in response to pre-treatment with the □$_1$/□$_2$ adrenoreceptor antagonist phentolamine (10 mg/kg). Data (mean±SE) are presented for changes in mean arterial pressure (Panel A), femoral artery blood flow (Panel B) and vascular resistance across the gastrocnemius muscle (Panel C). * $p<0.05$ vs. LZR; † $p<0.05$ vs. OZR; n=6 animals under each condition.

Figure 2. Arterial pressor responses and gastrocnemius muscle perfusion in LZR and OZR following intravenous infusion of the TxA_2 mimetic U46619 (10 □g/kg) under control conditions and in response to pre-treatment with the PGH_2/TxA_2 receptor antagonist SQ-29548 (10 mg/kg). Data (mean±SE) are presented for changes in mean arterial pressure (Panel A), femoral artery blood flow (Panel B) and vascular resistance across the gastrocnemius muscle (Panel C). * $p<0.05$ vs. LZR; † $p<0.05$ vs. OZR; n=6 animals under each condition.

Figure 3. Arterial pressor responses and gastrocnemius muscle perfusion in LZR and OZR following intravenous infusion of the endothelium-dependent dilator agonist methacholine (10 □g/kg) under control conditions and in response to pre-treatment with the superoxide dismutase mimetic TEMPOL (50 mg/kg). Data (mean±SE) are presented for changes in mean arterial pressure (Panel A), femoral artery blood flow (Panel B) and vascular resistance across the gastrocnemius muscle (Panel C). * $p<0.05$ vs. LZR; † $p<0.05$ vs. OZR; n=6 animals under each condition.

Figure 4. Hemodynamic and oxygen uptake responses across gastrocnemius muscle of LZR and OZR under resting conditions. Data (mean±SE) are presented for femoral artery blood flow (Panel A), vascular resistance across the gastrocnemius muscle (Panel B), oxygen extraction (Panel C) and oxygen uptake (VO_2) by the muscle (Panel D). Values are presented under control conditions and following treatment of OZR with phentolamine (10 mg/kg), TEMPOL (50 mg/kg), SQ-29548 (10 mg/kg) or all three substances. * $p<0.05$ vs. LZR (n=5 animals); † $p<0.05$ vs. OZR (n=15 for control; n=5 for each treatment group; all oxygen extraction and VO_2 data are from n=5 animals). The legend for all panels is presented in Panel A.

Figure 5. Hemodynamic and oxygen uptake responses across gastrocnemius muscle of LZR and OZR in response to three minutes of 1 Hz muscle contraction. Data (mean±SE) are presented for femoral artery blood flow (Panel A), vascular resistance across the gastrocnemius muscle (Panel B), oxygen extraction (Panel C), oxygen uptake (VO_2) by the muscle (Panel D) and developed tension by the gastrocnemius (Panel E). Values are presented under control conditions and following treatment of OZR with phentolamine (10 mg/kg), TEMPOL (50 mg/kg), SQ-29548 (10 mg/kg) or all three substances. * $p<0.05$ vs. LZR (n=5 animals); † $p<0.05$ vs. OZR (n=15 for control; n=5 for each treatment group; all oxygen extraction and VO_2 data are from n=5 animals). The legend for all panels is presented in Panel A.

Figure 6. Hemodynamic and oxygen uptake responses across gastrocnemius muscle of LZR and OZR in response to three minutes of 3 Hz muscle contraction. Data (mean±SE) are presented for femoral artery blood flow (Panel A), vascular resistance across the gastrocnemius muscle (Panel B), oxygen extraction (Panel C), oxygen uptake (VO_2) by the muscle (Panel D) and developed tension by the gastrocnemius (Panel E). Values are presented under control conditions and following treatment of OZR with phentolamine (10 mg/kg), TEMPOL (50 mg/kg), SQ-29548 (10 mg/kg) or all three substances. * $p<0.05$

vs. LZR (n=5 animals); † $p<0.05$ vs. OZR (n=15 for control; n=5 for each treatment group; all oxygen extraction and VO_2 data are from n=5 animals). The legend for all panels is presented in Panel A.

Figure 7. Hemodynamic and oxygen uptake responses across gastrocnemius muscle of LZR and OZR in response to three minutes of 5 Hz muscle contraction. Data (mean±SE) are presented for femoral artery blood flow (Panel A), vascular resistance across the gastrocnemius muscle (Panel B), oxygen extraction (Panel C), oxygen uptake (VO_2) by the muscle (Panel D), normalized O_2 conductance across the muscle (Panel E) and developed tension by the gastrocnemius (Panel F). Values are presented under control conditions and following treatment of OZR with phentolamine (10 mg/kg), TEMPOL (50 mg/kg), SQ-29548 (10 mg/kg) or all three substances. * $p<0.05$ vs. LZR (n=5 animals); † $p<0.05$ vs. OZR (n=15 for control; n=5 for each treatment group; all oxygen extraction and VO_2 data are from n=5 animals). The legend for all panels is presented in Panel B.

Figure 8. Correlation between O_2 conductance (DmO_2) and muscle performance in LZR (n=5) and OZR (n=5-6) in response to three minutes of muscle contraction at a frequency of 5Hz. Values are presented under control conditions and following treatment of OZR with phentolamine (10 mg/kg), TEMPOL (50 mg/kg), SQ-29548 (10 mg/kg) or all three substances. Data are presented for individual animals and the equation for the line of best fit is determined using a least squares analysis.

Figure 1:

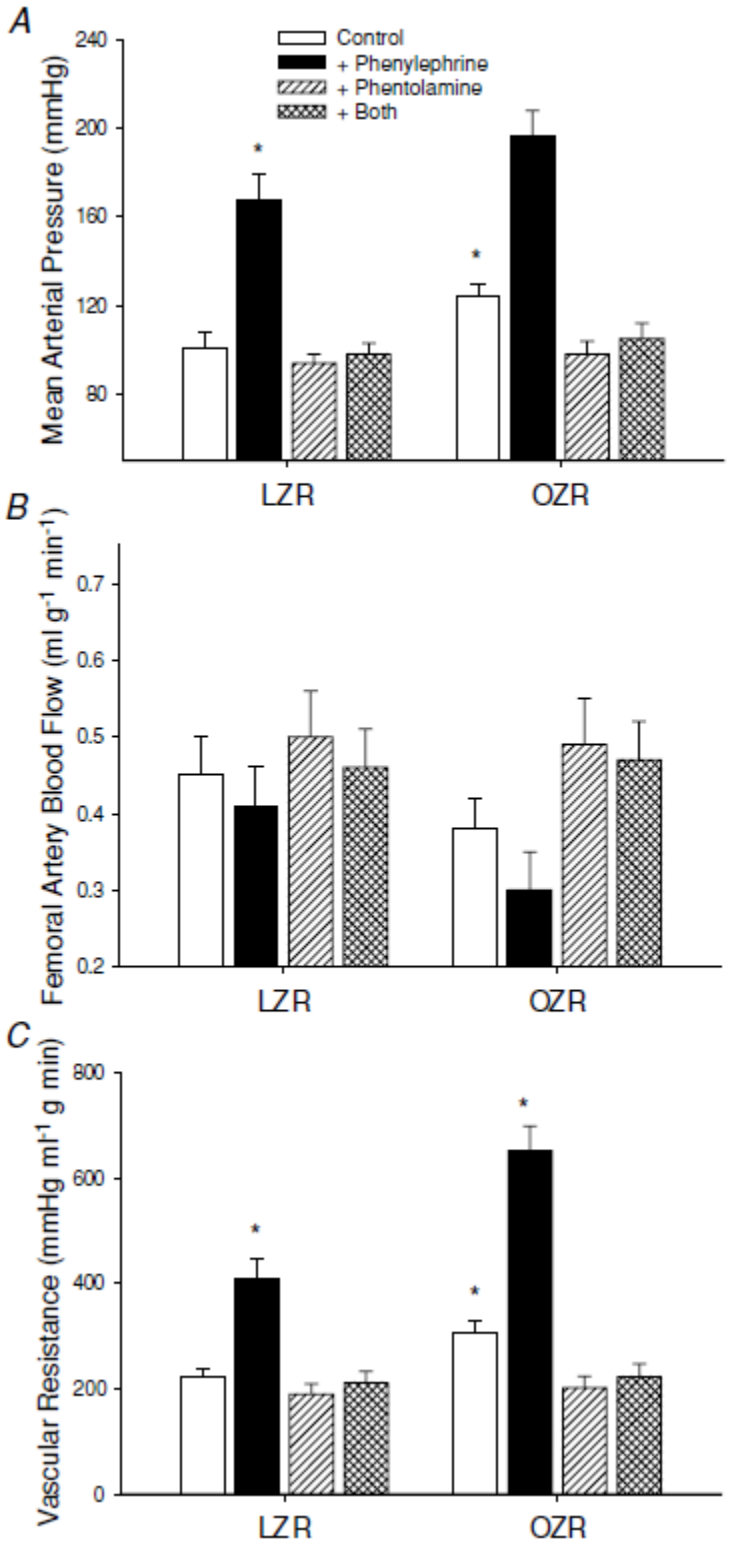
A
Control
+ Phenylephrine
+ Phentolamine
+ Both
Mean Arterial Pressure (mmHg)
240
200
160
120
80
*
*
LZR
OZR
B
Femoral Artery Blood Flow (ml g-1 min-1)
0.7
0.6
0.5
0.4
0.3
0.2
LZR
OZR
C
Vascular Resistance (mmHg ml-1 g min)
800
600
400
200
0
*
*
LZR
OZR

Figure 2:

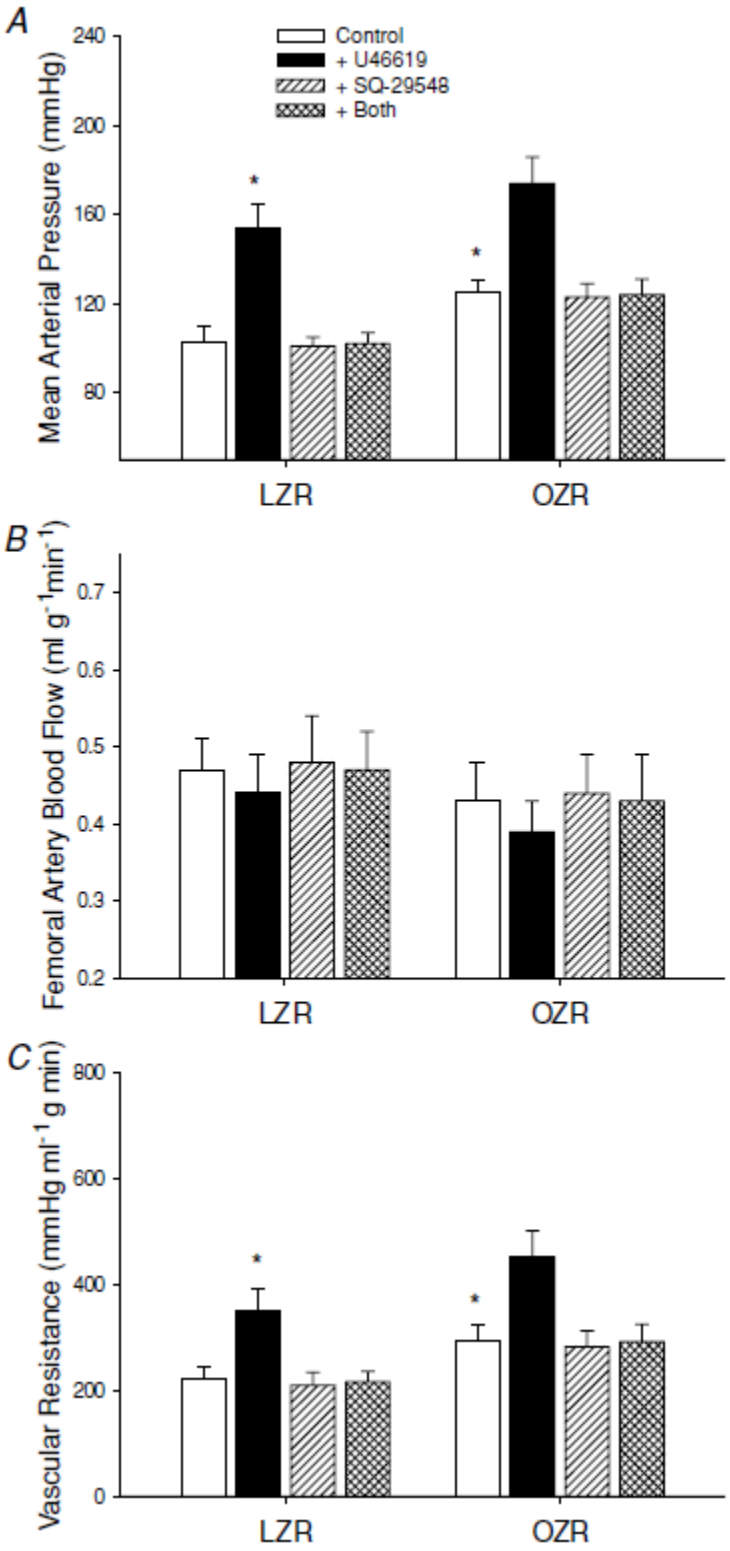
A
Control
+ U46619
+ SQ-29548
+ Both
Mean Arterial Pressure (mmHg)
240
200
160
120
80
*
*
LZR
OZR
B
Femoral Artery Blood Flow (ml g-1min-1)
0.7
0.6
0.5
0.4
0.3
0.2
LZR
OZR
C
Vascular Resistance (mmHg ml-1 g min)
800
600
400
200
0
*
*
LZR
OZR

Figure 3:

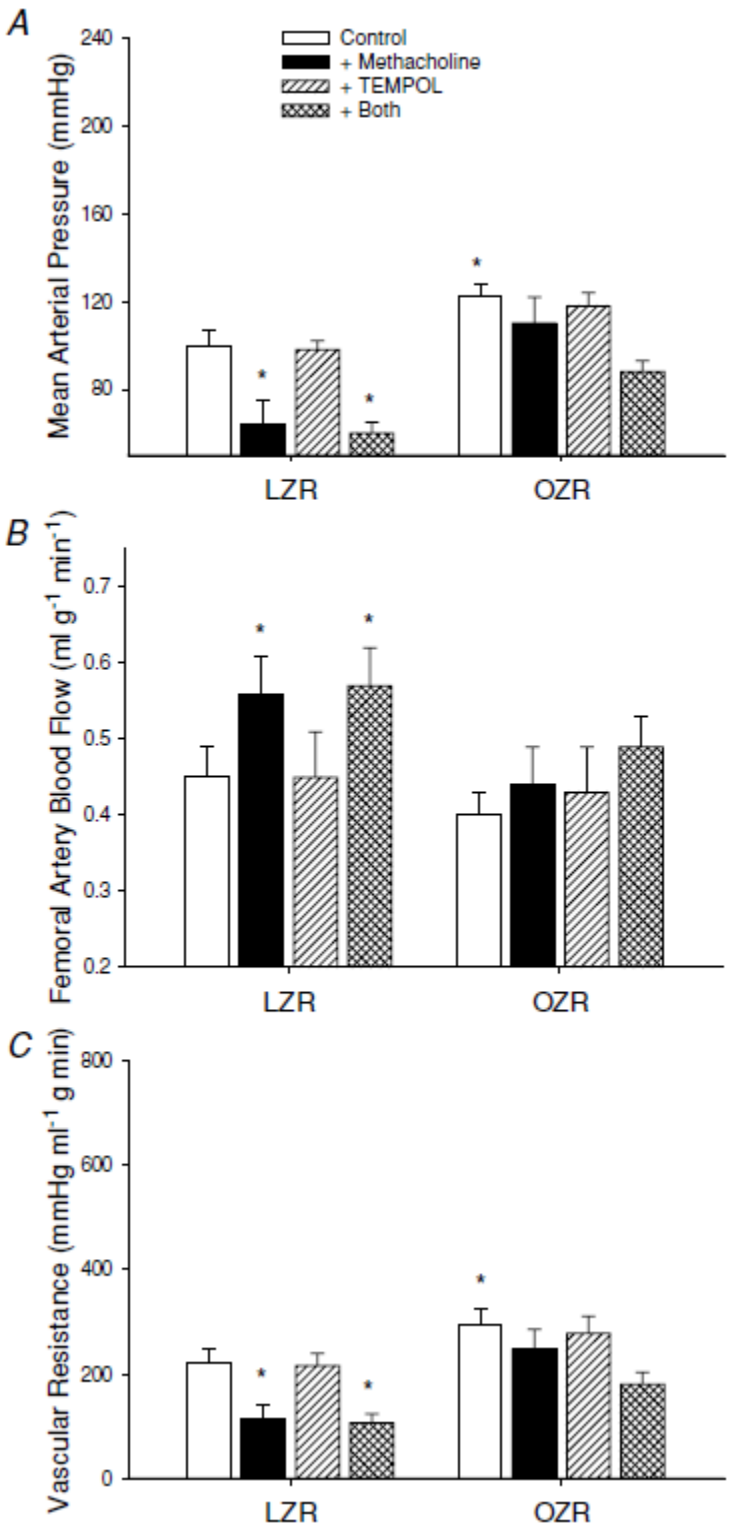
A
Control
+ Methacholine
+ TEMPOL
+ Both
Mean Arterial Pressure (mmHg)
240
200
160
120
80
LZR
OZR
B
Femoral Artery Blood Flow (ml g-1 min-1)
0.7
0.6
0.5
0.4
0.3
0.2
LZR
OZR
C
Vascular Resistance (mmHg ml-1 g min)
800
600
400
200
0
LZR
OZR

Figure 4:

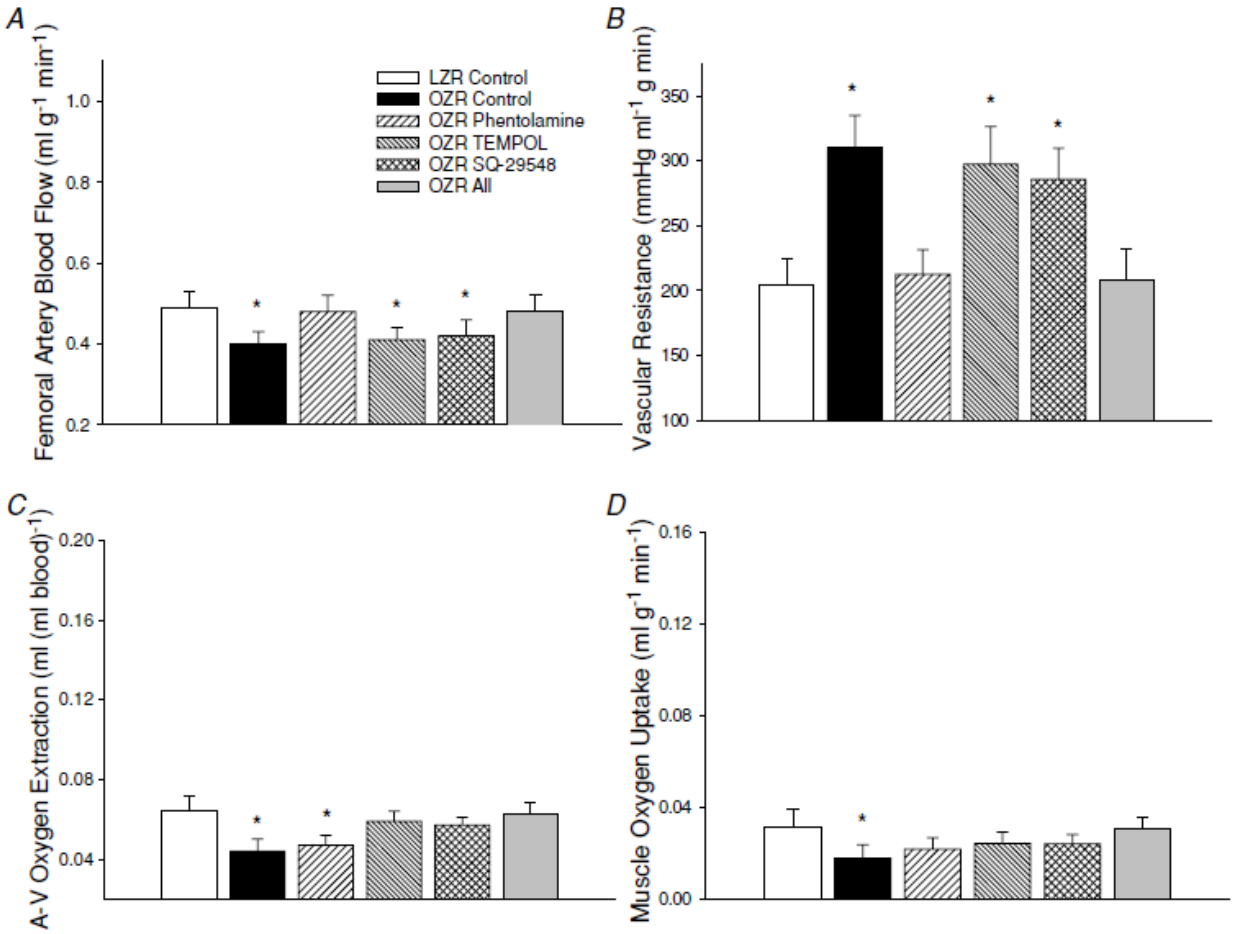
A
Femoral Artery Blood Flow (ml g-1 min-1)
1.0
0.8
0.6
0.4
0.2
LZR Control
OZR Control
OZR Phentolamine
OZR TEMPOL
OZR SQ-29548
OZR All
B
Vascular Resistance (mmHg ml-1 g min)
350
300
250
200
150
100
C
A-V Oxygen Extraction (ml (ml blood)-1)
0.20
0.16
0.12
0.08
0.04
D
Muscle Oxygen Uptake (ml g-1 min-1)
0.16
0.12
0.08
0.04
0.00

Figure 5:

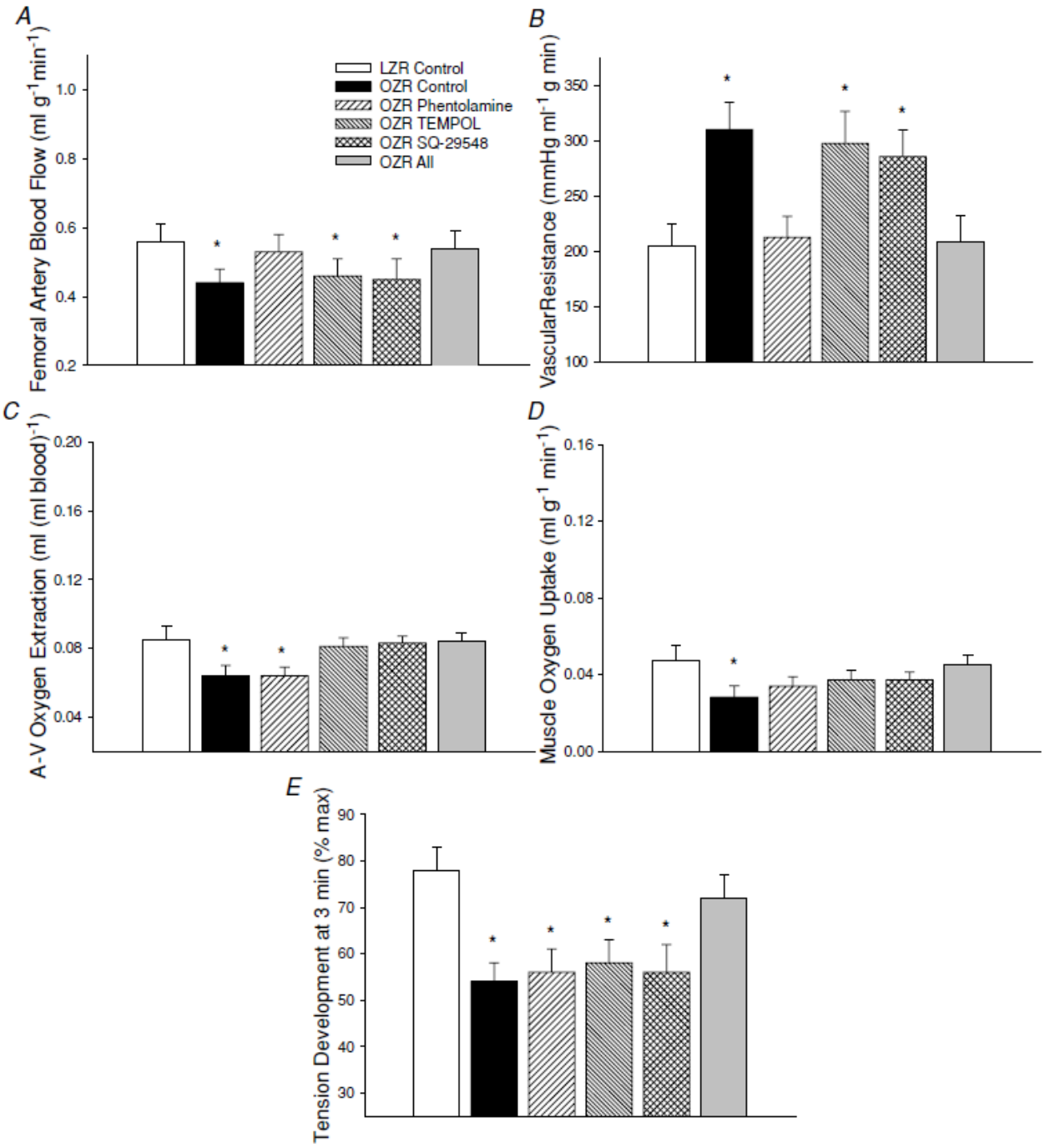
A
Femoral Artery Blood Flow (ml g-1 min-1)
1.0
0.8
0.6
0.4
0.2
LZR Control
OZR Control
OZR Phentolamine
OZR TEMPOL
OZR SQ-29548
OZR All
B
VascularResistance (mmHg ml-1 g min)
350
300
250
200
150
100
C
A-V Oxygen Extraction (ml (ml blood)-1)
0.20
0.16
0.12
0.08
0.04
D
Muscle Oxygen Uptake (ml g-1 min-1)
0.16
0.12
0.08
0.04
0.00
E
Tension Development at 3 min (% max)
90
80
70
60
50
40
30

Figure 6:

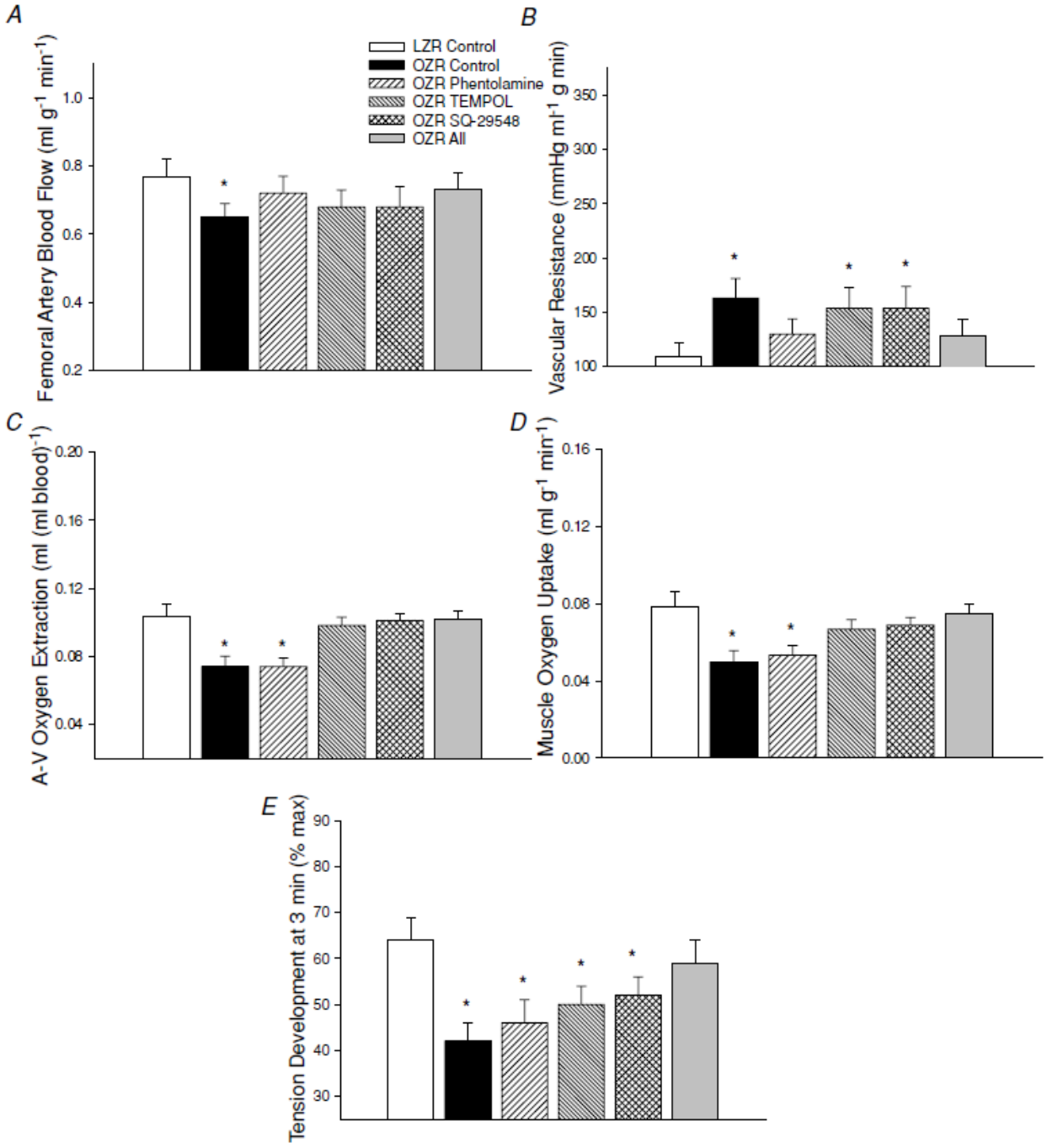
A
B
C
D
E
LZR Control
OZR Control
OZR Phentolamine
OZR TEMPOL
OZR SQ-29548
OZR All
Femoral Artery Blood Flow (ml g-1 min-1)
Vascular Resistance (mmHg ml-1 g min)
A-V Oxygen Extraction (ml (ml blood)-1)
Muscle Oxygen Uptake (ml g-1 min-1)
Tension Development at 3 min (% max)

Figure 7:

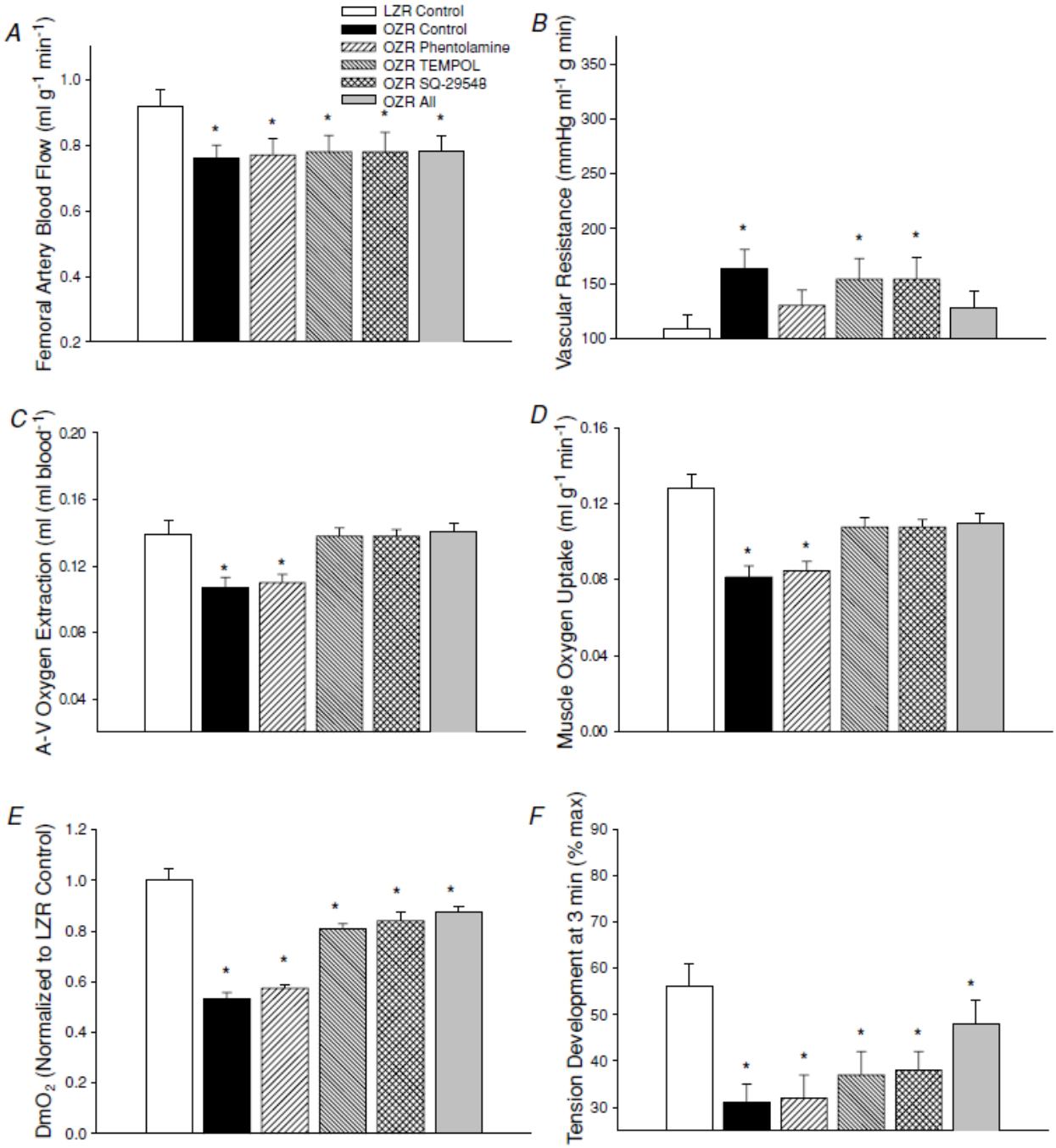
A
LZR Control
OZR Control
OZR Phentolamine
OZR TEMPOL
OZR SQ-29548
OZR All
Femoral Artery Blood Flow (ml g-1 min-1)
1.0
0.8
0.6
0.4
0.2
B
Vascular Resistance (mmHg ml-1 g min)
350
300
250
200
150
100
C
A-V Oxygen Extraction (ml (ml blood-1)
0.20
0.16
0.12
0.08
0.04
D
Muscle Oxygen Uptake (ml g-1 min-1)
0.16
0.12
0.08
0.04
0.00
E
DmO2 (Normalized to LZR Control)
1.2
1.0
0.8
0.6
0.4
0.2
0.0
F
Tension Development at 3 min (% max)
90
80
70
60
50
40
30

Figure 8:

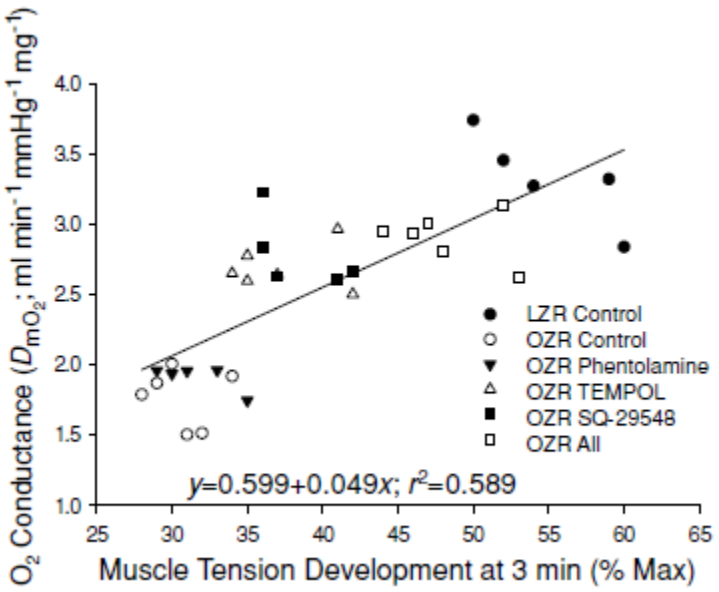
O_2 Conductance (D_{mO_2}; ml min^{-1} mmHg^{-1} mg^{-1})
4.0
3.5
3.0
2.5
2.0
1.5
1.0
25
30
35
40
45
50
55
60
65
Muscle Tension Development at 3 min (% Max)
LZR Control
OZR Control
OZR Phentolamine
OZR TEMPOL
OZR SQ-29548
OZR All
y=0.599+0.049x; r^2=0.589

Conceptual Framework

The second chapter is entitled "Divergence Between Arterial Perfusion and Fatigue Resistance in Skeletal Muscle in the Metabolic Syndrome". This chapter takes the vascular impairments that render the OZR unable to adequately match perfusion and demand, and give it functional relevance. It utilized the *in situ* blood perfused gastrocnemius preparation and revealed that the increase in the OZR microvasculature resistance is multifactorial in nature. There exists an impairment to bulk blood flow and also an inability to extract oxygen in the OZR compared to the LZR. These impairments exist at rest as well as at low, moderate, and high levels of electrical stimulus. The intervention that proved effective at restoring bulk blood flow was phentolamine, an alpha-adrenoreceptor antagonist. The antioxidant TEMPOL or TxA_2 receptor antagonist SQ-29548 proved effective at restoring oxygen uptake. However, none of the three interventions alone were effective at restoring tension development in the OZR. It was only when the combination of interventions was utilized that a significant improvement in performance was observed. The importance of these findings is two-fold. The first is that alteration to structure-function relationships via alpha-adrenergic and endothelial dysfunction has the ability to compromise functional hyperemia in the OZR. The second is the observation that oxygen extraction and uptake is compromised in the OZR. At this age (17 weeks) the OZR has the same activity and similar maximal developed tension and fiber types compared to the LZR control. Thus one would expect a significantly higher oxygen extraction with the estimated 25% rarefaction and lower blood flow accompanying this age group. This suggests that the impairments to OZR skeletal muscle performance are being significantly influenced by alterations to erythrocyte perfusion distribution.

Chapter 3

SPATIAL HETEROGENEITY IN SKELETAL MUSCLE MICROVASCULAR BLOOD FLOW DISTRIBUTION IS INCREASED IN THE METABOLIC SYNDROME

Jefferson C. Frisbee[1], Fan Wu[2], Adam G. Goodwill[1], Joshua T. Butcher[1] and Daniel A. Beard[2]

Department of Physiology and Pharmacology and Center for Cardiovascular and Respiratory Sciences, West Virginia University HSC, Morgantown, WV[1]

Department of Physiology and Biotechnology and Bioengineering Center, Medical College of Wisconsin, Milwaukee, WI[2]

Running Title: Muscle blood flow and vascular disease

Address for Correspondence:

Jefferson C. Frisbee, Ph.D.

Center for Cardiovascular and Respiratory Sciences

Department of Physiology and Pharmacology

West Virginia University Health Sciences Center; 3152 HSN

1 Medical Center Drive

Morgantown, WV 26506

Phone: (304) 293-6527

Fax: (304) 293-5513

Email: jfrisbee@hsc.wvu.edu

ABSTRACT

Previous studies have demonstrated that the metabolic syndrome is associated with impaired skeletal muscle arteriolar function, although integrating observations into a conceptual framework for impaired perfusion in peripheral vascular disease (PVD) has been limited. This study builds on previous work to evaluate *in situ* arteriolar hemodynamics in cremaster muscle of obese Zucker rats (OZR) to integrate existing knowledge into a greater understanding of impaired skeletal muscle perfusion. In OZR cremaster muscle, perfusion distribution at microvascular bifurcations (□) was consistently more heterogeneous than in controls. However, while consistent, the underlying mechanistic contributors were spatially

divergent as altered adrenergic constriction was the major contributor to altered at proximal microvascular bifurcations, with a steady decay with distance, while endothelial dysfunction was a stronger contributor in distal bifurcations with no discernible role proximally. Using measured values of , simulations predict that successive alterations to in OZR caused more heterogeneous perfusion distribution in distal arterioles than in controls; an effect that could only be rectified by combined adrenoreceptor blockade and improvements to endothelial dysfunction. Intravascular ^{125}I-albumin tracer washout from *in situ* gastrocnemius muscle of OZR provided independent support for these observations, indicating increased perfusion heterogeneity that was corrected only by combined adrenoreceptor blockade and improved endothelial function. These results suggest that a defining element of PVD in the metabolic syndrome may be an altered at microvascular bifurcations, that its contributors are heterogeneous and spatially distinct, and that interventions to rectify this negative outcome must take a new conceptual framework into account.

Key Words: rodent models of obesity; microcirculation; skeletal muscle blood flow regulation; models of peripheral vascular disease; blood flow heterogeneity; vascular dysfunction

INTRODUCTION

For myriad social, biological and behavioral reasons (14, 26), Western societies and economies are experiencing a robust growth in both the incidence and prevalence of obesity, impaired glycemic control (both from insulin resistance and the more severe type II diabetes mellitus). While there are multiple venues through which these conditions can impact public health, patient quality of life and mortality (13, 26), one of the most common is via an elevated risk for the development of peripheral vascular disease (PVD), which can generally be considered as an evolving condition wherein the ability of the vasculature to effectively deliver and distribute blood perfusion relative to local metabolic demand becomes increasingly compromised. While the presence of PVD based on structural alterations to larger conduit arteries, including atherosclerotic plaques/lesions and other structural abnormalities that intrude on the vascular lumen represents a major contributor to the overall prevalence of PVD (1, 9), the presence of an array of 'microvasculopathies' that are not a function of structural hindrances to perfusion can also represent a powerful contributor to a growing PVD under 'non-atherosclerotic' conditions (17, 34).

In the obese Zucker rat, classically considered as a model of the metabolic syndrome based on chronic hyperphagia subsequent to a disruption of leptin signaling at its receptor, we (16, 19) and others (40, 41) have demonstrated that basal perfusion and/or functional hyperemia can be compromised through adrenergic-based elevations in vascular resistance (19, 35) or increased adrenergic signaling (31), alterations to vascular endothelial function that can impact myogenic activation (21) and multiple parameters of dilator responses (7, 8, 16, 23, 25, 37). However, an understanding of how this array of contributors to an integrated vascular/perfusion-based outcome relevant for skeletal muscle performance or fatigue resistance has proven to be an exceptionally difficult process owing to difficulties in translating results in isolated tissues/*ex vivo* preparations to the functioning intact system, the inherent complexity of studying multiple processes simultaneously and the challenges of accurately integrating the concepts of space (location) and time into system behaviors and outcomes.

In our recent studies, we have provided evidence that the ability of *in situ* skeletal muscle of OZR to resist fatigue under conditions of elevated metabolic demand is partially a function of the inability to reduce the aggregate vascular resistance through the microvascular network (which was largely dependent on reducing adrenergic constrictor tone) and elevate oxygen extraction and conductance within the distal microcirculation (which was predominantly related to elevated vascular oxidant stress and the effects of the increased vascular production of thromboxane A_2; TxA_2) (15, 16). While alterations to skeletal muscle performance with either adrenoreceptor blockade or antioxidant treatment/PGH_2/TxA_2 receptor antagonism were trivial, the combination of these interventions effectively resulted in a maximal improvement to perfusion, O_2 extraction, O_2 conductance (a lumped parameter describing skeletal muscle oxygen flux that reflects all of the resistances for O_2 in moving from red cell to muscle fiber mitochondria; Ref. 38), resulting in significant improvements to muscle oxygen uptake (VO_2) and contractile performance. These observations, which help to identify the specific role of microvascular dysfunction in limiting VO_2 and muscle performance at low, moderate and near maximal metabolic demand, are especially intriguing given the results from previous studies which suggested that one of the defining characteristics of PVD and a poor perfusion outcome in OZR is an increasingly heterogeneous blood flow distribution at microvascular bifurcations within skeletal muscle (16). While that study provided an initial insight revealing the presence of increased perfusion heterogeneity at bifurcations, those results focused on only the distal microcirculation and provided no insight into either the presence of perfusion heterogeneity at different levels of the microcirculation or how contributing elements to this effect might vary with longitudinal position within the networks (16). In addition, those previous data provided no information regarding the functional outcomes or implications that result from the increased perfusion heterogeneity.

The primary purpose of the present study was to interrogate the presence of the increased perfusion heterogeneity at four distinct levels of the skeletal muscle microcirculation of OZR, to determine the physiological mechanistic contributors to this process (and if they vary with position within

the microcirculation), and to predict the functional implications of this process for perfusion patterns within the distal levels of the microcirculation. A secondary purpose of the present study was to utilize indicator dilution analyses in intact skeletal muscle to determine the presence and impact of increased microvascular perfusion heterogeneity in skeletal muscle of OZR and the role of the physiological mechanisms determined at the higher level of resolution (individual bifurcations) in contributing to these outcomes. Specifically, these studies tested the hypothesis that the presence of increased heterogeneity of perfusion distribution at successive bifurcations within the skeletal muscle microcirculation results in severe impairments to distal arteriolar blood flow distribution, and is a major contributor to the impaired muscle performance outcomes that have been previously demonstrated in OZR (15, 20).

MATERIALS AND METHODS

Animals: Male lean (total n=26) and obese Zucker rats (total n=102), purchased from Harlan, were fed standard chow and drinking water *ad libitum* and were housed in the animal care facility at the West Virginia University Health Sciences Center or the Medical College of Wisconsin. All protocols received prior IACUC approval. At ~17 weeks of age, rats were anesthetized with injections of sodium pentobarbital (50 mg/kg, i.p.), and received tracheal intubation to facilitate maintenance of a patent airway. In all rats, a carotid artery and an external jugular vein were cannulated for determination of arterial pressure and for infusion of supplemental anesthetic and pharmacological agents, as necessary. Any animal in which mean arterial pressure was found to be below 85 mmHg, or where MAP had decreased by more than 15% from that following equilibration (without any pharmacological intervention) was not used in the present study. Blood samples were drawn from the venous cannula for determination of glucose and insulin concentrations (Millipore, Billerica, MA) as well as cholesterol/triglyceride levels (Wako Diagnostics, Richmond, VA), and nitrotyrosine (Oxis International. Foster City, CA). Unless otherwise noted, all drugs and chemicals were purchased from Sigma-Aldrich (St. Louis, MO, USA).

Preparation of In Situ Cremaster Muscle: In each rat (LZR n=16; OZR n=74), an *in situ* cremaster muscle was prepared for study using intravital microscopy as described previously (16). After completion of the *in situ* cremaster muscle preparation, the tissue was continuously superfused with physiological salt solution (PSS) equilibrated with a 5% CO_2-95% N_2 gas mixture, and maintained at 35°C as it flowed over the muscle. Volume flow rate was ~3.0 ml/min. The ionic composition of the PSS was as follows (mM): NaCl 119.0, KCl 4.7, $CaCl_2$ 1.6, NaH_2PO_4 1.18, $MgSO_4$ 1.17, $NaHCO_3$ 24.0, and disodium EDTA 0.03. Arteriolar diameters were measured with a video-micrometer. Following a 30 minute period of equilibration following the surgical preparation, arterioles and bifurcations within five distinct diameter categories were selected for investigation; ~100 □m (1A), ~80 □m (2A), ~60 □m (3A), ~40 □m (4A), and ~20 □m (5A) in diameter. This resulted in four "bifurcation categories": 1) ~100 □m 'parent' to ~80 □m 'daughters' (1A-2A), 2) ~80 □m 'parent' to ~60 □m 'daughters' (2A-3A), 3) ~60 □m 'parent' to ~40 □m 'daughters' (3A-4A), and 4) ~40 □m 'parent' to ~20 □m 'daughters' (4A-5A). Arterioles/bifurcations were selected based on the following criteria: 1) distance from any site of incision, 2) presence of significant vascular tone (assessed by brisk dilator response to challenge with 10^{-3} M adenosine), 3) clearly discernible walls, 4) a rapid and stable level of erythrocyte perfusion, and 5) the presence of two clearly defined 'daughter' branches that also met criteria 1-4. Please see Figure 1 for a schematic representation of these concepts.

The mechanical (using on-screen videomicroscopy) and perfusion (using optical Doppler velocimetry) responses of both the 'parent' and 'daughter' arterioles within a bifurcation class were assessed under resting conditions within the cremaster muscle of each rat. All procedures were performed under control conditions in LZR and OZR, and following treatment of the *in situ* cremaster muscle with the anti-oxidant TEMPOL (10^{-3} M), the TxA_2 receptor antagonist SQ-29548 (10^{-4} M), the nitric oxide synthase inhibitor L-NAME (10^{-4}M), and/or the α_1/α_2 adrenergic receptor antagonist phentolamine (10^{-5} M); within the superfusate solution. All treatments to the cremaster were of a minimum of 40 minutes duration prior to any subsequent experimental manipulation.

Interrogation of Arteriolar Bifurcations: Within each animal, the numbers of bifurcations of each order that were studied differed depending on longitudinal position in the arteriolar network. Bifurcations spanning 1A-2A arterioles averaged 1-2/animal, while bifurcations spanning 3A-4A and 4A-5A arterioles averaged between 3-4/animal. For an individual measurement, arteriolar diameter and erythrocyte velocity were sampled for 10 seconds. All arterioles and bifurcations were selected on the basis of the criteria outlined above and were placed into their categories by size rather than by strict branch number. This was done as our experience demonstrated that branch order classification limited data collection as frequently not all inclusion criteria could be satisfied.

No cremaster muscle was exposed to all interventions as this would have compromised data quality owing to experiments of excessive duration. In addition to the collection of responses under control conditions, individual cremaster preparations were exposed to a maximum of three interventions, each separated by ~30 minutes of washout. Treatment or washout effectiveness was verified by determining abolition or recovery of mechanical responses following challenge with appropriate agonists (e.g., the α_1 adrenergic antagonist phenylephrine, the stable TxA_2 mimetic U-46619, and the endothelium dependent dilator agonist acetylcholine). Maximum experimental duration from preparation to termination was approximately five hours, after which time all animals were humanely euthanized by an intravenous overdose of anesthetic followed by a bilateral pneumothoracotomy.

In the present study, blood flow within a parent arteriole was measured directly, with α reflecting the proportion in the daughter arteriole with the higher perfusion. Within an individual arteriolar bifurcation, the maximum disparity between parent arteriole blood flow and the summated daughter arteriolar perfusion did not exceed 15%. If this error was consistent in terms of magnitude and direction, this could lead to a biased outcome on the distal arteriolar perfusion distributions. However, there is no a priori reason to believe that this would be a consistent error in terms of artificially increasing or decreasing Q determination, and it is more likely that measurement errors would be randomly distributed. To the extent possible, all measurements within an experiment were taken at the same arteriolar

bifurcation sites within a specific animal. However, this was not possible in every animal, owing to alterations to visibility that can develop with time and interventions in this experimental preparation.

Preparation of In Situ Blood Perfused Hindlimb: In a separate set of age-matched LZR (n=10) and OZR (n=28), the left hindlimb of each animal was isolated *in situ* (20) with minor modifications. Heparin (500 IU/kg) was infused via the jugular vein to prevent blood coagulation. Subsequently, an angiocatheter was inserted into the femoral artery, proximal to the origin of the gastrocnemius muscle to allow for bolus tracer injection. Additionally, a small shunt was placed in the femoral vein draining the gastrocnemius muscle that allowed for diversion of flow into a port which facilitated sampling of the venous effluent. Finally, a microcirculation flow probe (Transonic; 0.5/0.7 PS) was placed on the femoral artery to monitor muscle perfusion. In individual experiments, rats received intravenous infusion of the α_1/α_2 adrenoreceptor antagonist phentolamine (10 mg/kg), TEMPOL (50 mg/kg) and/or SQ-29548 (10 mg/kg). Effectiveness of these interventions was assessed by monitoring the changes in arterial pressure in response to intravenous infusion of phenylephrine (10 μg/kg), methacholine (10 μg/kg) or U-46619 (10 μg/kg), respectively (15, 16).

Upon completion of the surgical preparation, the gastrocnemius muscle was allowed 30 minutes of self-perfused rest. At this point, 20 μl of ^{125}I-albumin (10 μCi; Perkin-Elmer, Shelton, CT) was injected as a spike bolus (injection time <0.5 s) into the arterial angiocatheter and venous effluent samples were collected at a rate of 1/s for the subsequent 35 seconds. Venous effluent samples were then immediately transferred into silicate tubes and placed into a gamma counter for activity determination. Each rat received an intravenous infusion of homologous donor erythrocytes suspended in PSS at the individual animal's hematocrit (~45%) to replace the lost volume, and this was allowed a minimum of 20 minutes for circulation prior to subsequent intervention. In order to assess the potential for leakage of the labeled albumin from the intravascular space as a source for error, the gastrocnemius muscle was cleared by perfusion with physiological salt solution following euthanasia. Subsequent to a determination of mass, the muscle was placed in the counter for determination of residual activity. Residual activity within the gastrocnemius

muscle did not exceed 200 cpm/animal; a level that was far lower than those determined in the venous blood aliquots. All protocols had received prior approval from the Radiation Safety Office at the WVU Health Science Center.

Data and Statistical Analyses: Arteriolar perfusion in both parent and daughter vessels within *in situ* cremaster muscle of LZR and OZR was calculated as:

$$Q = (V \times 1.6^{-1})(\pi r^2)(0.001) \qquad \text{Equation 1}$$

where, Q represents arteriolar perfusion (nl•s^{-1}), V represents the measured red cell velocity from the optical Doppler velocimeter (mm•s^{-1}; with V/1.6 representing an estimated average velocity; Ref. 11), and r represents arteriolar radius (m; Ref. 3). The total volume perfusion in the daughters was determined as the sum of the individual perfusion rates, and the proportion of flow within each was determined as the quotient of the individual branch divided by the total. is defined as the ratio of the greater of the two flows in the daughter vessel to the total flow in the parent vessel. As an example, if flow distribution was homogeneous between daughters, for that bifurcation would be 0.5 in both daughter arterioles, while if the proportion of flow in one daughter arteriole was 60%, for that bifurcation would be 0.6, with flow distribution being 0.6 in the 'high perfusion' arteriole and 0.4 in the 'low perfusion' arteriole (5). Please see Figure 1 for additional clarification.

To predict the outcomes of the successive levels of for distal microvascular perfusion distribution in the distal microcirculation, the individual measured levels of from the experiments utilizing the cremaster muscle were inserted into a simulation of a dichotomous branching network with each outflow (daughter) arteriole arising from an inflow (parent) arteriole receiving either or (1-) as the distribution of perfusion. These respective values of daughter arteriolar perfusion then become in the inflow perfusion (parent) values for the next generation bifurcation. The process was repeated over a total of eight bifurcations, resulting in 2^8 or 256 parallel arterioles. This simulation utilized the measured value of for

the 1A-2A, the 2A-3A values of □ for the next two generations, the 3A-4A values of □ for the next two generations, and three 4A-5A values of □ to generate flows in the final three generations.

For the ^{125}I-albumin washout, four standard parameters describing characteristics of tracer washout curves, including mean transit time ($\bar{t}$), relative dispersion (*RD*), skewness (β_1), and kurtosis (β_2), were computed as functions of the transport function h(*t*) (6). The tail of tracer washout curves are extrapolated in the form of single exponential time course to allow for computing the four parameters by the integration for sufficiently long time for Equation 3 to converge (24). In this study, experimentally-measured time courses are extrapolated to 100 seconds, at which C(*t*) is estimated to be less than 10^{-9} of the maximum washout tracer activity. The transport function h(t) is estimated from

$$\mathrm{h}(t) = \mathrm{C}(t) \Big/ \int_0^\infty \mathrm{C}(t)dt \qquad \text{Equation 2}$$

where C(*t*) is the time course of activity of intravascular tracer in outlet flow exiting the collecting tube. The mean transit time $\bar{t}$ is calculated from experimentally measured washout curves according to:

$$\bar{t} = \int_0^\infty t \cdot \mathrm{h}(t)dt \qquad \text{Equation 3}$$

The *RD* of h(*t*) is a measure of the relative temporal spread of h(*t*) and computed as the ratio of standard deviation of h(t) to the mean transit time from:

$$RD = \left(\int_0^\infty \left(t - \bar{t}\right)^2 \cdot \mathrm{h}(t)\mathrm{d}t \right)^{1/2} / \bar{t} \qquad \text{Equation 4}$$

The skewness (β_1) is a measure of asymmetry of h(*t*) and computed from:

$$\beta_1 = \int_0^\infty \left(t - \bar{t}\right)^3 \cdot \mathrm{h}(t)\mathrm{d}t \Big/ \left(\int_0^\infty \left(t - \bar{t}\right)^2 \cdot \mathrm{h}(t)\mathrm{d}t \right)^{3/2} \qquad \text{Equation 5}$$

Skewness is a measure of the asymmetry of the perfusion distribution. In other words, it is a measure of the extent to which the perfusion distribution is skewed (as opposed to simply being shifted) to higher or

lower values of perfusion. The kurtosis (β_2) is a measure of deviation of h(t) from a normal distribution and computed from:

$$\beta_2 = \int_0^\infty \left(t-\bar{t}\right)^4 \cdot \mathrm{h}(t)\mathrm{d}t \Big/ \left(\int_0^\infty \left(t-\bar{t}\right)^2 \cdot \mathrm{h}(t)\mathrm{d}t \right)^{4/2} - 3 \quad . \qquad \text{Equation 6}$$

Kurtosis is a measure of the "sharpness of the peak" of the perfusion distribution. The familiar Gaussian bell-shaped curve has $\beta_2 = 0$; positive values of β_2 indicate a sharper peak than a Gaussian. The four parameters are estimated based on the above equations for each animal in each experimental group.

All data throughout the manuscript are presented as mean±SE. Statistically significant differences in measured and calculated parameters were determined using a one sample *t*-test (differences from zero), Student's *t*-test or analysis of variance (ANOVA) with Student-Newman-Keuls post-hoc test used as needed. Analyses of the simulation results for distal arteriolar perfusion distribution (Figure 6) utilized descriptive statistics (variance, skewness, kurtosis, range, maximum, minimum, quartiles (25%, 50% and 75%) and the 75-25% interquartile difference). Statistically significant differences between the frequency distributions for the simulations were evaluated using the Kruskal-Wallis test, although because indices of central tendency were not different between groups (due to the normalization procedures), multiple post-hoc comparisons were not possible. In all cases, $p<0.05$ was taken to reflect statistical significance.

RESULTS

Baseline characteristics describing the animals used in the present study are summarized in Table 1. At ~17 weeks of age, male OZR were significantly heavier than LZR and, in addition to a moderate hypertension, hypercholesterolemia and hyperglycemia, also exhibited a severe elevation in plasma levels of insulin, triglycerides and nitrotyrosine. Data describing the perfusion characteristics of the individual cremasteric arteriolar segments (described above) under the experimental conditions of the present study are summarized in Table 2. These data clearly demonstrate general differences between arteriolar

diameter and perfusion characteristics that are distributed longitudinally throughout the cremasteric microcirculation under the conditions of the present study.

Figure 2 presents the magnitude of the perfusion distribution coefficient (□) at bifurcations spanning 1A (100 □m) parent arterioles to 2A (80 □m) daughter arterioles in LZR and OZR under control conditions and in response to the interventions employed in the present study (Panel A) and the extent to which specific interventions restore □ in OZR to levels determined in LZR (Panel B). Specifically, the ordinate in Figure 2B is defined as:

$$\text{Recovery}(\%) = \left(1 - \frac{\gamma_{OZR-*} - \gamma_{LZR}}{\gamma_{OZR} - \gamma_{LZR}}\right) \cdot 100\% = \left(\frac{\gamma_{OZR} - \gamma_{OZR-*}}{\gamma_{OZR} - \gamma_{LZR}}\right) \cdot 100\% \qquad \text{Equation 7}$$

where γ_{OZR-*} represents one of the treatments indicated. Full (100%) recovery indicates that the indicated treatment restores □ to the LZR value. Zero (0%) recovery indicates that the treatment has no effect on □.

In these proximal resistance arterioles, γ was significantly elevated in OZR as compared to LZR, although this was restored by treatment of the cremaster muscle with the adrenoreceptor antagonist phentolamine (either alone or in combination with any other agent). In contrast, treatment with TEMPOL, SQ-29548, or L-NAME, either alone or in any combination was without effect in terms of restoring the normal magnitude of γ unless phentolamine was also present.

The magnitude of γ (Panel A), and its recovery following intervention (Panel B), in arteriolar bifurcations spanning 2A (80 μm) parent to 3A (60 μm) daughter arterioles in cremaster muscle of LZR and OZR are summarized in Figure 3. In contrast to the data presented in Figure 2, the ability of phentolamine to restore normal levels of γ in OZR at this level of the cremasteric microcirculation, while still statistically significant, was blunted as compared to responses at the more proximal bifurcation. Neither TEMPOL nor SQ-29548 elicited a significant improvement in □ at this level of the

microcirculation when applied individually. Further, when either TEMPOL or SQ-29548 was co-administered with phentolamine, these restorative effects appeared to be partially additive, as the improvement to was substantially elevated as compared to any single intervention. Interestingly, L-NAME treatment alone did not result in a significant change to in OZR, and this was not impacted by amelioration of vascular oxidant stress by co-administration with TEMPOL.

The magnitude of (Panel A), and its recovery following intervention (Panel B), in 3A (60 m) parent to 4A (40 m) and 4A to 5A (20 m) daughter arteriolar bifurcations in cremaster muscle of LZR and OZR are presented in Figures 4 and 5 respectively. At these levels of the cremasteric microcirculation, adrenoreceptor blockade was without significant effect in terms of restoration of in OZR to the levels determined in LZR. However, improvements to endothelial function from TEMPOL and SQ-29548, alone or in combination nearly restored the normal levels of in the OZR microcirculation at these positions within the networks. As with the data presented above, we were unable to determine an apparent role for nitric oxide bioavailability in terms of regulating γ in the cremasteric microcirculation of OZR.

Using the data presented above for γ distribution at the different levels of the cremasteric microcirculation of LZR and OZR under the employed experimental interventions, Figure 6 presents the predicted outcomes on perfusion distribution within the terminal arterioles, and Table 3 summarizes the results of the statistical analyses of the distribution outcomes presented in Figure 6. These predictions are based on a dichotomous branching network of eight bifurcations between the major perfusing arteriole and the terminal arterioles, resulting in a total of 256 terminal arterioles. These data clearly predict that the shifts in γ identified through direct examination of the cremaster muscle result in profound alterations in the outcomes for distal arteriolar perfusion distribution. While the distribution for volume flow in any single arteriole, relative to the mean flow across all 256 arterioles, was relatively tight in LZR as compared to OZR (Figure 6, Panel A versus Panel B), demonstrating much lower degrees of variability, skewness and kurtosis, with a much lower inter-quartile difference (Table 3), treatment with the

individual interventions of phentolamine, TEMPOL and SQ-29548 (Figure 6, Panels C-E, respectively) all results in moderate improvements to the variability, skewness, kurtosis and interquartile difference of the distributions (Table 3). However, the greatest magnitude of improvement was identified under conditions of adrenoreceptor blockade combined with either TEMPOL or SQ-29548 (or both). These perfusion outcome predictions and statistical analyses also suggest that vascular nitric oxide bioavailability, either under control conditions in OZR skeletal muscle at rest or following reductions to vascular oxidant stress that have been repeatedly demonstrated to increase NO bioavailability, may not play a significant role in terms of regulating or the distal arteriolar perfusion outcomes.

Figure 7 presents the mean tracer washout curves for ^{125}I-albumin from the isolated gastrocnemius muscle of LZR and OZR following the pharmacological treatments described above. Figure 8 summarizes data describing the aggregate washout curves. Mean transit time of the tracer across the gastrocnemius was very similar across all groups, suggesting that the relationship between bulk blood flow to the gastrocnemius muscle and vascular volume under the experimental conditions of the present study were very similar across groups (Panel A). The relative dispersion of tracer across the muscle (RD; Panel B) was significantly elevated in OZR as compared to LZR under control conditions, indicative of an increased perfusion heterogeneity throughout the microcirculation of the gastrocnemius muscle. Treatment of OZR with phentolamine (with or without TEMPOL or SQ-29548) significantly improved RD, although treatment with TEMPOL and/or SQ-29548 in the absence of the adrenoreceptor blockade was generally less effective. Both the skewness (Panel C) and the kurtosis (Panel D) of the tracer washout curves were reduced in OZR as compared to LZR, and these shifts in the washout patterns were improved toward the level in LZR as a result of the experimental interventions, with the greatest impact being determined in response to combined treatment with phentolamine and TEMPOL/SQ-29548. Based on the data presented in Figures 2-6, this final group of experiments and analyses did not involve direct manipulations to vascular nitric oxide bioavailability.

DISCUSSION

A recent study has demonstrated that the increased rate of skeletal muscle fatigue in OZR, defined as the percent decline in developed tension over the duration of the imposed bout of contraction, is not necessarily improved subsequent to an improved functional hyperemic response (15). However, one of the central observations of that study was that the vascular dysfunction in the skeletal muscle microcirculation of OZR impacted muscle performance outcomes through two distinct patterns, such that impairments within the proximal microcirculation restricted volume perfusion and responses in the distal microcirculation impaired normal patterns of perfusion:demand matching. Further, that study also implicated the possibility that the physiological and cellular mechanisms underlying the vascular dysfunction within the skeletal muscle microcirculation may be spatially distinct, with alterations to adrenergic constraint on perfusion dominating with regard to the regulation of bulk perfusion, and the endothelial dysfunction playing a stronger role in terms of the higher resolution matching of blood flow distribution to metabolic demand (15). When taken into account with our previous studies demonstrating the potential for increased perfusion heterogeneity at microvascular bifurcations as a defining characteristic of the metabolic syndrome in skeletal muscle of OZR (16), a greater understanding of the impact of the metabolic syndrome on integrated microvascular function represented a critical need. As such, the present studies were designed to determine whether the initial observation of perfusion heterogeneity at arteriolar bifurcations is present throughout microvascular networks, what the contributing mechanisms to this effect are, if they are spatially distinct, and what the functional outcomes of the successive perfusion distribution events would be for blood flow at the level of the terminal arterioles.

The foremost observation from the present study was that the increased heterogeneity at microvascular bifurcations within skeletal muscle (γ) of OZR was identified over four distinct bifurcation classes spanning five arteriolar diameter ranges. While γ at bifurcations in LZR tended to be slightly lower than 0.54 across all levels of arteriolar/bifurcation ranges, this value was elevated toward 0.60 in OZR. The axis limits on the ordinates in Figures 2-5 were chosen to reflect the observed range of □.

While on the absolute scale the observed differences in γ are relatively small, these differences are significant statistically and their cumulative effects translate into physiologically significant differences in function. The consistency of the elevated γ within the microcirculation of OZR afflicted with the metabolic syndrome suggests that this increased heterogeneity of perfusion at bifurcations may represent a defining characteristic of PVD in this animal model. This observation suggests that, as blood flow enters into the microvascular networks of the skeletal muscle of OZR, there is an increased heterogeneity of distribution at bifurcations involving the larger resistance arterioles, where the result is the generation of 'high flow' and 'low flow' daughter arterioles arising at this bifurcation. Essentially, this represents a source for increased variability as compared to perfusion distribution in LZR, and through a repetitive iteration at successive bifurcations will result in a striking increase to the heterogeneity of arteriolar perfusion within the distal microcirculation; predicted in Figure 6.

Our recent study that initially identified the presence of an altered γ in the skeletal muscle microcirculation of OZR suggested that this effect was a function of combined alterations to adrenergic tone and the evolving endothelial dysfunction in the metabolic syndrome, as acute interventions against these negative outcomes changed γ to levels that were similar to those determined in LZR (16). While the present results provide compelling evidence of the consistency of the alteration to throughout a microvascular network within OZR skeletal muscle, data from these experiments also demonstrated a significant heterogeneity in terms of the physiological/cellular mechanisms which contribute to the establishment of in the metabolic syndrome. In the proximal resistance arterioles, spanning 1A and 2A arterioles, the alteration in in OZR was strongly a function of alterations to adrenergic behavior at the microvessel, as treatment with the adrenoreceptor antagonist almost completely removed the change in this parameter, and resulted in of ~0.5. What was particularly striking in the present results was that acute interventions designed to ameliorate microvascular dysfunction, the antioxidant TEMPOL and the PGH_2/TxA_2 receptor antagonist SQ-29548, had no discernible impact on at the level of the 1A and 2A arteriolar bifurcations and only were associated with an improved under conditions where

adrenoreceptor blockade was also evident. This relationship gradually changed with longitudinal position in the microvascular networks, such that in smaller diameter bifurcations (2A-3A and 3A-4A), the impact of phentolamine on improving at bifurcations was progressively diminished, while the effects of TEMPOL and SQ-29548 on restoring to levels identified in LZR was increased. This effect continued to the most distal levels of the microcirculation (4A-5A), where adrenoreceptor blockade was entirely without significant effect and restoring endothelial function resulted in a maximal recovery in . In support our previous initial observations, combined treatment with an adrenoreceptor antagonist and either an antioxidant or the PGH_2/TxA_2 receptor blocker restores to levels determined in LZR throughout the microvascular network. With the incorporation of the results from the present study, the amelioration of different contributing mechanisms of dysfunction, while varying in proportion across levels of the microcirculation, suggests that a multi-faceted approach against the microvasculopathy in OZR is required to significantly improve integrated perfusion outcomes.

One of the more intriguing results of the present study is the lack of demonstrated evidence for a role for vascular nitric oxide bioavailability in the establishment of in OZR. The observation that treatment of OZR with L-NAME was without effect on in microvascular networks in that strain was not surprising, as multiple previous studies have demonstrated that vascular NO bioavailability is dramatically reduced in OZR at this age and treatment and that further antagonism of nitric oxide synthase (NOS) is without effect (18). However, as previous studies have demonstrated that antioxidant treatment improves vascular NO bioavailability in OZR (16, 17, 22), the lack of an effect on following treatment with TEMPOL and L-NAME (where TEMPOL alone improved) provides compelling evidence that physiological levels of NO bioavailability may not play a significant role in establishing in OZR. The current study employed pharmacological interventions targeted at determining the role of NO bioavailability (L-NAME and TEMPOL) treatments. As such, this study does not rule out the possibility that NO in other ‘stored’ forms, such as nitrosothiols could contribute, as any roles for these sources for NO were not directly interrogated.

While there is considerable ongoing effort to identify the molecular signaling cascades that underlying specific identified sites of vascular dysfunction in the metabolic syndrome (2, 29, 30, 32), these efforts can suffer from a lack of contextual relevance as it becomes exceptionally difficult to integrate these myriad observations from highly reduced preparations into either a functioning tissue type (e.g., vascular smooth muscle cell, isolated microvessel) or into an integrated system (e.g., blood perfused skeletal muscle). The present study incorporates individual levels of into a predictive outcome for tissue perfusion distribution at in the distal microcirculation. Using a dichotomous branching network of eight successive bifurcations and the determined levels of from the present study, we are able to predict the perfusion distribution in a network consisting of 256 terminal arterioles (5A). In these initial simulations, the resulting frequency distributions reveal that distal arteriolar perfusion in OZR was substantially more heterogeneous than in LZR, with a distribution characterized by an increased inter-quartile difference that reflects the genesis of a large number of ischemic pathways and a small number of very high flow pathways that may represent functional thoroughfares. While adrenoreceptor blockade and improving endothelial dysfunction with TEMPOL or SQ-29548 each resulted in some improvement to the perfusion distribution characteristics in the distal microcirculation, only combined interventions with both phentolamine and TEMPOL/SQ-29548 allowed for a maximal improvement (i.e., recovery) in the frequency distribution and its descriptive characteristics (Table 3) toward levels predicted in LZR. Obviously, distal arteriolar perfusion distribution within the skeletal muscle will be neither discrete nor clustered, and this is an artifact of the simulation employed. However, our simulation does illustrate both a real broadening of the distribution with the presence of PVD in OZR, and the capacity for ameliorating these negative outcomes with appropriately targeted interventions.

Although these predicted perfusion distributions are based on observation of at individual microvascular bifurcations in resting muscle, they may provide a partial explanation for the results from our recent study that evaluated the fatigue resistance of in situ skeletal muscle of OZR across levels of elevated metabolic demand (15). In that study, while the gastrocnemius muscle fatigue rate was elevated in OZR as compared to that in LZR, single pharmacological interventions were of extremely limited

effectiveness in improving the ultimate functional outcome of increased muscle performance. While adrenoreceptor blockade with phentolamine improved bulk perfusion and active hyperemia, improvements to muscle oxygen extraction, uptake (VO_2) and oxygen conductance (DmO_2) were minimal. Further, improving endothelial function with TEMPOL or SQ-29548 tended to improve extraction, VO_2 and DmO_2, although minimal impacts on bulk perfusion and muscle performance were identified. A significant improvement in muscle fatigue resistance was identified only when combined interventions with phentolamine and TEMPOL/SQ-29548 were applied, and this was also associated with the improvements to bulk perfusion, O_2 extraction, VO_2 and DmO_2 (15, please see ref. 37 for full review). When combined with the results of the present study, these data strongly suggest that the multi-faceted approach to reducing proximal resistance to bulk perfusion in combination with improving distal microvascular perfusion:demand matching represent a requisite condition to lessen the impact of PVD on muscle performance outcomes.

One of the main considerations that must be addressed in the present study is that of the level of resolution for the data. The *in situ* cremaster muscle preparation allows for very high resolution measurements of multiple arterioles throughout the tissue for both their mechanical (dimension) and hemodynamic (RBC flux, volume blood flow) status. However, this preparation does not lend itself well to the integrated study of the entire network at one time. We have employed the *in situ* gastrocnemius muscle preparation for the integrated assessment of network function using tracer washout kinetics, as the anatomy and the range of blood flow volumes to the muscle allow for an effective tracer washout protocol that is not possible in the cremaster. While the strong associations between in cremaster muscle, its physiological mechanistic contributors and its distribution with the results in the *in situ* gastrocnemius muscle in our previous study is compelling, the intravascular washout experiments summarized in Figures 8 and 9 provide independent data that reflect the flow distributions throughout the gastrocnemius muscle circulation. Since the washout of ^{125}I-albumin (which is confined to the intravascular space) introduced into the femoral artery immediately proximal to the gastrocnemius muscle reflects the whole-network

flow distribution, any potential for a selection bias is eliminated. As presented in Figures 7 and 8, striking differences in the washout kinetics were determined between LZR and OZR under the conditions of the present study. In general, OZR manifested an earlier appearance time of tracer than in LZR as well as a longer retention in the microcirculation. Speculatively, this change could reflect the combined influence of both the 'high flow' and 'low flow' pathways that are demonstrated at bifurcations, and is consistent with the frequency distributions of predicted distal arteriolar perfusion summarized in Figure 6. While treatment of OZR with phentolamine, TEMPOL or SQ-29548 all exhibited the ability to partially restore the washout kinetics to levels determined in LZR, combined therapy, which would result in an improved microvascular function and across all levels of the networks, resulted in the greatest restoration of the tracer washout kinetics. One particularly intriguing element of the present study was also revealed through the use of the tracer washout approach. Given that the mean transit times for tracer washout was at least 15 seconds under all conditions, despite arteriolar perfusion velocities that would suggest a more rapid tracer appearance, this suggests that a significant dispersion of the tracer may have also occurred across the capillary beds and within the post-capillary venular networks. While alterations to venular function have been unexplored in this model, interrogating how alterations to venular reactivity and hemodynamics can impact perfusion responses may represent an exciting area for future investigation. The reader is directed to our computational modeling manuscript (39), where these tracer washout kinetics are analyzed using a computational model for microvascular perfusion distributions in OZR versus LZR skeletal muscle, revealing additional insights into network flow distributions associated with these washout data.

The description of a novel perfusion distribution parameter, , alterations to which contributes to a substantially increased heterogeneity in blood flow distribution within the distal microcirculation of the skeletal muscle of OZR, is strikingly relevant to the concept of the 'network Fahraeus effect' described by Pries *et al.* in the late 1980s (33). As a brief summary, the non-uniform distribution of perfusion at successive bifurcations within a microvascular network, contributes to a reduction in the mean

microvascular hematocrit (H_{MV}) measured within the distal microcirculation and capillaries (12, 28). This process is distinct from the classically described 'vessel Fahraeus effect', wherein the differential mean velocities of plasma and erythrocytes within individual microvessels causes a reduction in the instantaneous 'tube' hematocrit within a microvessel (4, 27). However, the combined influence of the normal contributing mechanisms to hematocrit reduction within the microcirculation and the effects of an increased or accentuated network Fahraeus effect could lead to a reduction from normal H_{MV} within OZR versus LZR that could contribute to the impaired muscle fatigue resistance demonstrated in our previous studies (15, 20). It is important to state that the results from present study do not account for the effects of plasma skimming at bifurcations, inherent within the network Fahraeus effect (33), on our measurements of arteriolar blood flow and that this process may have impacted the washout kinetics of ^{125}I-albumin in an uncontrolled fashion (as this is an intravascular tracer). Bearing this in mind, further studies will be required to interrogate the speculative argument outlined above as well as the potential impact of targeted interventions in improving H_{MV} in OZR.

In keeping with this concept, the results from a several earlier studies resulted in a competing argument regarding the degree of heterogeneity in capillary perfusion. While results from Tyml's group suggested that capillary perfusion heterogeneity was reduced with elevated metabolic demand and the inherent vasodilation, suggesting a significant, yet unidentified, control mechanism (36), results from Duling's group did not support this concept, suggesting that capillary perfusion heterogeneity was not a controlled variable in skeletal muscle (10). The results of the present study may be conservatively interpreted as supporting the former argument, where treatment with phentolamine in OZR increased flow and narrowed the perfusion frequency distribution (Table 3). Further, as an improvement to endothelial function in OZR following treatment with TEMPOL and/or SQ-29548 also decreased perfusion heterogeneity, this also suggests that the normal vascular and endothelial function may contribute to the regulation of capillary perfusion heterogeneity. However, as these previous studies (10, 36) utilized a metabolic stimulus as the primary intervention where the current study was conducted in resting muscle,

additional experiments must be performed to provide for a stronger argument regarding the degree of control over capillary perfusion heterogeneity.

The results of the present study provide for a new conceptual framework with regard to the study of PVD in the metabolic syndrome. Foremost, these results highlight the critical importance of integration across levels of resolution in efforts to interrogate complex disease states. While previous work has identified multiple signaling pathways and elements that may contribute to specific indices of vascular dysfunction (2, 29, 30, 32), there has been a limited effort to determine how these actually impact perfusion responses in specific vessels (16, 41) and almost no study of how these integrate to produce an impaired perfusion response across an entire network. A description of network flow heterogeneity introduced here, with values of the bifurcation ratio determined as a function of arteriolar generation, can help to reveal specific mechanistic contributors to PVD, including alterations to adrenergic constriction, vascular oxidant stress and increased actions of TxA_2. This new conceptual framework is strongly predictive of the most translationally relevant outcomes associated with amelioration of PVD, and will be useful in designing and interpreting future studies of PVD in the metabolic syndrome.

ACKNOWLEDGEMENTS

This study was supported by grants from the National Institutes of Health (NIH DK R01 64668 and RR 2865AR) and the American Heart Association (AHA SDG 0330194N and EIA 0740129N). The authors also wish to express their gratitude for the expert technical assistance, support and insight from Dr. Julian H. Lombard and Mr. Tianjian Huang from the Department of Physiology at the Medical College of Wisconsin, Ms. Milinda James from the Department of Physiology and Pharmacology, and Dr. Stephanie J. Frisbee from the Department of Community Medicine at West Virginia University and for

support provided through the Translational Research Facility in the Center for Cardiovascular and Respiratory Sciences at the West Virginia University HSC.

LITERATURE CITED

1. **Aboyans, V., P. Lacroix and M.H. Criqui.** Large and small vessels atherosclerosis: similarities and differences. *Prog Cardiovasc Dis.* 50(2):112-25, 2007.

2. **Ali, M.I., P. Ketsawatsomkron, E.J. Belin de Chantemele, J.D. Mintz, K. Muta, C. Salet, S.M. Black, M.L. Tremblay, D.J. Fulton, M.B. Marrero and D.W. Stepp.** Deletion of protein tyrosine phosphatase 1b improves peripheral insulin resistance and vascular function in obese, leptin-resistant mice via reduced oxidant tone. *Circ Res.* 105(10):1013-22, 2009.

3. **Baker, M. and H. Wayland.** On-line volume-flow rates and velocity profile measurements for blood in microvessels. *Microvasc. Res.* 7:131-143, 1974.

4. **Barbee, J.H. and G.R. Cokelet.** The Fahraeus effect. *Microvasc Res.* 3(1):6-16, 1971.

5. **Bassingthwaighte, J.B., L.S. Liebovitch and B.J. West.** "Intraorgan flow heterogeneities." In: *Fractal Physiology*. Oxford University Press, New York, 1994. p. 236-262.

6. **Bassingthwaighte, J.B. and C.A. Goresky.** "Modeling in the analysis of solute and water exchange in the microvasculature." In: *Handbook of Physiology Sect 2, The Cardiovascular System Vol IV, The Microcirculation*, eds. Renkin, E.M. and Michel, C.C. Bethesda, MD: Am. Physiol. Soc., 1984, p. 549-626.

7. **Bohlen, H.G.** Protein kinase betaII in Zucker obese rats compromises oxygen and flow-mediated regulation of nitric oxide formation. *Am J Physiol Heart Circ Physiol.* 286(2):H492-7, 2004.

8. **Bouvet, C., E. Belin de Chantemèle, A.L. Guihot, E. Vessières, A. Bocquet, O. Dumont, A. Jardel, L. Loufrani, P. Moreau and D. Henrion.** Flow-induced remodeling in resistance arteries from obese Zucker rats is associated with endothelial dysfunction. *Hypertension.* 50(1):248-54, 2007.

9. **Cooke, J.P. and A.M. Wilson.** Biomarkers of peripheral arterial disease. *J Am Coll Cardiol.* 55(19):2017-23, 2010.

10. **Damon, D.H. and B.R. Duling.** Evidence that capillary perfusion heterogeneity is not controlled in striated muscle. *Am. J. Physiol.* 249:H386-92, 1985.

11. **Davis, M.J.** Determination of volumetric flow in capillary tubes using an optical Doppler velocimeter. *Microvasc Res* 34:223-30, 1987.

12. **Desjardins, C. and B.R. Duling.** Microvessel hematocrit: measurement and implications for capillary oxygen transport. *Am J Physiol.* 252(3 Pt 2):H494-503, 1987.

13. **Dunbar, J.A., P. Reddy, N. Davis-Lameloise, B. Philpot, T. Laatikainen, A. Kilkkinen, S.J. Bunker, J.D. Best, E. Vartiainen, S. Kai Lo and E.D. Janus.** Depression: an important comorbidity with metabolic syndrome in a general population. *Diabetes Care.* 31(12):2368-2373, 2008.

14. **Ford, E.S. and A.H. Mokdad.** Epidemiology of obesity in the Western Hemisphere. *J Clin Endocrinol Metab* 93: S1-8, 2008.

15. **Frisbee, J.C., J.T. Butcher, A.G. Goodwill and I.M. Olfert.** Divergence between arterial perfusion and fatigue resistance in skeletal muscle in the metabolic syndrome. *Exp Physiol.* (in press), 2011.

16. **Frisbee, J.C., J.M. Hollander, R.W. Brock, H.G. Yu and M.A. Boegehold.** Integration of skeletal muscle resistance arteriolar reactivity for perfusion responses in the metabolic syndrome. *Am J Physiol Regul Integr Comp Physiol.* 296(6):R1771-82, 2009.

17. **Frisbee, J.C. and M.D. Delp.** Vascular function in the metabolic syndrome and the effects on skeletal muscle perfusion: lessons from the obese Zucker rat. *Essays Biochem.* 42:145-61, 2006.

18. **Frisbee, J.C.** Reduced nitric oxide bioavailability contributes to skeletal muscle microvessel rarefaction in the metabolic syndrome. *Am J Physiol Regul Integr Comp Physiol.* 289(2):R307-R316, 2005.

19. **Frisbee, J.C.** Enhanced arteriolar alpha-adrenergic constriction impairs dilator responses and skeletal muscle perfusion in obese Zucker rats. *J Appl Physiol.* 97(2):764-72, 2004.

20. **Frisbee, J.C.** Impaired skeletal muscle perfusion in obese Zucker rats. *Am J Physiol Regul Integr Comp Physiol.*285(5):R1124-34, 2003.

21. **Frisbee, J.C., K.G. Maier and D.W. Stepp.** Oxidant stress-induced increase in myogenic activation of skeletal muscle resistance arteries in obese Zucker rats. *Am J Physiol Heart Circ Physiol.* 283(6):H2160-8, 2002.

22. **Fulton, D., Harris, M.B., Kemp, B.E., Venema, R.C., Marrero M.B. and D.W. Stepp.** Insulin resistance does not diminish eNOS expression, phosphorylation or binding to HSP-90. *Am J Physiol Heart Circ Physiol*. 287:H2384-93, 2004.

23. **Goodwill, A.G., M.E. James and J.C. Frisbee.** Increased vascular thromboxane generation impairs dilation of skeletal muscle arterioles of obese Zucker rats with reduced oxygen tension. *Am J Physiol Heart Circ Physiol*. 295(4):H1522-8, 2008.

24. **Hamilton, W.F., J.W. Moore, J.M. Kinsman and R.G. Spurling.** Studies on the circulation IV. Further analysis of the injection method, and of changes in hemodynamics under physiological and pathological conditions. *Am J Physiol* 99: 534-551, 1932.

25. **Johnson, F.K., R.A. Johnson, W. Durante, K.E. Jackson, B.K. Stevenson and K.J. Peyton.** Metabolic syndrome increases endogenous carbon monoxide production to promote hypertension and endothelial dysfunction in obese Zucker rats. *Am J Physiol Regul Integr Comp Physiol*. 290(3):R601-8, 2006.

26. **Kannan, H., S. Thompson and S.C. Bolge.** Economic and humanistic outcomes associated with comorbid type-2 diabetes, high cholesterol, and hypertension among individuals who are overweight or obese. *J Occup Environ Med* 50: 542-549, 2008.

27. **Klitzman, B. and B.R. Duling.** Microvascular hematocrit and red cell flow in resting and contracting striated muscle. *Am J Physiol.* 237(4):H481-90, 1979.

28. **Keller, M.W., D.N. Damon and B.R. Duling.** Determination of capillary tube hematocrit during arteriolar microperfusion. *Am J Physiol*. 266(6 Pt 2):H2229-38, 1994.

29. **Ma, L., S. Ma, H. He, D. Yang, X. Chen, Z. Luo, D. Liu and Z. Zhu.** Perivascular fat-mediated vascular dysfunction and remodeling through the AMPK/mTOR pathway in high-fat diet-induced obese rats. *Hypertens Res*. 33(5):446-53, 2010.

30. **Marchesi, C., T. Ebrahimian, O. Angulo, P. Paradis and E.L. Schiffrin.** Endothelial nitric oxide synthase uncoupling and perivascular adipose oxidative stress and inflammation contribute to vascular dysfunction in a rodent model of metabolic syndrome. *Hypertension.* 54(6):1384-92, 2009.

31. **Naik, J.S., L. Xiang and R.L. Hester.** Enhanced role for RhoA-associated kinase in adrenergic-mediated vasoconstriction in gracilis arteries from obese Zucker rats. *Am J Physiol Regul Integr Comp Physiol.* 290(1):R154-61, 2006

32. **Payne, G.A., L. Borbouse, S. Kumar, Z. Neeb, M. Alloosh, M. Sturek and J.D. Tune.** Epicardial perivascular adipose-derived leptin exacerbates coronary endothelial dysfunction in metabolic syndrome via a protein kinase C-beta pathway. *Arterioscler Thromb Vasc Biol.* 30(9):1711-7, 2010.

33. **Pries, A.R., K. Ley and P. Gaehtgens.** Generalization of the Fahraeus principle for microvessel networks. *Am J Physiol.* 251(6 Pt 2):H1324-32, 1986.

34. **Rattigan, S., C. Wheatley, S.M. Richards, E.J. Barrett and M.G. Clark.** Exercise and insulin-mediated capillary recruitment in muscle. *Exerc Sport Sci Rev.* 33(1):43-8, 2005.

35. **Stepp, D.W. and J.C. Frisbee.** Augmented adrenergic vasoconstriction in hypertensive diabetic obese Zucker rats. *Am J Physiol Heart Circ Physiol.* 282(3):H816-20, 2002.

36. **Tyml, K. and L. Cheng.** Heterogeneity of red blood cell velocity in skeletal muscle decreases with increased flow. *Microcirculation.* 2:181-93, 1995.

37. **Vessieres, E., E. Belin de Chantemèle, Toutain, B., Guihot, A.L., Jardel, A. Loufrani, L. and D. Henrion.** Cyclooxygenase-2 inhibition restored endothelium-mediated relaxation in old obese Zucker rat mesenteric arteries. *Front. Physio.* doi: 10.3389/fphys.2010.00145

38. **Wagner PD.** Gas exchange and peripheral diffusion limitation. *Med Sci Sports Exerc*. 24(1):54-8, 1992.

39. **Wu, F., D.A. Beard and J.C. Frisbee.** Computational analyses of intravascular tracer washout reveal altered capillary-level flow distributions in obese Zucker rats. *J. Physiol.* (in press), 2011.

40. **Xiang, L., J. Dearman, S.R. Abram, C. Carter and R.L. Hester.** Insulin resistance and impaired functional vasodilation in obese Zucker rats. *Am J Physiol Heart Circ Physiol*. 294(4):H1658-66, 2008.

41. **Xiang, L., J.S. Naik, B.L. Hodnett and R.L. Hester.** Altered arachidonic acid metabolism impairs functional vasodilation in metabolic syndrome. *Am J Physiol Regul Integr Comp Physiol.* 290(1):R134-8, 2006.

Table 1. Baseline characteristics of ~17 week-old LZR and OZR used in the present study. * $p<0.05$ versus LZR. Data are presented as mean±SE.

	LZR (n=26)	**OZR (n=102)**
Mass (g)	366±8	684±11*
MAP (mmHg)	101±5	124±6*
$[Glucose]_{plasma}$ (mg/dl)	111±10	184±14*
$[Insulin]_{plasma}$ (ng/ml)	2.0±0.4	9.4±1.1*
$[Cholesterol]_{plasma}$ (mg/dl)	78±9	138±12*
$[Triglycerides]_{plasma}$ (mg/dl)	84±11	348±19*
$[Nitrotyrosine]_{plasma}$ (ng/ml)	14±4	48±8*

Table 2. Arteriolar perfusion in LZR and OZR. Data are presented for arteriolar inner diameter (ID; □m), centerline erythrocyte velocity (V_{RBC}; mm/s), and volume perfusion within the arteriole (Q; nl/s). * $p<0.05$ versus LZR; † $p<0.05$ versus OZR. Data are presented as mean±SE; -P represents treatment with phentolamine, -T represents treatment with TEMPOL, -SQ represents treatment with SQ-29548, -LN represents treatment with L-NAME; with combinations representing treatment with multiple agents.

		LZR	OZR	O-P	O-T	O-SQ	O-LN	O-PT	O-PSQ	O-PLN	O-TLN	O-TSQ	O-PTSQ
1A	ID	94±4	85±6	92±3	87±6	88±5	84±6	93±3	93±4	90±4	86±3	86±4	93±3
	V_{RBC}	56±5	46±6	48±5	45±6	49±7	38±6*	52±6	53±5	46±5	48±5	48±4	53±5
	Q	245±14	165±20*	200±15	169±14*	186±9*	134±15*	219±6†	224±14†	183±13*	175±13*	176±14*	227±17†
2A	ID	75±4	66±5	72±3	69±6	68±6	64±5	73±4	74±4	71±5	67±6	69±5	74±4
	V_{RBC}	40±6	35±5	40±5	36±6	36±5	32±4	39±5	39±4	36±6	37±5	38±6	40±4
	Q	112±10	74±12*	100±9	84±9*	82±5*	65±6*	102±5	105±8	89±9	82±11*	89±12	108±6†
3A	ID	53±4	48±7	50±5	53±6	53±5	47±6	52±5	53±5	48±5	52±5	53±6	53±5
	V_{RBC}	20±4	14±3	17±4	14±3	14±3	12±3	18±3	18±4	15±4	12±3	14±4	20±2
	Q	28±4	16±4*	21±3	19±4	19±3	13±3*	24±5	25±5	17±3	16±3	19±4	28±4*
4A	ID	36±4	30±3	31±3	33±5	32±4	28±3	34±5	34±4	29±4	32±5	35±4	35±3
	V_{RBC}	12±3	8±2	12±3	9±2	10±3	8±2	11±2	12±2	8±2	9±2	9±2	12±2
	Q	7.8±1.9	3.7±1.5	5.5±1.7	4.7±1.1	4.8±1.3	3.1±0.8*	6.1±1.6	6.6±1.3	3.5±0.9	4.3±1.2	5.5±1.4	7.2±1.6
5A	ID	21±3	18±3	18±2	20±3	19±3	18±3	19±2	20±3	18±2	19±3	19±2	20±2
	V_{RBC}	7±1	4±1	5±2	4±1	4±1	3±1	6±2	7±2	5±2	5±2	5±1	7±1
	Q	1.5±0.3	0.7±0.2*	0.8±0.2	0.8±0.2	0.7±0.2*	0.5±0.2*	1.1±0.3	1.3±0.2	0.8±0.2	0.8±0.2	0.8±0.3	1.4±0.3

Table 3. Statistical analysis of the individual frequency distributions of predicted distal arteriolar perfusion heterogeneity presented in Figure 6. Data are presented for variance, skewness, kurtosis and ranges of the individual distributions, as well as the quartiles and the inter-quartile difference (IQ Diff.). Results from the Kruskal-Wallis test indicated that there are significant differences across the different distributions ($p<0.001$). -P represents treatment with phentolamine, -T represents treatment with TEMPOL, -SQ represents treatment with SQ-29548, -LN represents treatment with L-NAME; with combinations representing treatment with multiple agents.

		LZR	OZR	O-P	O-T	O-SQ	O-LN	O-PT	O-PSQ	O-PLN	O-TLN	O-TSQ	O-PTSQ
Variance		0.015	0.384	0.195	0.086	0.106	0.298	0.026	0.024	0.204	0.070	0.070	0.013
Skewness		0.319	1.678	1.131	0.673	0.744	1.470	0.422	0.407	1.175	0.631	0.555	0.302
Kurtosis		-0.083	4.193	1.625	0.171	0.311	3.168	0.033	0.009	1.829	0.184	-0.183	-0.104
Range		0.690	4.210	2.590	1.525	1.705	3.590	0.918	0.888	2.716	1.427	1.280	0.653
Minimum		0.706	0.166	0.291	0.469	0.430	0.206	0.632	.6418	0.278	0.495	0.526	0.722
Maximum		1.397	4.376	2.881	1.994	2.135	3.795	1.551	1.530	2.994	1.921	1.806	1.375
Percentiles	25	0.914	0.571	0.687	0.783	0.755	0.617	0.878	0.895	0.697	0.800	0.795	0.918
	50	0.994	0.853	0.916	0.967	0.959	0.883	0.990	0.991	0.912	0.975	0.975	0.996
	75	1.081	1.275	1.223	1.194	1.216	1.263	1.117	1.098	1.194	1.187	1.195	1.082
IQ Diff. (75-25)		0.167	0.704	0.536	0.411	0.461	0.646	0.239	0.203	0.497	0.387	0.400	0.164

FIGURE LEGENDS

Figure 1. Schematic representation of the *in situ* cremasteric arteriolar bifurcation used for assessing 'parent' and 'daughter' arteriolar mechanical and hemodynamic/perfusion responses to pharmacological challenge. Open arrows represent parent or daughter arteriolar diameter in response to a specific condition; filled arrows represent parent or daughter arteriolar erythrocyte velocity in response to a specific challenge. These data are utilized to determine both arteriolar flow volume and perfusion heterogeneity at bifurcations ( ). Please see text for additional details.

Figure 2. Microvascular perfusion distribution ( ) at bifurcations spanning 1A (parent) and 2A (daughter) arterioles within *in situ* cremaster muscle. Data are presented as mean±SE for LZR under control conditions and in OZR under control conditions and following treatment with the adrenoreceptor antagonist phentolamine (P), the antioxidant TEMPOL (T), the PGH_2/TxA_2 receptor blocker SQ-29548 (SQ), the nitric oxide synthase inhibitor L-NAME (LN) or combinations of these agents. Panel A presents data describing the magnitude of at the 1A-2A bifurcation under the specific experimental conditions and Panel B presents the % recovery (to the level determined in LZR) in at that bifurcation as a result of the imposed pharmacological challenge. Please see text for additional details. For Panel A, * $p<0.05$ vs. LZR; † $p<0.05$ vs. OZR. For Panel B, * $p<0.05$ versus no change.

Figure 3. Microvascular perfusion distribution ( ) at bifurcations spanning 2A (parent) and 3A (daughter) arterioles within *in situ* cremaster muscle. Data are presented as mean±SE for LZR under control conditions and in OZR under control conditions and following treatment with the adrenoreceptor antagonist phentolamine (P), the antioxidant TEMPOL (T), the PGH_2/TxA_2 receptor blocker SQ-29548 (SQ), the nitric oxide synthase inhibitor L-NAME (LN) or combinations of these agents. Panel A presents data describing the magnitude of at the 2A-3A bifurcation under the specific experimental conditions and Panel B presents

the % recovery (to the level determined in LZR) in □ at that bifurcation as a result of the imposed pharmacological challenge. Please see text for additional details. For Panel A, * $p<0.05$ vs. LZR; † $p<0.05$ vs. OZR. For Panel B, * $p<0.05$ versus no change.

Figure 4. Microvascular perfusion distribution (□) at bifurcations spanning 3A (parent) and 4A (daughter) arterioles within *in situ* cremaster muscle. Data are presented as mean±SE for LZR under control conditions and in OZR under control conditions and following treatment with the adrenoreceptor antagonist phentolamine (P), the antioxidant TEMPOL (T), the PGH_2/TxA_2 receptor blocker SQ-29548 (SQ), the nitric oxide synthase inhibitor L-NAME (LN) or combinations of these agents. Panel A presents data describing the magnitude of □ at the 3A-4A bifurcation under the specific experimental conditions and Panel B presents the % recovery (to the level determined in LZR) in □ at that bifurcation as a result of the imposed pharmacological challenge. Please see text for additional details. For Panel A, * $p<0.05$ vs. LZR; † $p<0.05$ vs. OZR. For Panel B, * $p<0.05$ versus no change.

Figure 5. Microvascular perfusion distribution (□) at bifurcations spanning 4A (parent) and 5A (daughter) arterioles within *in situ* cremaster muscle. Data are presented as mean±SE for LZR under control conditions and in OZR under control conditions and following treatment with the adrenoreceptor antagonist phentolamine (P), the antioxidant TEMPOL (T), the PGH_2/TxA_2 receptor blocker SQ-29548 (SQ), the nitric oxide synthase inhibitor L-NAME (LN) or combinations of these agents. Panel A presents data describing the magnitude of □ at the 4A-5A bifurcation under the specific experimental conditions and Panel B presents the % recovery (to the level determined in LZR) in □ at that bifurcation as a result of the imposed pharmacological challenge. Please see text for additional details. For Panel A, * $p<0.05$ vs. LZR; † $p<0.05$ vs. OZR. For Panel B, * $p<0.05$ versus no change.

Figure 6. Predicted perfusion distributions in the distal microcirculation of skeletal muscle of LZR and OZR under the conditions of the present study. Frequency distributions are calculated based on an eight bifurcation network using the microvascular perfusion distribution coefficients (□) determined in the *in situ* cremaster muscle presented in Figures 2-5. Individual panels present the distribution of perfusion across of 256 (2^8) parallel arterioles under each experimental condition as a result of the simulation of a dichotomous branching network. Please see text for additional details.

Figure 7. Data describing the washout of ^{125}I-albumin from the *in situ* gastrocnemius muscle of LZR and OZR under the conditions of the present study. Data are presented as mean±SE for LZR (n=10) under control conditions and OZR under control conditions (total n=28) and following intravenous treatment with the adrenoreceptor antagonist phentolamine (P; n=10), the antioxidant TEMPOL (T; n=9), the PGH_2/TxA_2 receptor blocker SQ-29548 (SQ; n=9), or for combinations of these agents (n=8-10 for each).

Figure 8. Data (presented as mean±SE) describing the four moments of the washout of ^{125}I-albumin from the *in situ* gastrocnemius muscle of LZR and OZR under the conditions of the present study. Data are shown for the mean transit time of the washout (Panel A), the relative dispersion of the washout (RD; Panel B), the distribution skewness (Panel C) and kurtosis (Panel D). Please see text for details. * $p<0.05$ vs. LZR; † $p<0.05$ vs. OZR.

Figures:

Figure 1:

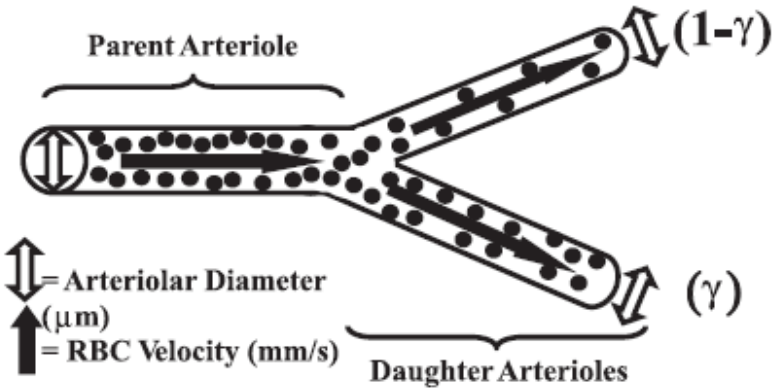

Figure 2:

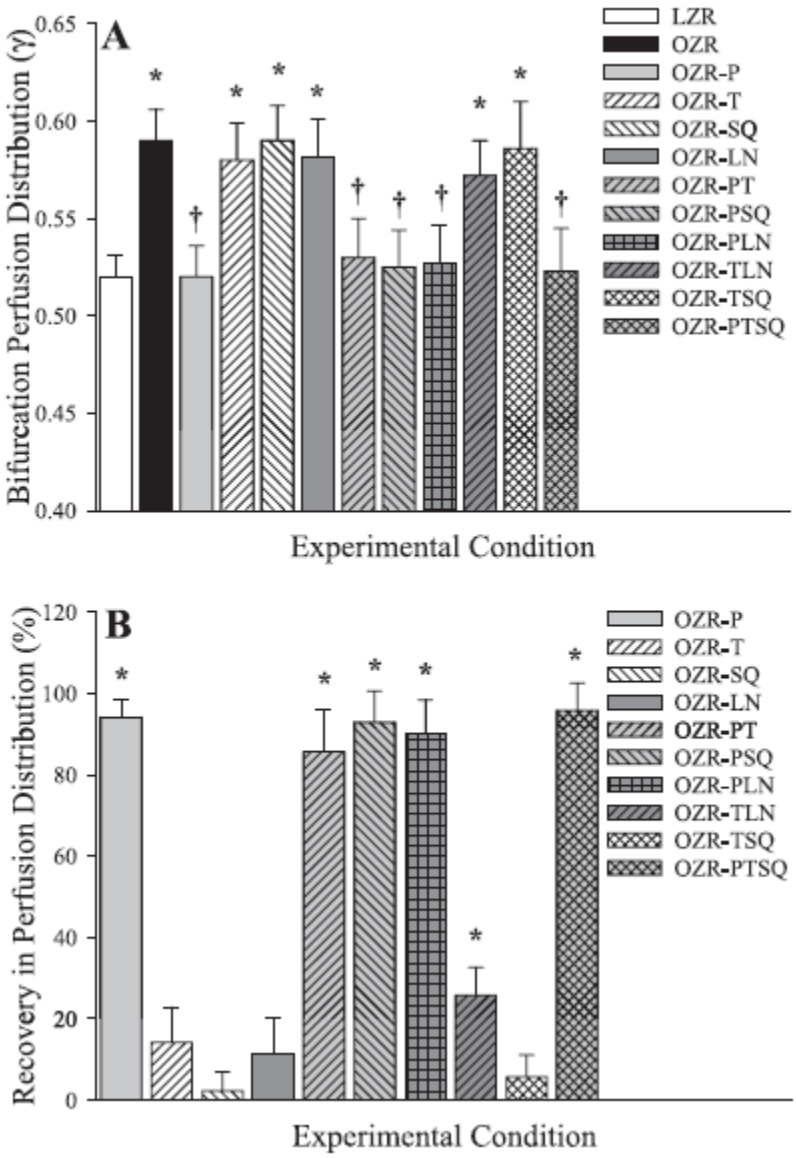
A
Bifurcation Perfusion Distribution (γ)
0.65
0.60
0.55
0.50
0.45
0.40
LZR
OZR
OZR-P
OZR-T
OZR-SQ
OZR-LN
OZR-PT
OZR-PSQ
OZR-PLN
OZR-TLN
OZR-TSQ
OZR-PTSQ
Experimental Condition
B
Recovery in Perfusion Distribution (%)
120
100
80
60
40
20
0
OZR-P
OZR-T
OZR-SQ
OZR-LN
OZR-PT
OZR-PSQ
OZR-PLN
OZR-TLN
OZR-TSQ
OZR-PTSQ
Experimental Condition

Figure 3:

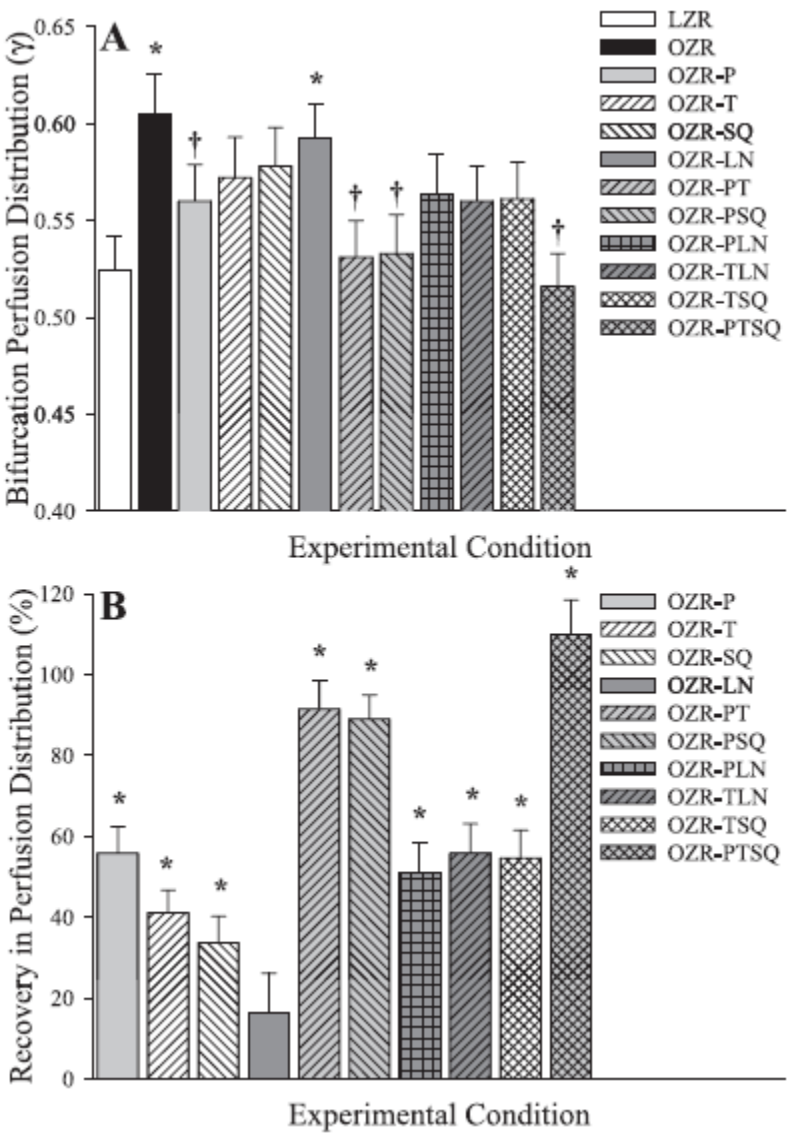
A
Bifurcation Perfusion Distribution (γ)
0.65
0.60
0.55
0.50
0.45
0.40
Experimental Condition
LZR
OZR
OZR-P
OZR-T
OZR-SQ
OZR-LN
OZR-PT
OZR-PSQ
OZR-PLN
OZR-TLN
OZR-TSQ
OZR-PTSQ
B
Recovery in Perfusion Distribution (%)
120
100
80
60
40
20
0
Experimental Condition
OZR-P
OZR-T
OZR-SQ
OZR-LN
OZR-PT
OZR-PSQ
OZR-PLN
OZR-TLN
OZR-TSQ
OZR-PTSQ

Figure 4:

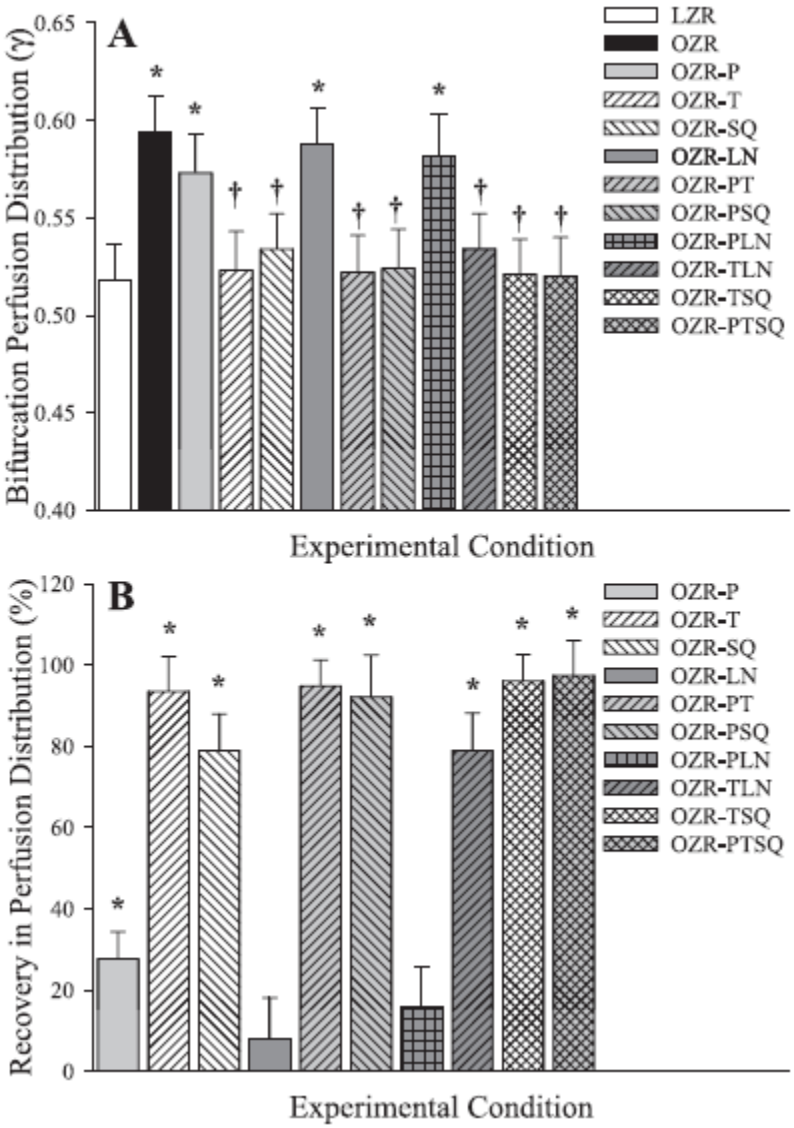
A
Bifurcation Perfusion Distribution (γ)
0.65
0.60
0.55
0.50
0.45
0.40
LZR
OZR
OZR-P
OZR-T
OZR-SQ
OZR-LN
OZR-PT
OZR-PSQ
OZR-PLN
OZR-TLN
OZR-TSQ
OZR-PTSQ
Experimental Condition
B
Recovery in Perfusion Distribution (%)
120
100
80
60
40
20
0
OZR-P
OZR-T
OZR-SQ
OZR-LN
OZR-PT
OZR-PSQ
OZR-PLN
OZR-TLN
OZR-TSQ
OZR-PTSQ
Experimental Condition

Figure 5:

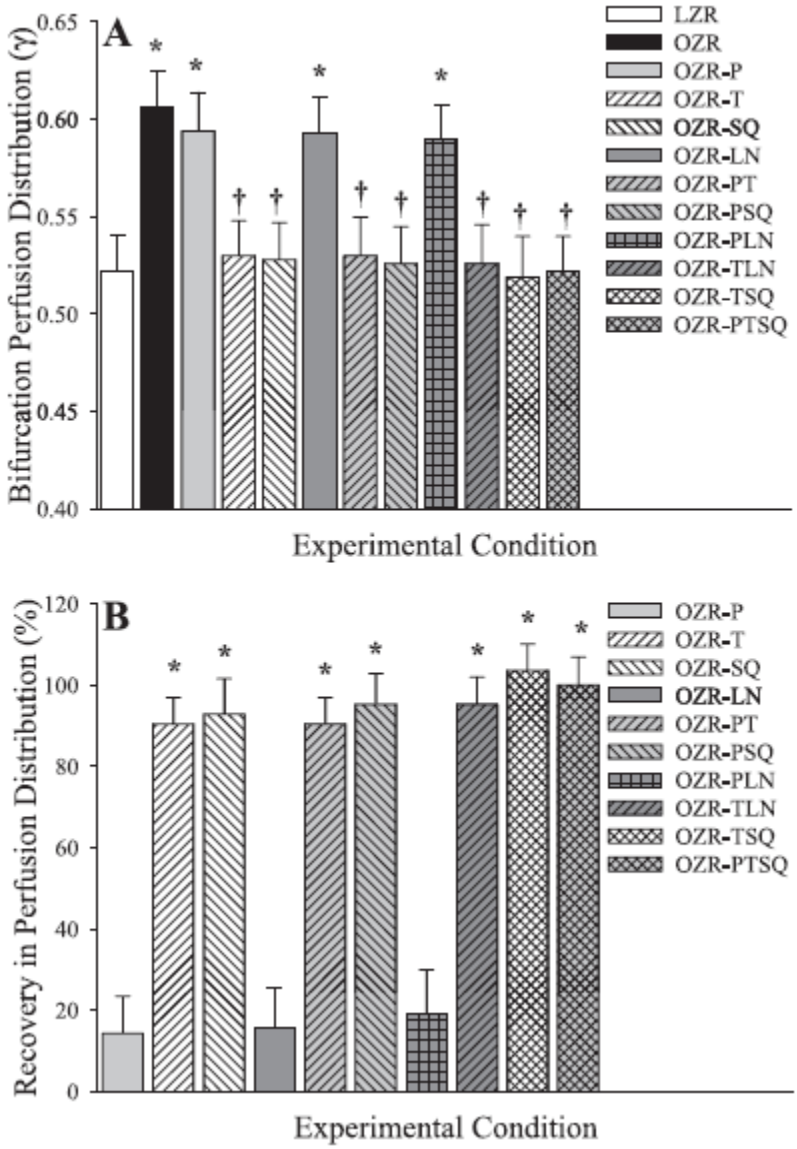
A
Bifurcation Perfusion Distribution (γ)
0.65
0.60
0.55
0.50
0.45
0.40
Experimental Condition
LZR
OZR
OZR-P
OZR-T
OZR-SQ
OZR-LN
OZR-PT
OZR-PSQ
OZR-PLN
OZR-TLN
OZR-TSQ
OZR-PTSQ
B
Recovery in Perfusion Distribution (%)
120
100
80
60
40
20
0
Experimental Condition
OZR-P
OZR-T
OZR-SQ
OZR-LN
OZR-PT
OZR-PSQ
OZR-PLN
OZR-TLN
OZR-TSQ
OZR-PTSQ

Figure 6:

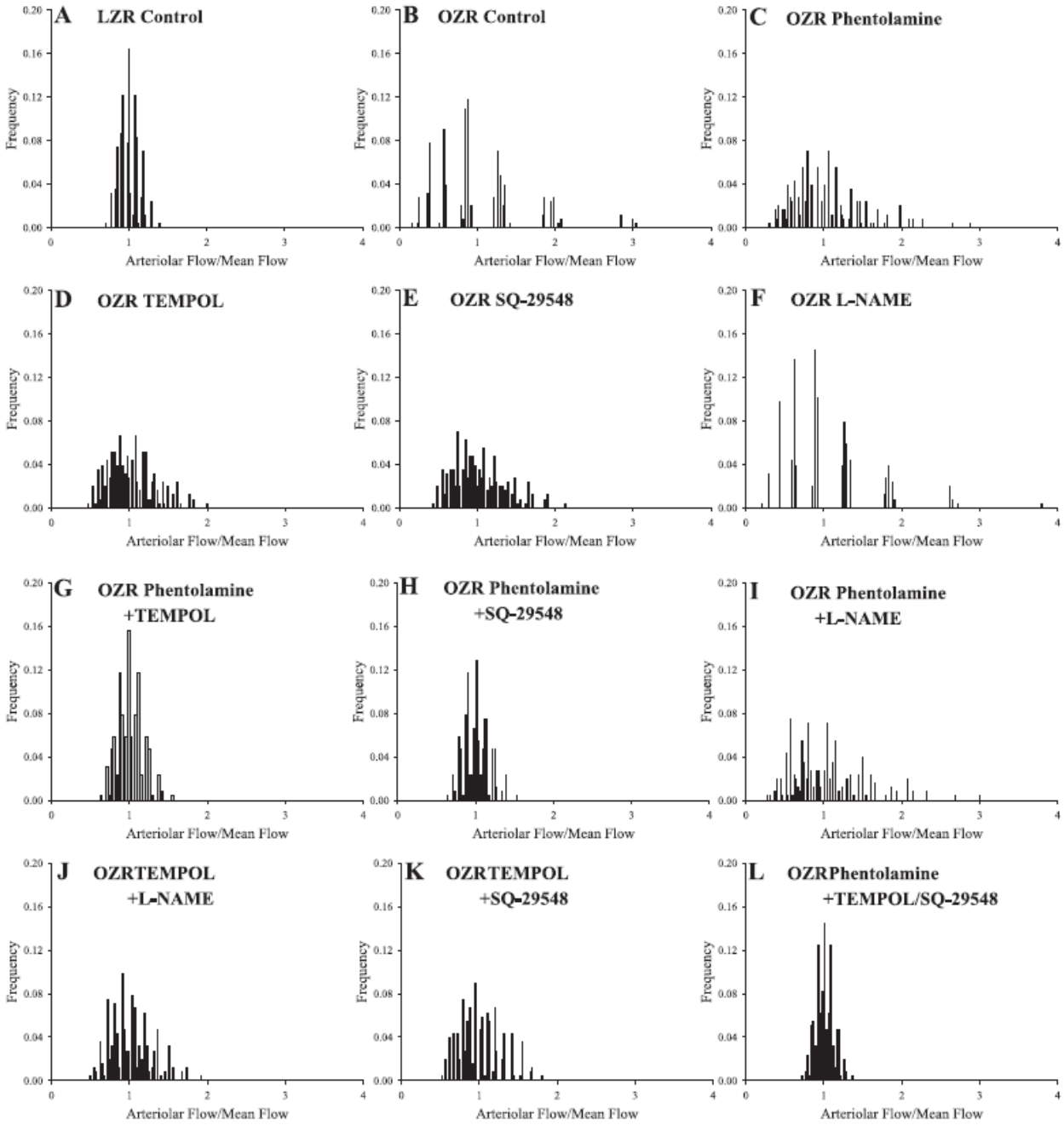
A LZR Control
B OZR Control
C OZR Phentolamine
D OZR TEMPOL
E OZR SQ-29548
F OZR L-NAME
G OZR Phentolamine +TEMPOL
H OZR Phentolamine +SQ-29548
I OZR Phentolamine +L-NAME
J OZRTEMPOL +L-NAME
K OZRTEMPOL +SQ-29548
L OZRPhentolamine +TEMPOL/SQ-29548
Frequency
Arteriolar Flow/Mean Flow

Figure 7:

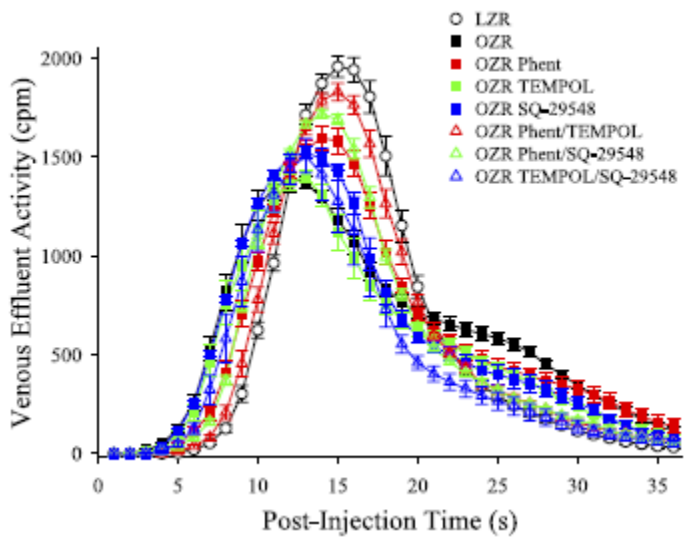

Figure 8:

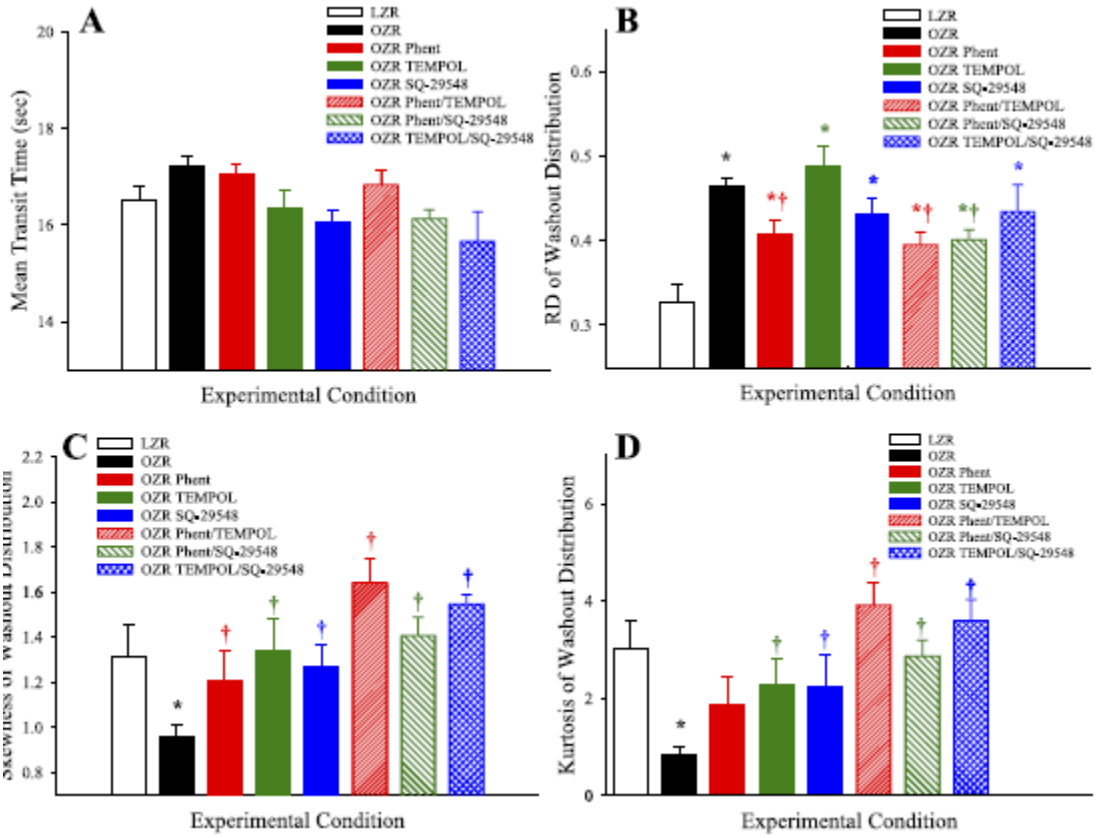

Conceptual Framework

The third chapter is entitled "Spatial Heterogeneity in Skeletal Muscle Microvascular Blood Flow Distribution is Increased in the Metabolic Syndrome". It followed from the above paper, and was based on the data suggesting that the inability of the OZR skeletal muscle to resist fatigue lies within dysfunctional alpha-adrenergic behavior and endothelial dysfunction predominantly driven by oxidant stress and altered AA metabolism. However, these mechanisms suggest spatial differences, thus this paper uses the *in situ* cremaster preparation and the *in situ* blood perfused hindlimb with I^{125} labeled albumin to examine an entire microvascular network with intact blood flow. It allowed for the determination of blood flow distributions at bifurcations at different levels of resolution. In the OZR it identified an increased perfusion distribution compared to the LZR, but revealed that the mechanisms that affect the distribution are spatially distinct. The proximal microcirculation perfusion distribution appears largely impacted by alpha-adrenergic dysfunction, while the distal microcirculation perfusion distribution is altered by oxidant stress and TxA_2. The result of these impairments to perfusion is a "low flow" and a "high flow" pathway that it iterated at each bifurcation across the entire microvasculature network. The indicator solution washout analysis was included to ensure that the results of the high resolution bifurcation study was not a result of selection bias, as the I^{125} albumin is an intravascular tracer used for integrated assessment of network function. The results indicate significant disparity between the mean transit time, dispersion, skewness, and kurtosis of the OZR compared to the LZR, which suggestively confirm the "high/low flow" pathways at bifurcations and matches previous predictive models.

Chapter 4

BLUNTED TEMPORAL ACTIVITY OF MICROVASCULAR PERFUSION HETEROGENEITY IN METABOLIC SYNDROME: A NEW ATTRACTOR FOR PERIPHERAL VASCULAR DISEASE?

Joshua T. Butcher, Adam G. Goodwill, Shyla C. Stanley and Jefferson C. Frisbee

Department of Physiology and Pharmacology and Center for Cardiovascular and Respiratory Sciences

West Virginia University HSC, Morgantown, WV

Running Title: Microcirculation and peripheral vascular disease

Address for Correspondence:

Jefferson C. Frisbee, Ph.D.

Center for Cardiovascular and Respiratory Sciences

Department of Physiology and Pharmacology

West Virginia University Health Sciences Center; 3152 HSN

1 Medical Center Drive

Morgantown, WV 26506

Phone: (304) 293-6527

Fax: (304) 293-5513

Email: jefrisbee@hsc.wvu.edu

ABSTRACT

A key clinical outcome for peripheral vascular disease (PVD) in patients is a progressive decay in skeletal muscle performance and its ability to resist fatigue with elevated metabolic demand. We have demonstrated that PVD in obese Zucker rats (OZR) is partially due to increased perfusion distribution heterogeneity at successive microvascular bifurcations within skeletal muscle. As this increased heterogeneity (γ) is longitudinally present in the network, its cumulative impact is a more heterogeneous distribution of perfusion between terminal arterioles than normal, causing greater regional tissue ischemia. To minimize this negative outcome, a likely compensatory mechanism against an increased γ should be an increased temporal switching at arteriolar bifurcations to minimize downstream perfusion deficits. Using *in situ* cremaster muscle, we determined that temporal activity (the cumulative sum of absolute differences between successive values of γ, taken every 20 seconds) was lower in OZR than in control animals, and this difference was present in both proximal (1A-2A) and distal (3A-4A) arteriolar bifurcations. While adrenoreceptor blockade (phentolamine) improved temporal activity in 1A-2A arteriolar bifurcations in OZR, this was without impact in the distal microcirculation, where only interventions against oxidant stress (TEMPOL) and thromboxane A_2 activity (SQ-29548) were effective. Analysis of the attractor for γ indicated that it was not only elevated in OZR, but also exhibited severe reductions in range, suggesting that the ability of the microcirculation to respond to any challenge is highly restricted, and may represent the major contributor to the manifestation of poor muscle performance at this age in OZR.

Key Words: rodent models of obesity; microcirculation; skeletal muscle blood flow regulation; models of peripheral vascular disease; blood flow heterogeneity; vascular dysfunction

INTRODUCTION

With ongoing study, there is increasing appreciation that the transition from 'healthy' physiology to disease states represents a change in the overall system of control from an existing normal structure (46). It is also generally unclear whether this transition represents a failure of the 'healthy' system or evolving compensations to attempt to optimize the most critical biological outcomes despite progression of a challenged environment (38, 57). For this reason, a detailed understanding of which major contributing processes to an outcome are altered with pathology and the extent for which these are compensated is critical for developing appropriate therapeutic interventions. Failure to elucidate both the key sites of impairment and the compensatory mechanisms, as well as how these impact functional outcomes, has resulted in poorly targeted interventional measures.

While the existing literature contains extensive prior interrogation into the effects of atherosclerotic peripheral vascular disease on perfusion and performance outcomes in multiple model systems as well as the identification of many putative mechanistic contributors to plaque/lesion development (1, 9, 20, 27, 30, 39), investigation into the impact of non-atherosclerotic peripheral vascular disease (PVD) has received a much more limited investment. While underrepresented to date, this is an exceedingly important area of investigation, as a growing body of evidence suggests that an increasing number of human subjects are afflicted with the symptomology of PVD in the absence of overt plaque/lesion development (12, 19, 31, 44, 45).

Based on its origin in a dysfunctional leptin receptor gene, destroying the satiety reflex, the obese Zucker rat (OZR) experiences a chronic hyperphagia, developing severe obesity, a progressive worsening of glycemic control and plasma lipid profiles and, ultimately, the development of moderate hypertension (32, 37). The importance of the OZR model for studying non-atherosclerotic PVD is considerable, as the genesis of the pathological state lies within the leptin resistance-induced hyperphagia, which is found in the human population (53, 56). Further, the severity of the elevated risk factors for a negative cardiovascular outcome has repeatedly been demonstrated to be comparable to that determined in afflicted patients, and these animals do not develop atherosclerotic lesions.

Recent study has provided clear and compelling evidence that impairments to skeletal muscle performance that are associated with development of non-atherosclerotic PVD in OZR are not adequately predicted by basic indices such as the mechanical responses of resistance arterioles to stimuli or by bulk blood flow responses to skeletal muscle (25). Rather, we have recently demonstrated that a defining characteristic of non-atherosclerotic PVD in OZR skeletal muscle is an increasingly asymmetric blood flow distribution at successive microvascular bifurcations, resulting in pronounced heterogeneity of perfusion across the distal arterioles within the network (24, 59). While this increased spatial heterogeneity of perfusion distribution was improved by interventions against reactive oxygen stress, the actions of thromboxane, and altered function within adrenergic vasoconstriction (24, 59), the question of the system compensation for this increased perfusion heterogeneity in OZR is entirely unknown. Conceptually, a likely compensation for the increased spatial heterogeneity of perfusion in the microcirculation of OZR could be via increased temporal switching at arteriolar bifurcations. As the spatial heterogeneity between parallel daughter arterioles would create relative degrees of downstream ischemic signals between the parallel perfused regions, a compensation that resulted in increased temporal switching between 'high flow' and 'low flow' daughter arterioles would help to minimize the severity and duration of the resulting ischemic regions and could act to maintain muscle performance to the greatest possible extent.

Given this conceptual framework, the purpose of the present study was to determine the degree of temporal switching at arteriolar bifurcations within the resting skeletal muscle microcirculation of OZR versus LZR, the extent to which this acts as a compensatory physiological mechanism to the increased spatial perfusion heterogeneity and to determine the major contributing mechanisms to differences between the two conditions. This study tested the hypothesis that temporal switching at arteriolar bifurcations is increased in skeletal muscle of OZR as a means for compensating for the increased spatial perfusion heterogeneity and helping to maintain skeletal muscle performance at optimal levels despite the evolving pathological state.

MATERIALS AND METHODS

Animals: Male lean (total n=20; Harlan) and obese Zucker rats (total n=38; *fa-/fa-*; Harlan) were fed standard chow and drinking water *ad libitum* and were housed in the animal care facility at the West Virginia University Health Sciences Center or the Medical College of Wisconsin. All protocols received prior IACUC approval. At ~17 weeks of age, rats were anesthetized with injections of sodium pentobarbital (50 mg/kg, i.p.), and received tracheal intubation to facilitate maintenance of a patent airway. In all rats, a carotid artery and an external jugular vein were cannulated for determination of arterial pressure and for infusion of supplemental anesthetic and pharmacological agents, as necessary. Any animal in which mean arterial pressure was found to be below 85 mmHg, or where MAP had decreased by more than 15% from that following this initial surgery (without any pharmacological intervention) was not used in the present study. Blood samples were drawn from the venous cannula for determination of glucose and insulin concentrations (Millipore; Billerica, MA) as well as cholesterol/triglyceride levels (Wako Diagnostics; Richmond, VA), and nitrotyrosine (Oxis International; Foster City, CA). Unless otherwise noted, all drugs and chemicals were purchased from Sigma-Aldrich (St. Louis, MO, USA).

Preparation of In Situ Cremaster Muscle: In each rat (LZR n=20; OZR n=38), an *in situ* cremaster muscle was prepared for intravital microscopy (2, 26, 35), and was continuously superfused with physiological salt solution (PSS) equilibrated with a 5% CO_2-95% N_2 gas mixture, maintained at 35°C, as it flowed over the muscle. Volume flow rate was ~3.0 ml/min. The ionic composition of the PSS was as follows (mM): NaCl 119.0, KCl 4.7, $CaCl_2$ 1.6, NaH_2PO_4 1.18, $MgSO_4$ 1.17, $NaHCO_3$ 24.0, and disodium EDTA 0.03. After a 30 minute period of equilibration following the surgical preparation, arterioles and bifurcations within two distinct "bifurcation categories" were selected for investigation: 1) ~100 μm 'parent' to ~80 μm 'daughters' (1A-2A) and 2) ~60 μm 'parent' to ~40 μm 'daughters' (3A-4A). Arterioles/bifurcations were selected based on the following criteria: 1) distance from any site of incision, 2) presence of significant vascular tone (assessed by brisk dilator response to challenge with 10^{-3} M adenosine), 3) clearly discernible walls, 4) a rapid and stable level of erythrocyte perfusion, and 5) the

presence of two clearly defined 'daughter' branches that also met criteria 1-4. Please see Figure 1 for a schematic representation (also reference 24).

The mechanical (using on-screen videomicroscopy) and perfusion (using optical Doppler velocimetry) responses of both the 'parent' and 'daughter' arterioles within a bifurcation class were assessed under resting conditions within the cremaster muscle of each rat. All procedures were performed under control conditions in LZR and OZR, and following treatment of the *in situ* cremaster muscle with the anti-oxidant TEMPOL (10^{-3} M), the TxA_2 receptor antagonist SQ-29548 (10^{-4} M), and/or the α_1/α_2 adrenergic receptor antagonist phentolamine (10^{-5} M); within the superfusate solution. All treatments to the cremaster were of a minimum of 40 minutes duration prior to any subsequent experimental manipulation/data collection.

Interrogation of Arteriolar Bifurcations: Within each animal, one 1A-2A bifurcation and one 3A-4A bifurcation was studied within the arteriolar network. For an individual measurement, arteriolar diameter and erythrocyte velocity were monitored for 5 minutes, with measurements taken every 20 seconds. All arterioles and bifurcations were selected on the basis of the criteria outlined above and were placed into their categories by size rather than by strict branch number within the network.

In order to maintain preparation and collected data quality, no cremaster muscle was exposed to all interventions and combinations listed above. In addition to the collection of responses under control conditions, individual cremaster preparations were exposed to a maximum of four interventions, each separated by ~30 minutes of washout. Treatment or washout effectiveness was verified by determining abolition or recovery of mechanical responses following challenge with appropriate agonists (e.g., the α_1 adrenergic antagonist phenylephrine, the stable TxA_2 mimetic U-46619, and the endothelium-dependent dilator agonist acetylcholine for the appropriate initial treatments). Maximum experimental duration from preparation to termination was approximately four hours, after which time all animals were humanely euthanized by an intravenous overdose of anesthetic followed by a bilateral pneumothoracotomy, *as per* approved IACUC protocols.

Data and Statistical Analyses: Arteriolar perfusion in both parent and daughter vessels within *in situ* cremaster muscle of LZR and OZR was calculated as:

$$Q = (V \times 1.6^{-1})(\pi r^2)(0.001)$$

where Q represents arteriolar perfusion (nl•s^{-1}), V represents the measured red cell velocity from the optical Doppler velocimeter (mm•s^{-1}; with V/1.6 representing an estimated average velocity assuming a parabolic flow profile; Ref. 18), and r represents arteriolar radius (μm; Ref. 4).

The total volume perfusion in the daughters was determined as the sum of the individual perfusion rates, and the proportion of flow within each was determined as the quotient of the individual branch divided by the total. γ is defined as the ratio of the greater of the two flows in the daughter vessel to the total flow in the parent vessel. As an example, if flow distribution was homogeneous between daughters, γ for that bifurcation would be 0.5 in both daughter arterioles, while if the proportion of flow in one daughter arteriole was 60%, for that bifurcation would be 0.6, with flow distribution being 0.6 in the 'high perfusion' arteriole and 0.4 in the 'low perfusion' arteriole (Figure 1, and Ref. 6).

Monitoring γ throughout the observation period and analyzing those resulting data used three initial approaches. The first of these was simply to determine the mean±SE of the individual measurements throughout the 5 minute observation window, providing the mean value for γ. However, this is clearly not sufficiently informative in terms of understanding the temporal behavior for γ at a bifurcation. The second approach was to determine the cumulative change in γ from each of the 15 successive measurements:

$$\sum_{t=1}^{15} (\gamma_{(t)} - \gamma_{(t+1)})$$

where γ represents the perfusion distribution at any given bifurcation and *t* represents the measurement time from 1 (initial) to 15 (final). While these data can provide us with evidence of broader changes in γ with longer durations, it was apparent that a more sensitive marker is needed to provide sufficient insight into

temporal switching at an arteriolar bifurcation. As such, the final approach is to summate the absolute values of the differences in γ from one time point to the next to provide for a superior index of total activity:

$$\sum_{t=1}^{15} ABS\{(\gamma_{(t)} - \gamma_{(t+1)})\}$$

This final index (summating absolute difference in γ), will provide insight into the total temporal switching at any arteriolar bifurcation within the data collection window.

In order to determine the effectiveness of any intervention on improving the behavior of γ over the data collection window in OZR, the values for the γ (cumulative, absolute differences) that were collected for arteriolar bifurcations in LZR under control conditions (A) were set as the overall control value. As such, the impact of pathology (development of the metabolic syndrome) is determined from the data collected in OZR under control conditions (B) and is the absolute difference between these two values: $x = ABS\ (A - B)$. The extent to which any intervention in OZR can improve normal behavior is given by the value of γ (cumulative, absolute) following the intervention (C), and is represented by: $y = ABS\ (B - C)$. Given this, the percent effectiveness of any intervention in restoring the normal behavior of γ at a bifurcation in OZR is provided by: $z = (y/x) \times 100$.

An attractor is generally defined as the set of conditions towards which a given variable evolves over time. To a significant extent, this can be considered as the representation of the behavior of a dynamic system over a period of time, and this can be extremely useful in understanding the limits of a system (i.e., what behaviors are either not possible, not generally attainable or are extremely unlikely) and the effects on system behavior (either beneficial or detrimental) subsequent to an imposed intervention. The most informative manner in presenting an attractor is as an iterated map, where the current state of the parameter under study is plotted at a given moment, and then its change in position re-plotted at the next time interval. This process is iterated repeatedly, to the conclusion of the data set, and the shape and location of the attractor

on the co-ordinate system becomes evident. This approach also facilitates comparisons between experimental conditions and the impact these have on the location and shape of the attractor.

All data throughout the manuscript are presented as mean±SE. Statistically significant differences in measured and calculated parameters were determined using a one sample *t*-test (differences from zero), Student's *t*-test or analysis of variance (ANOVA) with Student-Newman-Keuls post-hoc test used as needed. In all cases, $p<0.05$ was taken to reflect statistical significance.

RESULTS

Table 1 presents the baseline characteristics of animals used in the present study. By ~17 weeks of age, OZR demonstrated striking obesity and had a significantly higher mass than LZR. Further, OZR exhibited statistically significant elevation in mean arterial pressure, and both plasma insulin and nitrotyrosine concentrations. Data describing the dimension and perfusion characteristics of the cremasteric arteriolar bifurcation segments (described above) under the conditions of the present study are summarized in Table 2. These data clearly demonstrate general differences between arteriolar diameter and perfusion characteristics that are distributed longitudinally throughout the cremasteric microcirculation under the conditions of the present study.

Figure 2 presents representative data describing the distribution of the magnitude of γ and its temporal behavior across 1A-2A (Panels A and B, respectively) and 3A-4A (Panels C and D, respectively) arteriolar divisions. As suggested by these data, in addition to a shift in the frequency distribution of γ between LZR and OZR at both microvascular divisions, the changes in γ (measured every 20 seconds over the course of 5 minutes) were less extensive in both proximal and distal bifurcations of the resting cremaster muscle microcirculation of OZR as compared to LZR.

Proximal Resistance Arterioles: The summarized results of the average magnitude of γ at 1A-2A arteriolar bifurcations over the observation period are presented in Figure 3. In LZR (Panel A), γ was

approximately 0.51 under control conditions, and was not altered by acute pharmacological intervention. In contrast, average γ over the 5 minute period in OZR (Panel B) was much higher, approximately 0.58 under control conditions. While interventions containing phentolamine (regardless of the presence of any other substance) reduced average γ to levels determined in LZR, treatment against either the increased TxA_2 production (SQ-29548) or the elevated vascular oxidant stress (TEMPOL) in OZR were not effective, resulting in minimal changes to γ.

Data describing the changes in γ in 1A-2A bifurcations between LZR and OZR over the 5 minute observation window are summarized in Figure 4. When presented as the cumulative change in γ, neither LZR (Panel A) nor OZR (Panel B) exhibited a difference between strains or a clear pattern in terms of the cumulative change in γ within a strain. However, when the cumulative changes in γ are presented as the sum of the absolute changes, striking differences are evident. While a clear reduction in the cumulative change in γ (absolute) was evidence in OZR (Panel D) as compared to LZR (Panel C), blockade of adrenoreceptors (alone or with any other pharmacological intervention) in 1A-2A bifurcations in LZR reduced activity at the bifurcation. In contrast, treatment of elevated oxidant stress with TEMPOL or blockade of TxA_2 with SQ-29548 has no discernible impact. In 1A-2A bifurcations from OZR, treatment with phentolamine (either alone or with TEMPOL and/or SQ-29548) significantly increased the cumulative change in γ (absolute) over the data collection window (Panel D). Similarly to LZR, treatment with TEMPOL and/or SQ-29548 in the absence of phentolamine did not have a significant impact.

Distal Resistance Arterioles: Comparable to data presented for proximal resistance arterioles, the average γ for 3A-4A arteriolar bifurcations over the 5 minute period was ~0.5 in LZR under control conditions (Figure 5, Panel A) and this was elevated in OZR (Panel B). However, while treatment interventions were without effect in LZR, application of either TEMPOL or SQ-29548 in OZR significantly reduced mean γ toward 0.5. In contrast to the results from more proximal resistance arterioles, γ was largely

unaffected by phentolamine treatment and interventions targeted at rectifying endothelial dysfunction were required in order to cause a significant restoration of γ.

Figure 6 presents the cumulative changes in γ over the 5 minute period in 3A-4A arteriolar bifurcations from LZR (Panels A and C) and OZR (Panels B and D). When the changes in γ are presented as simple accumulation, there were no significant differences between LZR (Panel A) and OZR (Panel B) or within a strain as a result of any intervention. However, when the changes in γ are summated as absolute differences, clear differences were identified. In 3A-4A arteriolar bifurcations of LZR (Panel C), acute treatment with phentolamine reduced the accumulated changes to γ, while the presence of TEMPOL and/or SQ-29548 resulted in minimal total changes or marginal change (when applied in combination with each other or with phentolamine). In contrast, application of TEMPOL and/or SQ-29548 significantly improved the cumulative changes to γ (absolute) in 3A-4A arteriolar bifurcations of OZR, while the effects of phentolamine application were muted (Panel D).

Effects of Adenosine: To simulate the impact of elevated metabolic demand on the temporal stability of γ throughout the cremaster muscle microcirculation, increasing concentrations of adenosine were added to the preparation superfusate. While application of adenosine had minimal impact on average γ in LZR, it reduced average γ in OZR, at both 1A-2A (Panel A) and 3A-4A (Panel C) bifurcations to levels that were very similar to that determined in LZR, with the greatest impact being observed with the highest level of adenosine (Figure 7). Adenosine did not impact the cumulative change in γ over the 5 minute period in either strain, at either bifurcation location (data not shown). However, when the changes in are summated as absolutes, application of increasing concentrations of adenosine reduced temporal activity in LZR at both 1A-2A (Panel B) and 3A-4A (Panel D) bifurcations, although it had minimal impact on activity in the bifurcations of OZR (Panels B and D).

Effectiveness of Interventions in Restoring Normal Behavior: Figure 8 summarizes the impact of the interventions on restoring normal temporal activity at 1A-2A (Panel A) and 3A-4A (Panel B) arteriolar

bifurcations in OZR (where the activity at those bifurcation levels in untreated LZR is defined as control/normal). As shown in Panel A, while there is a significant recovery in function with treatment with the adrenoreceptor antagonist alone, combined therapy of phentolamine with the agents targeted at improving endothelial dysfunction resulted in a dramatic improvement in the temporal behavior of at the proximal arteriolar bifurcations of OZR. Conversely, the reverse pattern was evident for distal arteriolar bifurcations of OZR, as treatment with SQ-29548 and/or TEMPOL resulted in significant improvements to the temporal activity of , while the combined application with phentolamine resulted in a further marginal improvement to this outcome.

Establishment of a New Attractor for PVD: Figure 9 presents the attractor for at 1A-2A arteriolar bifurcations in cremaster muscle of LZR and OZR (control conditions). As show in Panel A, the attractor for changes in in OZR was shifted from that in LZR, exhibiting a higher and a smaller range over which can move. Treatment with phentolamine (Panel B) was effective in restoring the magnitude of the attractor in OZR compared to that in LZR, although range remained restricted. In contrast, treatment of the cremasteric network with TEMPOL and/or SQ-29548 was of minimal benefit in restoring the attractor in OZR to that in LZR (Panel C). However, combined treatment with phentolamine and TEMPOL/SQ-29548 almost completely restored the magnitude and the shape of the attractor in OZR to that in LZR. This situation was reversed in distal arteriolar bifurcations of OZR and LZR (Figure 10), as the shift in the attractor for OZR versus LZR under control conditions (Panel A) was much more strongly impacted by treatment with TEMPOL and/or SQ-29548 (Panel C) than with phentolamine (Panel B); although combined treatment with phentolamine and TEMPOL/SQ-29548 still resulted in near complete restoration of the attractor shape and magnitude determined in LZR (Panel D).

The effects of increasing adenosine concentration on the attractor in arteriolar bifurcations of OZR are summarized in Figure 11. In both proximal (Panel A) and distal (Panel B) arteriolar bifurcations, treatment with high concentrations of adenosine (10^{-3}M) restored the attractor magnitude, but not the full extent of the shape. Lower concentrations of adenosine (10^{-7} or 10^{-5}M) were without

discernible effect (data not shown). The temporal behavior of suggested that, with the highest concentrations of adenosine, there was a less heterogeneous distribution of perfusion at bifurcations, but also that the activity of over time remained reduced.

DISCUSSION

It has long been understood that the development of non-atherosclerotic PVD, with its implicit failure of appropriate matching of blood perfusion to meet requisite metabolic demand, is associated with a severely compromised ability of the skeletal muscle to maintain performance (i.e., developed tension levels; refs. 19, 44). However, using the OZR model of the metabolic syndrome, it has been clearly demonstrated that blood-perfused skeletal muscle rates of fatigue are increased as compared to LZR, and that this compromised performance is not simply a function of global ischemia (25). Rather, treatment with an adrenoreceptor antagonist and a substantial restoration of functional hyperemia, muscle fatigue rates and oxygen uptake (VO_2) remained compromised in OZR as compared to LZR. It was only after combined treatment with both the adrenoreceptor antagonist and interventions ameliorating endothelial dysfunction (the anti-oxidant TEMPOL and/or the PGH_2/TxA_2 receptor antagonist SQ-29548) that muscle performance and VO_2 were improved. These results strongly suggest a spatial divergence with regard to dysfunction wherein altered adrenoreceptor function primarily impacts bulk perfusion resistance while altered endothelial function primarily impairs perfusion:demand matching in the distal microvasculature (25). We have interrogated this spatial divergence in blood flow control in skeletal muscle of OZR and have determined that a defining characteristic of PVD in this model is an increasingly heterogeneous distribution of blood flow at successive bifurcations within the arteriolar network (defined by the proportionality parameter:). The deviation of from 0.5 (homogeneous distribution) is not only strongly predictive of poor muscle performance, it was determined to be longitudinally consistent down the arteriolar network, and was demonstrated to lead to severe increases in blood flow distribution at the pre-capillary level in OZR as compared to LZR (24, 59).

The elevated □ at arteriolar bifurcations and increased spatial heterogeneity of perfusion distribution represent a deviation from the normal system behavior identified in microvascular networks of LZR. However, as with the majority of biological systems, compensatory mechanisms that can minimize the impact of the increased spatial heterogeneity in perfusion should be present. Logically, the most likely compensatory mechanism would be an increased temporal 'switching' at the individual bifurcations (an increased rate of change with regard to which daughter represents the 'high' or 'low' flow branch, or at least in the severity of the change in □) which would serve to minimize the extent to which signals associated with any developed ischemic signals accumulate within a 'low flow' branch. While the nature of these signals is not fully clear at this time, with potential contributors stemming from the buildup of parenchymal tissue metabolic signals (10, 13, 17, 49), substances released from increasingly deoxygenated erythrocytes as they pass through the microcirculation (22, 29, 50, 51), or undefined signals that are propagated along myocyte and/or endothelial communication pathways (3, 7, 21, 55), the general principle appears to be valid regardless of the stimuli involved.

The data presented in this study refute our general hypothesis, as the accumulated shifts in □ with time at both 1A-2A (Figures 3/4) and 3A-4A (Figure 5/6) arteriolar bifurcations in resting skeletal muscle of OZR were significant reduced as compared to levels determined in LZR. This is a particularly striking observation, as it clearly suggests that not only does a change in temporal switching at arteriolar bifurcations not serve as a compensatory mechanism for the increased □ at arteriolar bifurcations in OZR, the reduction in temporal switching actually entrenches the negative outcomes for perfusion distribution associated with the increased □. The results from subsequent interventions demonstrated that this blunting of temporal activity in arteriolar bifurcations of OZR could be ameliorated. In proximal resistance arterioles, treatment of the resting cremaster muscle with phentolamine, to remove alterations to the distribution of adrenergic constriction throughout the network, significantly increased the cumulative □; an observation that was not identified in the distal microcirculation, where adrenoreceptor blockade was not associated with a significant change in □. Conversely, interventions targeted at

correcting endothelial dysfunction (TEMPOL and/or SQ-29548) had minimal impact on the temporal activity of perfusion distribution at proximal arterioles, but significantly improved this response in more distal 3A-4A bifurcations (Figure 8). In all cases, combined treatments improved to levels that were very similar to that determined for LZR under control conditions. It is particularly compelling that these interventions, and their sites of greatest impact parallel results in our previous studies with regard to correcting the spatial heterogeneity of throughout the microcirculation (24) and improving muscle fatigue resistance and VO_2 (24). Specifically, while treatment with either phentolamine or TEMPOL/SQ-29548 alone improved select or localized indices of vascular function (with no beneficial impact on muscle performance), only combined treatment with phentolamine and TEMPOL/SQ-29548 resulted in a widely distributed and significant improvement to muscle perfusion, VO_2 and performance (25). Taken together, this series of observations suggest that, with a combined intervention designed to remove alterations to adrenergic constriction and endothelial dysfunction in the OZR model of metabolic syndrome, blood flow hemodynamics at successive arteriolar bifurcations is improved to a condition which helps to restore the processes of mass transport and exchange in the microcirculation to a level that allows for a significant improvement to muscle performance. However the extent to which this is manifested as a change to the total surface area available for exchange in the muscle or an improvement to erythrocyte distribution within the terminal arterioles and capillary networks remains to be elucidated.

One of the benefits derived from the increased effort of acquiring temporal data is that it can allow for the determination of an attractor. In essence, an attractor is the set to which a variable will adhere over time (36, 58). Even following perturbation as a result of an imposed challenge, the variable will change its behavior over time to return to its attractor if possible (36, 58). In the present experiments, the attractor for both proximal (1A-2A) and distal (3A-4A) arteriolar bifurcations in LZR exhibited a wide range of states around a central region with approximating 0.5. This was dramatically different in both proximal (Figure 9) and distal (Figure 10) arteriolar bifurcations of OZR, where the central region of the attractor was shifted to ~0.58, with a narrowed range of achieved values. Beyond being an intriguing

scientific curiosity, this shift in the attractor has critical implications for blood flow control in OZR. The change in both magnitude and range of the attractor with the development of pathology in OZR indicates that the ability of arterioles and arteriolar bifurcations to respond to imposed challenges (e.g., changes in metabolic demand) will be severely compromised as the potential for perfusion redistribution will be constrained to a more limited set of attainable conditions. Essentially, the development of non-atherosclerotic PVD in OZR is defined by a loss of flexibility in the control systems contributing to the regulation of perfusion distribution in skeletal muscle, thus severely compromising the ability to effectively adapt to changing conditions. This is a particularly striking outcome and it may represent the more functionally integrated extension of a similar process identified by Tigno *et al.* (54) in diabetic monkeys, where the randomness of arterial vasomotion was found to be dampened with disease progression. Taken together, it is not simply that we have dysfunction and can identify it in a series of reduced preparations. It is that indices of dysfunction in simplified preparations, when integrated, produce an outcome wherein the pathology is partially defined by an impaired ability of the system to respond to stressors.

Despite numerous attempts, we were unable to acquire a sufficiently robust data set which outlined the impact of muscle contraction on in the cremaster muscle microcirculation. However, as a simulator of this condition, we utilized elevated concentrations of adenosine in the preparation superfusate and determined the resulting effects on . The results clearly indicate that superfusion with low (10^{-7}M) or moderate (10^{-5}M) levels of adenosine had a limited impact on the temporal behavior of or the resulting attractor in arteriolar bifurcations of OZR, while superfusion with high concentrations of adenosine (10^{-3}M) nearly restored to levels determined in arteriolar bifurcations in LZR, but did not restore the range of the attractor (Figure 11). These observations strongly suggest that the arteriolar networks in OZR may be resistant responding to elevated metabolic demand, until a 'threshold' is reached. Once a sufficient metabolic intensity (or build-up of the appropriate signal) has been attained, the system will respond, although to a constrained extent (i.e., magnitude of is restored, but range

remains blunted). As we have demonstrated previously (24), this high concentration of adenosine results in a maximal relaxation of *in situ* skeletal muscle arterioles in OZR, meaning that the entire vascular network should be without any significant source of tone. This would mean that any changes in would reflect only the impact of the architecture and geometric arrangement of the network, as well as the intrinsic physical processes associated with blood flow and erythrocyte distribution in vascular networks, as has been previously studied by Cokelet (14, 15) and Kiani (33), among others (23, 28). As presented in Figure 11, the attractor for under these conditions is very similar between LZR and OZR in terms of magnitude and shape, but with a restricted range.

Given the nature of the data in the present study, attention should be given to the impact of the method of anesthesia on outcomes and data interpretation. Numerous previous studies have demonstrated that both inhalational volatile and injectable general anesthetics can impact endothelial function and vasomotion (16, 41, 48), as well as baroreflex sensitivity and the sympathetic control of vascular tone (48). As such, either option presents a challenge for data interpretation in the present study, especially given the complications associated with altered baroreflex control (40, 47), sympathetic output (11, 47), and endothelial function (25) that has been demonstrated in the obese Zucker rat. While for this research, we have elected to utilize a barbiturate anesthetic (owing to the time between exposure and data collection, and to avoid the impact on vasomotion), these are issues that become extremely complicated and further investigation of the impact of anesthetic regimen on microvascular outomes in models of increased PVD risk may be warranted.

Obviously, the ultimate outcome for microvascular function, regardless of condition, is the ability of the networks to adequately support mass transport and exchange under both resting and challenged conditions. If we assume that the attractors identified for LZR under control conditions are representative of ‘health’, for the purposes of the present discussion it may be useful to consider this as ‘optimized’ (i.e., these attractors describe microvascular networks functioning optimally). Assuming this, the attractors for OZR would represent the resultant state of the microcirculation under conditions of the metabolic

syndrome. As such, it is important to estimate how these changes to perfusion distribution would impact indices such as tissue oxygenation or microvascular hematocrit. While these measurements are outside of the scope of the current study, previous research efforts can provide some potential insight. In particular, the work of Pries *et al.* (42, 43), has identified a 'network Fahraeus effect' that can represent a significant contributor to the ultimate reduction in microvascular hematocrit at successive bifurcations owing to a disproportionate distribution of flow (and therefore, erythrocytes) at arteriolar bifurcations. Under 'control' conditions, those authors suggested that this alone could cause a reduction in microvascular hematocrit approaching 20%, with direct implications for tissue oxygenation (8, 52). As the results from the present study clearly indicate that is increased in the arteriolar networks of OZR (versus 'control'), it would be logical to speculate that this would result in an exacerbation of the 'network Fahraeus effect', which, when taken in combination with other contributors to hematocrit reduction (e.g., the 'vessel Fahraeus effect' (15, 43) and other hemo-rheological parameters (5, 23, 34)), would result in a further reduction of microvascular hematocrit within the networks. While specific interventions such as adrenoreceptor blockade and inhibiting the actions of TxA_2 could provide some amelioration of this impairment, based on alterations to the shape of the attractors, only a combined interventional strategy would be sufficient to cause an improvement to arteriolar network function that would be sufficient to result in alterations to mass transport and exchange that were large enough to improve muscle fatigue resistance (25). Further investigation into the impact of these cumulative perfusion abnormalities in the skeletal muscle microcirculation of OZR could provide us with a far more complete understanding of how non-atherosclerotic PVD is manifest in this increasingly relevant animal model of the metabolic syndrome.

ACKNOWLEDGEMENTS

This study was supported by grants from the National Institutes of Health (NIH DK R01 64668, T32 HL 90610 and RR 2865AR) and the American Heart Association (AHA EIA 0740129N). The authors also wish to express their gratitude for the expert technical assistance from Ms. Milinda James from the Department of Physiology and Pharmacology at West Virginia University and for support provided through the Translational Research Facility in the Center for Cardiovascular and Respiratory Sciences at the West Virginia University HSC.

LITERATURE CITED

1. **Ait-Oufella H, Taleb S, Mallat Z, Tedgui A.** Recent advances on the role of cytokines in atherosclerosis. *Arterioscler Thromb Vasc Biol*. 31:969-79, 2011.

2. **Bagher P, Segal SS.** The mouse cremaster muscle preparation for intravital imaging of the microcirculation. *J Vis Exp*. 2011 Jun 10;(52). pii: 2874. doi: 10.3791/2874.

3. **Bagher P, Segal SS.** Regulation of blood flow in the microcirculation: role of conducted vasodilation. *Acta Physiol (Oxf).* 202:271-284, 2011.

4. **Baker M, Wayland H.** On-line volume-flow rates and velocity profile measurements for blood in microvessels. *Microvasc. Res.* 7:131-143, 1974.

5. **Baskurt OK, Yalcin O, Gungor F, Meiselman HJ.** Hemorheological parameters as determinants of myocardial tissue hematocrit values. *Clin Hemorheol Microcirc.* 35:45-50, 2006.

6. **Bassingthwaighte JB, Liebovitch LS, West BJ.** "Intraorgan flow heterogeneities." In: *Fractal Physiology*. Oxford University Press, New York, 1994. p. 236-262.

7. **Behringer EJ, Segal SS.** Spreading the signal for vasodilatation: Implications for skeletal muscle blood flow control and the effects of aging. *J Physiol.* 2012 Aug 13. [Epub ahead of print] PubMed PMID: 22890708.

8. **Bos C, Hoofd L, Oostendorp T.** Mathematical model of erythrocytes as point-like sources. *Math Biosci.* 125:165-189, 1995.

9. **Businaro R, Tagliani A, Buttari B, Profumo E, Ippoliti F, Di Cristofano C, Capoano R, Salvati B, Riganò R.** Cellular and molecular players in the atherosclerotic plaque progression. *Ann N Y Acad Sci.* 1262:134-41, 2012.

10. **Calbet JA, Joyner MJ.** Disparity in regional and systemic circulatory capacities: do they affect the regulation of the circulation? *Acta Physiol (Oxf)*. 199:393-406, 2010.

11. **Carlson SH, Shelton J, White CR, Wyss JM.** Elevated sympathetic activity contributes to hypertension and salt sensitivity in diabetic obese Zucker rats. *Hypertension.* 35:403-408, 2000.

12. **Chandra S, Singh V, Nehra M, Agarwal D, Singh N.** ST-segment elevation in non-atherosclerotic coronaries: a brief overview. *Intern Emerg Med.* 6:129-139, 2011.

13. **Clifford PS, Hellsten Y.** Vasodilatory mechanisms in contracting skeletal muscle. *J Appl Physiol.* 97:393-403, 2004.

14. **Cokelet GR.** Rheology and hemodynamics. *Annu Rev Physiol.* 42:311-324, 1980.

15. **Cokelet GR.** Experimental determination of the average hematocrit of blood flowing in a vessel. *Microvasc Res.* 7:382-384, 1974.

16. **Colantuoni A, Bertuglia S, Intaglieeta M.** Effects of anesthesia on the spontaneous activity of the microvasculature. *Int J Microcirc Clin Exp.* 3:13-28, 1984

17. **Davis MJ.** Perspective: physiological role(s) of the vascular myogenic response. *Microcirculation.* 19:99-114, 2012.

18. **Davis MJ.** Determination of volumetric flow in capillary tubes using an optical Doppler velocimeter. *Microvasc Res* 34:223-30, 1987.

19. **Dean SM.** Atypical ischemic lower extremity ulcerations: a differential diagnosis. *Vasc Med.* 13:47-54, 2008.

20. **Demer L, Tintut Y.** The roles of lipid oxidation products and receptor activator of nuclear factor-κB signaling in atherosclerotic calcification. *Circ Res.* 108:1482-93, 2011.

21. **Diep HK, Vigmond EJ, Segal SS, Welsh DG.** Defining electrical communication in skeletal muscle resistance arteries: a computational approach. *J Physiol.* 568:267-81, 2005.

22. **Ellsworth ML, Sprague RS.** Regulation of blood flow distribution in skeletal muscle: role of erythrocyte-released ATP. *J Physiol.* 590:4985-4991, 2012.

23. **Fenton BM, Carr RT, Cokelet GR.** Nonuniform red cell distribution in 20 to 100 micrometers bifurcations. *Microvasc Res.* 29:103-126, 1985.

24. **Frisbee JC, Wu F, Goodwill AG, Butcher JT, Beard DA.** Spatial heterogeneity in skeletal muscle microvascular blood flow distribution is increased in the metabolic syndrome. Am J Physiol Regul Integr Comp Physiol. 301:R975-R986, 2011.

25. **Frisbee JC, Goodwill AG, Butcher JT, Olfert IM.** Divergence between arterial perfusion and fatigue resistance in skeletal muscle in the metabolic syndrome. *Exp Physiol.* 96:369-383, 2011.

26. **Frisbee JC, Sylvester FA, Lombard JH.** Contribution of extrinsic factors and intrinsic vascular alterations to reduced arteriolar reactivity with high-salt diet and hypertension. *Microcirculation.* 7:281-289, 2000.

27. **Fuster JJ, Castillo AI, Zaragoza C, Ibáñez B, Andrés V.** Animal models of atherosclerosis. *Prog Mol Biol Transl Sci.* 105:1-23, 2012.

28. **Gaehtgens P.** Distribution of flow and red cell flux in the microcirculation. *Scand J Clin Lab Invest Suppl.* 156:83-87, 1981.

29. **Goldman D, Fraser GM, Ellis CG, Sprague RS, Ellsworth ML, Stephenson AH.** Toward a multiscale description of microvascular flow regulation: O(2)-dependent release of ATP from human erythrocytes and the distribution of ATP in capillary networks. *Front Physiol.* 3:246, 2012.

30. **Greenwald SE.** Ageing of the conduit arteries. *J Pathol.* 211:157-172, 2007

31. **Hill SF, Sheppard MN.** Non-atherosclerotic coronary artery disease associated with sudden cardiac death. *Heart.* 96:1119-1125, 2010.

32. **Kasiske BL, O'Donnell MP, Keane WF.** The Zucker rat model of obesity, insulin resistance, hyperlipidemia, and renal injury. *Hypertension.* 19(1Suppl):I110-5, 1992.

33. **Kiani MF, Pries AR, Hsu LL, Sarelius IH, Cokelet GR.** Fluctuations in microvascular blood flow parameters caused by hemodynamic mechanisms. *Am J Physiol.* 266:H1822-H1828, 1994.

34. **Lipowsky HH.** Microvascular rheology and hemodynamics. *Microcirculation.* 12:5-15, 2005.

35. **Lombard JH, Frisbee JC, Greene AS, Hudetz AG, Roman RJ, Tonellato PJ.** Microvascular flow and tissue PO(2) in skeletal muscle of chronic reduced renal mass hypertensive rats. *Am J Physiol Heart Circ Physiol.* 279:H2295-H2302, 2000.

36. **Mandelbrot BB**, "Fractal attractors and fractal ("chaotic') evolutions." In: *The Fractal Geometry of Nature.* pp. 193-199, 1983. W.H. Freeman and Company, New York, USA.

37. **Mathé D.** Dyslipidemia and diabetes: animal models. *Diabete Metab.* 21:106-11, 1995.

38. **Menolascina F, Siciliano V, di Bernardo D.** Engineering and control of biological systems: A new way to tackle complex diseases *FEBS Lett.* 586:2122–2128, 2012.

39. **Meru AV, Mittra S, Thyagarajan B, Chugh A.** Intermittent claudication: an overview. *Atherosclerosis.* 187:221-37, 2006.

40. **Pamidimukkala J, Jandhyala BS.** Evaluation of hemodynamics, vascular reactivity and baroreceptor compensation in the insulin resistance Zucker obese rats. *Clin Exp Hypertens.* 18:1089-1104, 1996.

41. **Park, KW, Dai HB, Lowenstein E, Sellke FW.** Effect of sevoflurane and desflurane on the myogenic constriction and flow-induced dilation in rat coronary arterioles. *Anesthesiology.* 90:1422-1427, 1999.

42. **Pries AR, Secomb TW, Gaehtgens P, Gross JF.** Blood flow in microvascular networks. Experiments and simulation. *Circ Res.* 67:826-834, 1990.

43. **Pries AR, Ley K, Gaehtgens P.** Generalization of the Fahraeus principle for microvessel networks. *Am J Physiol.* 251:H1324-H1332, 1986.

44. **Ren J.** Leptin and hyperleptinemia - from friend to foe for cardiovascular function. *J Endocrinol.* 181:1-10, 2004.

45. **Rioufol G, Finet G.** Non-atherosclerotic mild anterior myocardial ischaemia. *Arch Cardiovasc Dis.* 103:135-136, 2010.

46. **Rollie´ S, Mangold M, Sundmacher K.** Designing biological systems: Systems Engineering meets Synthetic Biology. *Chem Engineer Sci.* 69:1–29, 2012.

47. **Schreihofer AM, Mandel DA, Mobley SC, Stepp DW**. Impairment of sympathetic baroreceptor reflexes in obese Zucker rats. *Am J Physiol Heart Circ Physiol*. 293:H2543-H2549, 2007.

48. **Seagard JL, Bosnjak ZJ, Hopp Jr. FA, Kotrly KJ, Ebert TJ, Kampine JP.** Cardiovascular effects of general anesthesia. p. 149-170. In: "Effects of Anesthesia", Eds: Covino BR, Fozzard HA, Rehder K, Strichartz H., Waverly Press, Inc., Baltimore, MD, 1985.

49. **Segal SS.** Regulation of blood flow in the microcirculation. *Microcirculation.* 12:33-45, 2005.

50. **Sprague RS, Ellsworth ML.** Erythrocyte-derived ATP and perfusion distribution: role of intracellular and intercellular communication. *Microcirculation.* 19:430-439, 2012.

51. **Sprague RS, Bowles EA, Achilleus D, Stephenson AH, Ellis CG, Ellsworth ML.** A selective phosphodiesterase 3 inhibitor rescues low PO2-induced ATP release from erythrocytes of humans with type 2 diabetes: implication for vascular control. *Am J Physiol Heart Circ Physiol.* 301:H2466-H272, 2011.

52. **Stainsby WN, Snyder B, Welch HG.** A pictographic essay on blood and tissue oxygen transport. *Med Sci Sports Exerc.* 20:213-221, 1988.

53. **Tanofsky-Kraff M, Yanovski SZ.** Eating disorder or disordered eating? Non-normative eating patterns in obese individuals. *Obes Res.* 12:1361-1366, 2004.

54. **Tigno XT, Hansen BC, Nawang S, Shamekh R, Albano AM.** Vasomotion becomes less random as diabetes progresses in monkeys. *Microcirculation.* 18:429-439, 2011.

55. **Tran CH, Vigmond EJ, Plane F, Welsh DG.** Mechanistic basis of differential conduction in skeletal muscle arteries. *J Physiol.* 587:1301-1318, 2009.

56. **Unger RH, Scherer PE.** Gluttony, sloth and the metabolic syndrome: a roadmap to lipotoxicity. *Trends Endocrinol Metab.* 21:345-352, 2010.

57. **van der Greef J, Hankemeier T, McBurney RN.** Metabolomics-based systems biology and personalized medicine: moving towards n = 1 clinical trials? *Pharmacogenomics.* 7:1087-1094, 2006.

58. **Wagner CD, Nafz B, Persson PB.** Chaos in blood pressure control. *Cardiovasc Res.* 31:380-387, 1996.

59. **Wu F, Beard DA, Frisbee JC.** Computational analyses of intravascular tracer washout reveal altered capillary-level flow distributions in obese Zucker rats. *J Physiol.* 589:4527-4543, 2011.

Table 1. Baseline characteristics of ~17 week-old LZR and OZR used in the present study. * $p<0.05$ versus LZR. Data are presented as mean±SE.

	LZR (n=20)	**OZR (n=38)**
Mass (g)	357±9	676±10*
MAP (mmHg)	104±4	135±6*
$[Glucose]_{plasma}$ (mg/dl)	106±9	188±12*
$[Insulin]_{plasma}$ (ng/ml)	1.7±0.2	8.8±1.3*
$[Nitrotyrosine]_{plasma}$ (ng/ml)	17±4	53±7*

Table 2. Arteriolar perfusion in LZR and OZR. Data are presented for arteriolar inner diameter (ID; □m), centerline erythrocyte velocity (V_{RBC}; mm/s), and volume perfusion within the arteriole (Q; nl/s). * $p<0.05$ versus LZR; † $p<0.05$ versus OZR. Data are presented as mean±SE; -P represents treatment with phentolamine, -T represents treatment with TEMPOL, -SQ represents treatment with SQ-29548; with combinations representing treatment with multiple agents.

		LZR	OZR	O-P	O-T	O-SQ	O-PT	O-PSQ	O-TSQ	O-PTSQ
1A	ID	95±4	81±5	93±4	83±5	84±6	93±4	94±4	85±5	94±4
	V_{RBC}	56±6	42±6	53±6	46±5	44±5	53±5	53±6	47±4	54±5
	Q	248±12	135±15*	225±16†	156±13	152±11	225±9†	230±15†	167±11	234±12†
2A	ID	70±5	60±6	67±5	64±4	63±5	68±4	68±5	64±4	69±4
	V_{RBC}	50±4	34±6	47±6	38±6	36±4	46±5	48±4	41±5	49±5
	Q	120±12	60±7*	104±11†	76±10	70±6	104±6†	109±7†	82±12	115±7†
3A	ID	54±5	46±6	50±5	51±6	49±4	53±4	52±4	51±5	53±5
	V_{RBC}	35±6	24±4	34±6	25±5	27±4	35±4	36±4	27±4	36±4
	Q	50±5	25±4*	42±4†	32±6	32±4	48±5†	48±5†	33±5	50±6†
4A	ID	37±5	32±4	33±5	38±5	37±4	38±4	38±4	37±5	38±4
	V_{RBC}	35±5	20±5	30±5	24±4	23±3	32±4	33±5	24±5	36±5
	Q	24±3	10±3*	16±3	17±3	15±3	23±3†	23±4†	16±4	26±4†

FIGURE LEGENDS

Figure 1. Schematic representation of an arteriolar bifurcation used for study. Presented are the key measured parameters of arteriolar diameter and erythrocyte velocity, which are used to calculate blood flow volumes. Perfusion distribution volumes are given as the proportionality parameter □ and (1-□□□□in the two daughter arterioles arising from a parent. Please see text for additional details.

Figure 2. Frequency distribution and representative sample of the temporal changes in □ in 1A-2A (Panels A and B, respectively) and 3A-4A (Panels C and D, respectively) arteriolar bifurcations in LZR and OZR under control conditions. For data in Panels B and D, □□is determined every 20 seconds throughout a 5 minute collection window. Please see text for additional details.

Figure 3. The average □ in 1A-2A arteriolar bifurcations of LZR (Panel A) and OZR (Panel B) over the 5 minute collection period. Data (presented as mean±SE) are presented for LZR and OZR under control conditions and in OZR following treatment of the cremaster muscle with phentolamine (Phent), TEMPOL (TEM), SQ-29548, or combinations of these agents. * $p<0.05$ versus control in that strain. † $p<0.05$ versus LZR Control.

Figure 4. Data describing the cumulative changes in □ over the 5 minute collection period in 1A-2A arteriolar bifurcations in LZR and OZR. Data (presented as mean±SE) are presented for LZR and OZR under control conditions and in OZR following treatment of the cremaster muscle with phentolamine (Phent), TEMPOL (TEM), SQ-29548, or combinations of these agents. Cumulative changes in □ are summated either as differences between successive time points (Panels A and B) or as the absolute

differences between successive time points (Panels C and D). * $p<0.05$ versus control in that strain. † $p<0.05$ versus LZR control. Please see text for additional details.

Figure 5. The average in 3A-4A arteriolar bifurcations of LZR (Panel A) and OZR (Panel B) over the 5 minute collection period. Data (presented as mean±SE) are presented for LZR and OZR under control conditions and in OZR following treatment of the cremaster muscle with phentolamine (Phent), TEMPOL (TEM), SQ-29548, or combinations of these agents. * $p<0.05$ versus control in that strain. † $p<0.05$ versus LZR Control.

Figure 6. Data describing the cumulative changes in over the 5 minute collection period in 3A-4A arteriolar bifurcations in LZR and OZR. Data (presented as mean±SE) are presented for LZR and OZR under control conditions and in OZR following treatment of the cremaster muscle with phentolamine (Phent), TEMPOL (TEM), SQ-29548, or combinations of these agents. Cumulative changes in are summated either as differences between successive time points (Panels A and B) or as the absolute differences between successive time points (Panels C and D). * $p<0.05$ versus control in that strain. † $p<0.05$ versus LZR control. Please see text for additional details.

Figure 7. Data describing the changes in over the 5 minute collection window in proximal and distal arteriolar bifurcations of LZR and OZR in response to increasing concentrations of adenosine. Data (presented as mean±SE) are presented for 1A-2A arteriolar bifurcations either as average (Panel A) or as the cumulative changes in , summated as absolute differences (Panel B). Similarly, data for 3A-4A arteriolar bifurcations are presented as average (Panel C) or as the cumulative changes in , summated

as absolute differences (Panel D). * $p<0.05$ versus LZR under that condition. † $p<0.05$ versus LZR control.

Figure 8. The effectiveness of the employed interventions at restoring normal activity of □ (cumulative, absolute) at 1A-2A (Panel A) and 3A-4A (Panel B) bifurcations in OZR. Normal activity is defined as that determined in arteriolar bifurcations at those two sites in LZR. Data (presented as mean±SE) are presented for OZR following treatment of the cremaster muscle with phentolamine (Phent), TEMPOL (TEM), SQ-29548, or combinations of these agents. * $p<0.05$ versus no change under that condition.

Figure 9. Presentation of the attractor describing the overall spatial-temporal behavior of □ at 1A-2A arteriolar bifurcations in LZR (blue) and OZR (red) under control conditions (Panel A). The attractors are presented as iterated maps, where the respective value for □ is presented at multiple successive time points within that condition. In subsequent panels, the control data is greyed (light for LZR, dark for OZR) and the effects of the interventions on the attractor are presented in black. This is done for treatment with phentolamine (Panel B), TEMPOL and/or SQ-29548 (Panel C) and phentolamine and TEMPOL and/or SQ-29548 (Panel D).

Figure 10. Presentation of the attractor describing the overall spatial-temporal behavior of □ at 3A-4A arteriolar bifurcations in LZR (blue) and OZR (red) under control conditions (Panel A). The attractors are presented as iterated maps, where the respective value for □ is presented at multiple successive time points within that condition. In subsequent panels, the control data is greyed (light for LZR, dark for OZR) and the effects of the interventions on the attractor are presented in black. This is done for

treatment with phentolamine (Panel B), TEMPOL and/or SQ-29548 (Panel C) and phentolamine and TEMPOL and/or SQ-29548 (Panel D).

Figure 11. Presentation of the attractor describing the overall spatial-temporal behavior of at 1A-2A (Panel A) and 3A-4A (Panel B) arteriolar bifurcations in LZR and OZR under control conditions and in response to treatment with 10^{-3}M adenosine. As described in Figures 9 and 10, the control data is greyed (light for LZR, dark for OZR) and the effects of the elevated adenosine concentration in bifurcations in OZR are presented in black.

Figures:

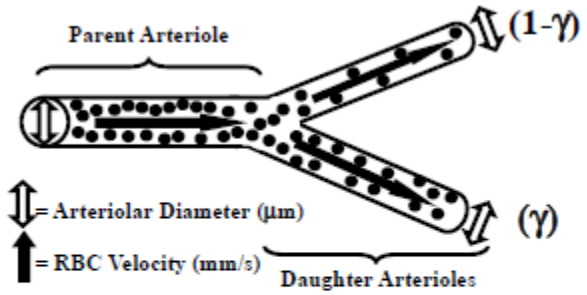

Figure 1.

Butcher et al.

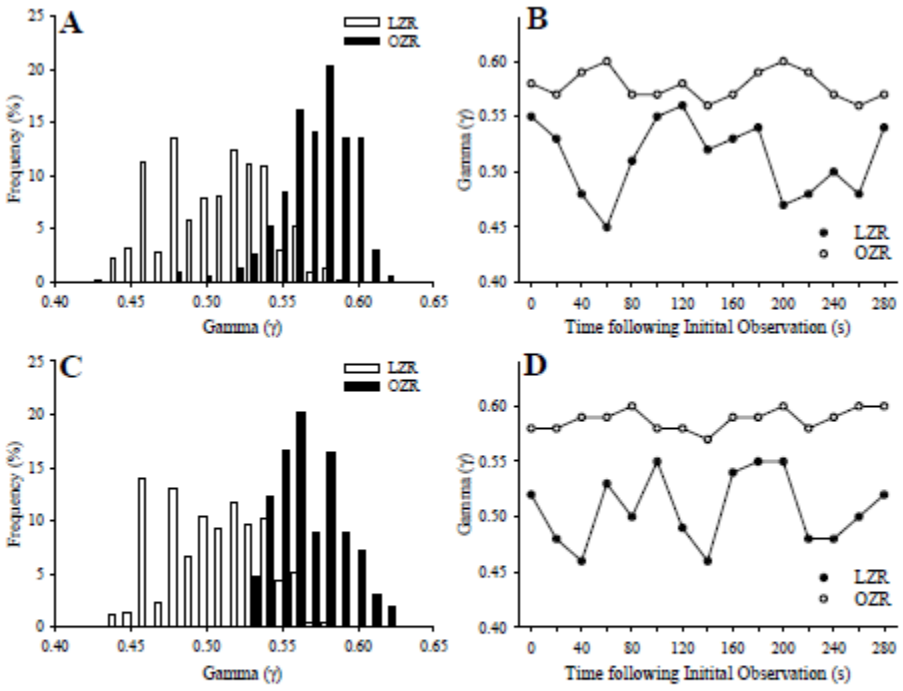

Figure 2.

Butcher et al.

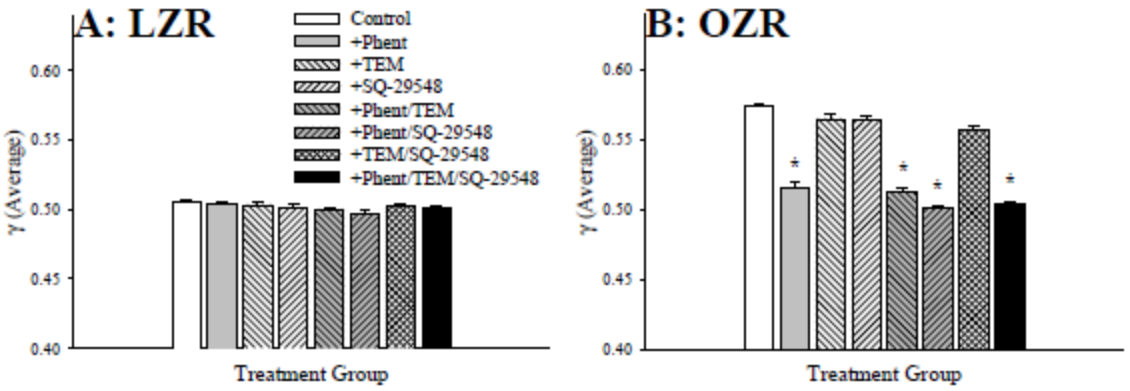

Figure 3.

Butcher et al.

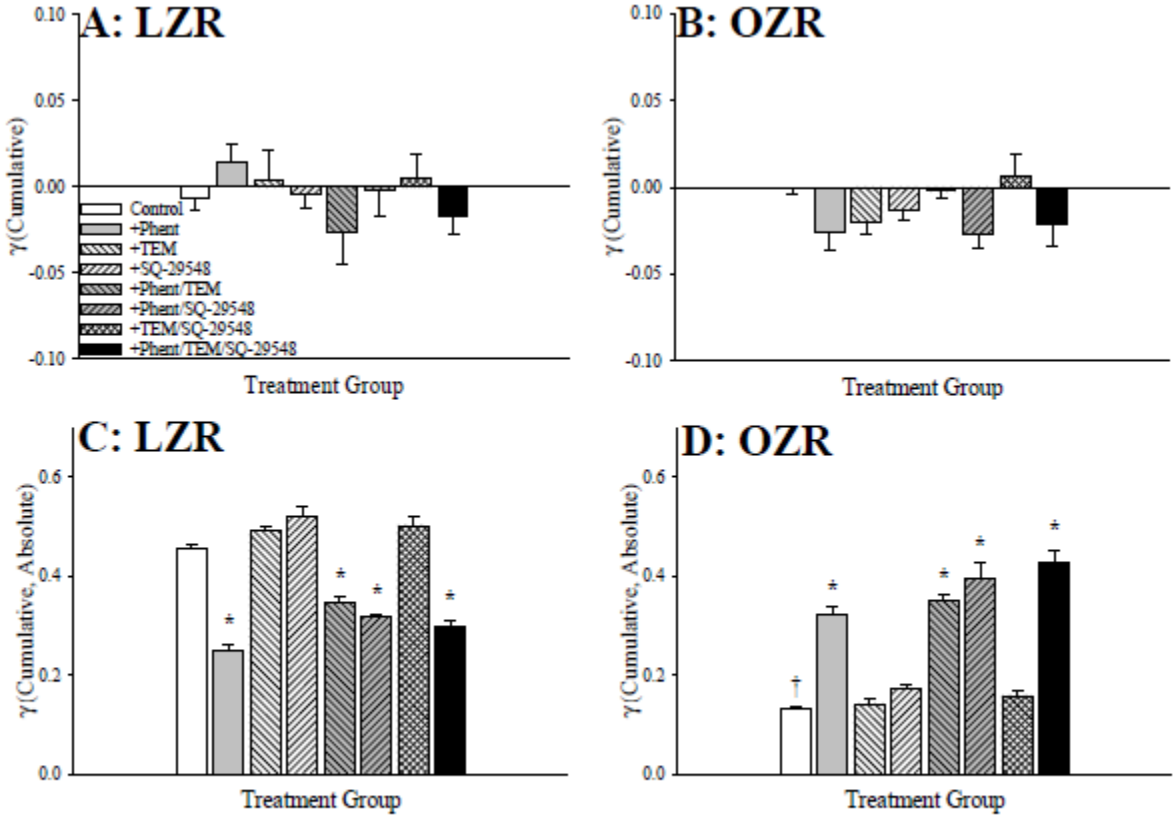

Figure 4.

Butcher et al.

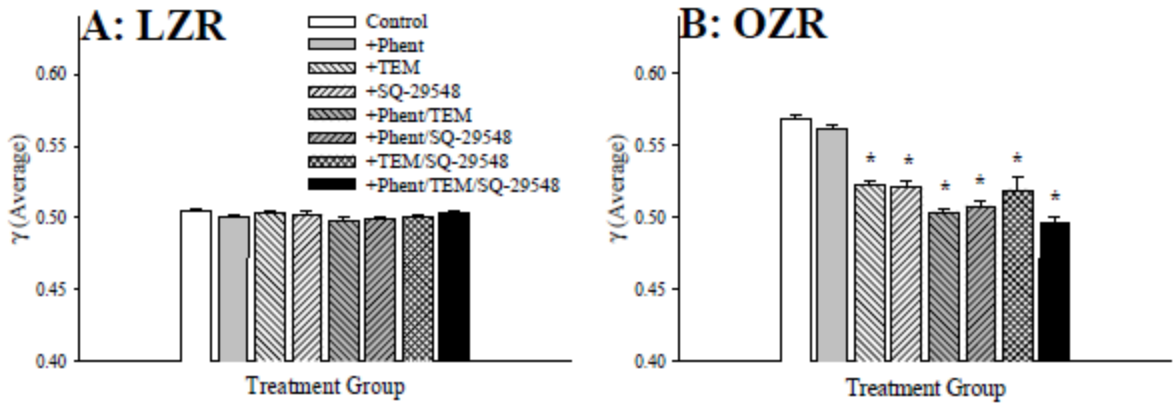

Figure 5.

Butcher et al.

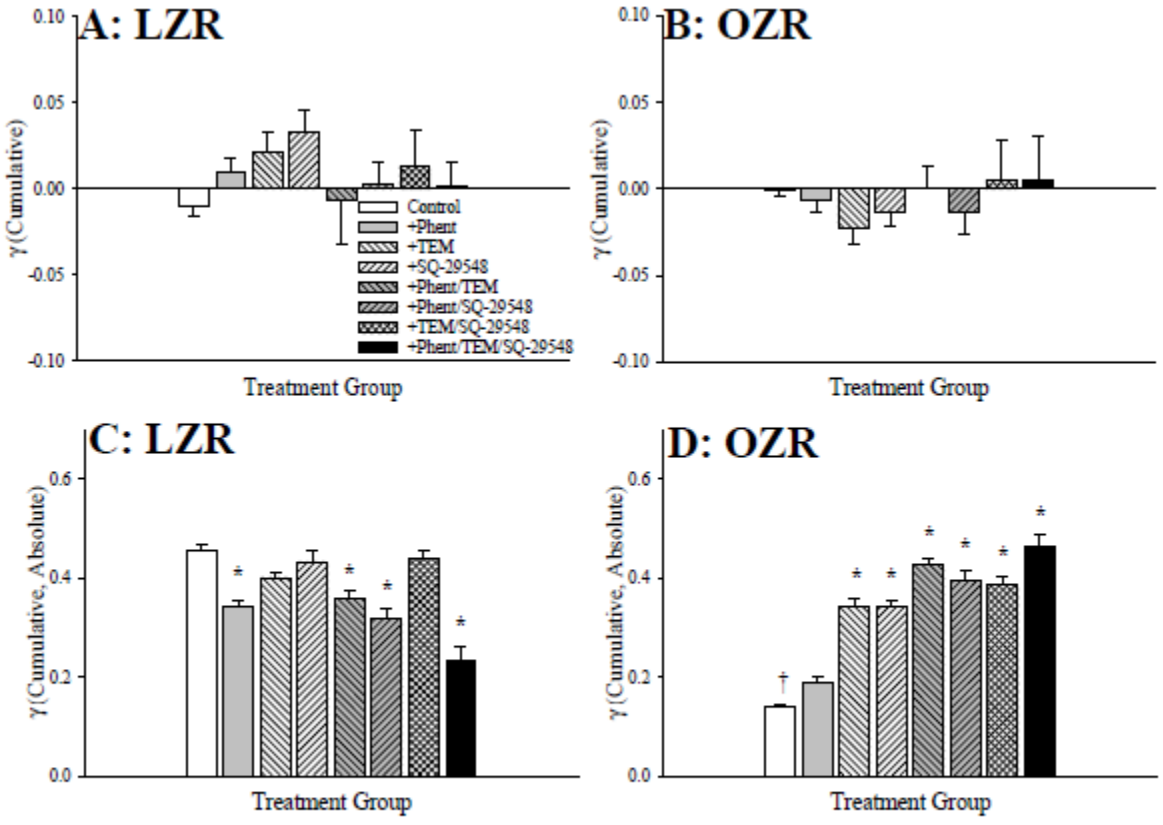

Figure 6.

Butcher et al.

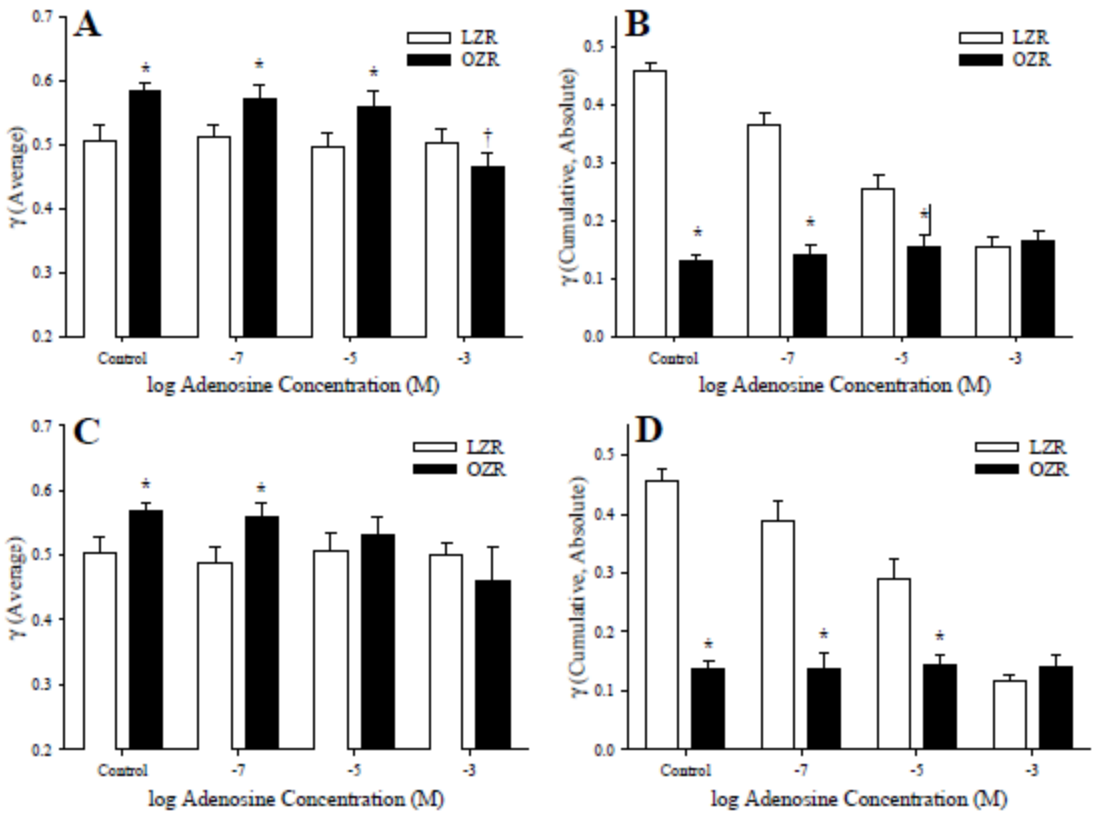

Figure 7.

Butcher et al.

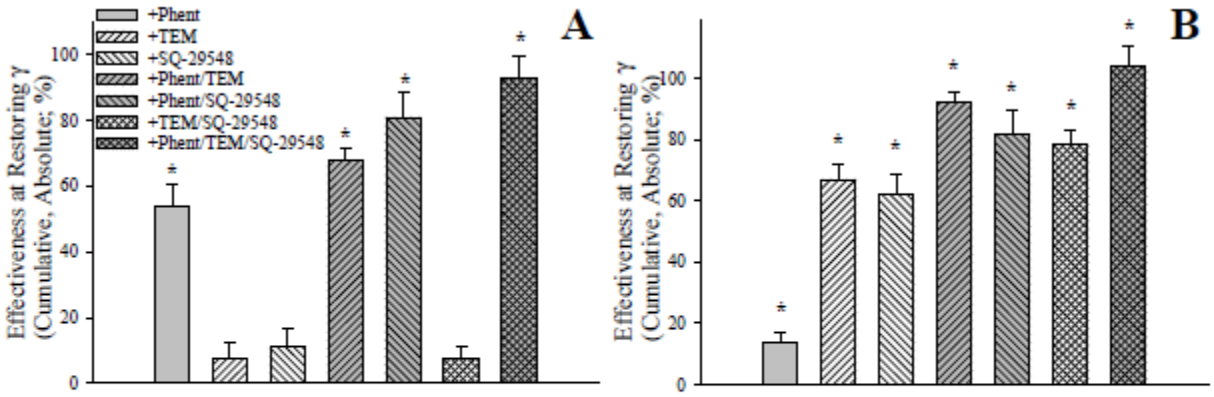

Figure 8.

Butcher et al.

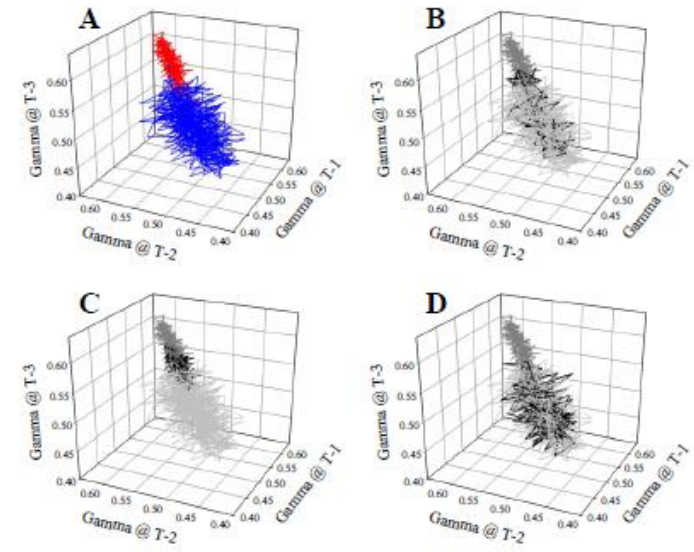

Figure 9.

Butcher et al.

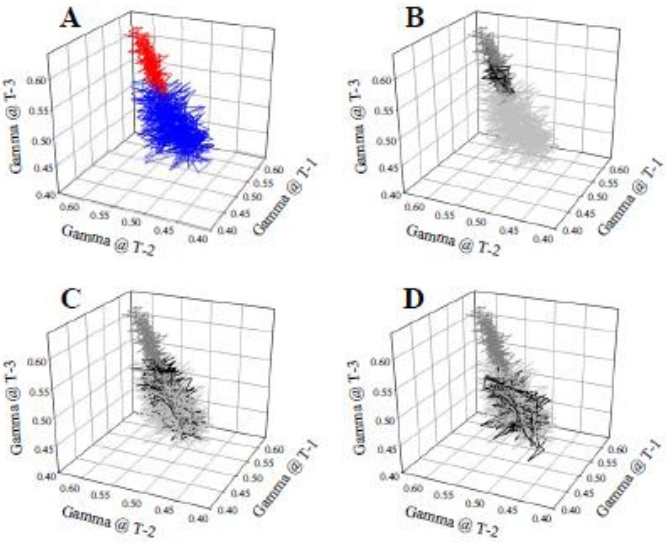

Figure 10.

Butcher et al.

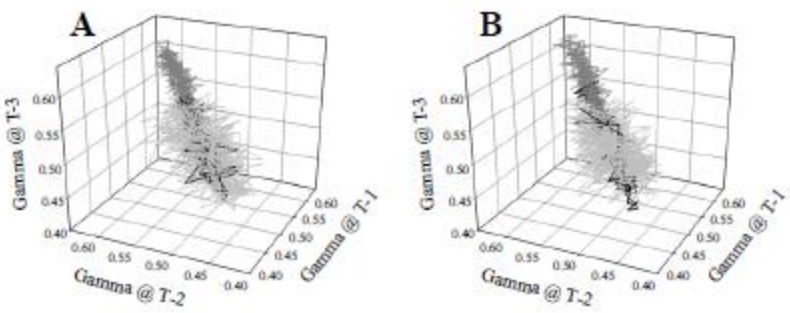

Figure 11.

Butcher et al.

Conceptual Framework

The fourth chapter is entitled "Blunted Temporal Activity of Microvascular Perfusion Heterogeneity in Metabolic Syndrome: A New Attractor for Peripheral Vascular Disease?". It addresses what we hypothesized would be the logical compensation for the increase in perfusion heterogeneity at bifurcations seen in the previous paper, what is known as "temporal switching". The perfusion heterogeneity at bifurcations is iterated longitudinally across the entire microvascular network and should lead to local regions of tissue with an accelerated buildup of metabolic dilators, thus increasing the temporal switching at bifurcations to meet that demand. Interestingly, the temporal activity was blunted in both the proximal and distal microcirculation. This suggests that the poor muscle performance in the OZR is the cumulative response of spatial and temporal impairments to blood flow regulation.

Of special relevance is the identification of an attractor for PVD, which is elucidated by the presentation of the temporal data as an iterated map. Beyond a scientific curiosity, an attractor is significant because it describes how a dynamic system will evolve toward a set of conditions over time. The attractor generated for a system demonstrates the ability of the system to respond to perturbations, and can infer the flexibility of a network as the system will seek to return to its attractor upon being disturbed. The attractor for the LZR, representing health, has a wide range and is centered on 0.5. This remains constant for both the proximal and distal microcirculation. The attractor for the OZR is not only elevated throughout the entire microcirculation, but also significantly limited in its range, suggesting that the system is limited in its ability to respond to perturbations. This compromised network flexibility could be a major contributor to the development of poor vascular outcomes in MetSyn subjects.

Chapter 5

Altered Hemodynamics within the Skeletal Muscle Microvasculature in the Obese Zucker Rats

Joshua T. Butcher, Fan Wu, Steven D. Brooks, Shyla C. Stanley, and Jefferson C. Frisbee

Department of Physiology and Pharmacology and Center for Cardiovascular and Respiratory Sciences

West Virginia University HSC, Morgantown, WV

Address for Correspondence:

Jefferson C. Frisbee, Ph.D.

Center for Cardiovascular and Respiratory Sciences

Department of Physiology and Pharmacology

West Virginia University Health Sciences Center; 3152 HSN

1 Medical Center Drive

Morgantown, WV 26506

Phone: (304) 293-6527

Fax: (304) 293-5513

Email: jefrisbee@hsc.wvu.edu

ABSTRACT

Increasing evidence has indicated that a key contributor to the development, maintenance, and progression of peripheral vascular disease (PVD) is altered microvascular structure, function, and reactivity. Recent research has observed an increasingly heterogeneous perfusion distribution within the skeletal muscle microvasculature of the obese Zucker rat, a model of PVD. This heterogeneous perfusion distribution is iterated throughout the microvascular network and dominated by spatially distinct mechanisms; driven by alpha-adrenergic dysfunction in proximal microvessels and oxidant stress based increases in vascular thromboxane A_2 in distal microvessels. Additional research demonstrated that a temporal compensation for the increased heterogeneous perfusion distribution was also blunted. Taken together, the spatial and temporal alterations to microvascular blood flow will serve to entrench a physiological state of inadequate blood flow regulation throughout skeletal muscle. One of the hallmark characteristics of PVD is an inability to resist the development of fatigue. The heterogeneous perfusion distribution within the microvasculature suggests that the OZR's inability to resist fatigue may be the result of a dysfunctional distribution of erythrocytes in the skeletal muscle microcirculation. To determine erythrocyte distribution with the capillaries and arterioles we utilized the *in situ* cremaster preparation with video microscopy to obtain a representative sample of capillary tube hematocrit and the blood perfused isolated hindlimb preparation with I^{125} labeled albumin and Cr^{51} labeled RBCs to obtain microvascular hematocrit. The analysis indicates that the cumulative sum of altered spatial and temporal regulation of microvascular perfusion distribution results in a lowered microvascular hematocrit and a large variation in capillary hematocrit in the OZR compared to the LZR. This altered erythrocyte distribution represents a significant contributor to the poor muscle performance observed in the OZR.

Key Words: microcirculation; microvascular hematocrit; obese zucker rat; peripheral vascular disease; microvascular dysfunction; network hemodynamics

INTRODUCTION

PVD is an insidious pathologic state that ultimately deprives organs of adequate blood flow and afflicts between 8-13 million Americans. The prevalence of PVD increases with age, afflicting 10-20% of the population over 60 years of age. Once diagnosed, PVD is largely irreversible barring surgery, and possesses a high direct and indirect cost burden to society[29, 30] . A growing subset of the population presents with the overt signs of PVD, but without the classically demonstrated atherosclerotic lesions, suggesting that a significant contributor to the development of PVD is microvascular dysfunction.

Human subjects diagnosed with the Metabolic Syndrome (MetSyn) possess a significantly greater risk of developing PVD. The significance of this cannot be understated, as ~34% of the U.S. meet the diagnosable criteria for MetSyn today[29, 31-34]. The rate of the overweight, obese, and extremely obese adults within the U.S. population is over 75%[35]. Given that obesity is generally understood to be the initiating condition for the development of MetSyn, there is concern that a significant portion of the population is at risk for developing MetSyn and the associated pathologies at a much younger age.

The obese Zucker rat (OZR) is a rodent model for studying the development of MetSyn. Owing to its dysfunctional leptin receptor the OZR possesses an impaired satiety reflex, which results in chronic hyperphagia. Thus, by ≈17 weeks of age, the OZR experiences significant increases in mass, moderate hypertension, insulin resistance, loss of glycemic control, and a pro-inflammatory and pro-thrombotic state. The OZR is an appropriate model for examining the development of MetSyn and non-atherosclerotic PVD. Recent studies have demonstrated that MetSyn in the OZR results in a progressive decay of skeletal muscle performance[36, 37]. There appears to be dual contributors to this inability of skeletal muscle to resist fatigue. One of the contributors appears to be alpha-adrenergic in origin and restricts bulk blood flow delivery to the skeletal muscle. Another contributor is impaired oxygen uptake, resulting from an increase in oxidant stress, which reduces NO bioavailability as well as altering arachidonic acid metabolism to increase vascular production of thromboxane A_2 (TxA_2). The simultaneous treatment of both altered systems results in improved performance outcomes in the OZR. Additional studies concluded that the above mentioned contributors to impaired skeletal muscle

performance impact the microcirculatory system in a spatially distinct manner. The dysfunction in the proximal microcirculation is dominated by altered alpha-adrenergic based elements to vascular tone, while the dysfunction within the distal microcirculation is characterized by endothelial dysfunction, specifically via altered metabolism of arachidonic acid (AA)[38, 39]. However, both serve to increase perfusion heterogeneity at bifurcations in the microvasculature. The interpretation of the above work suggests PVD promotes perfusion heterogeneity at microvascular bifurcations through spatially distinct mechanisms[40, 41]. Further research postulated that, due to the increased perfusion heterogeneity at bifurcations, temporal switching between the low flow and high flow branch would increase due to accelerated buildup of metabolites, or other regulatory signals, downstream within the low flow pathway. However, our most recent data suggested that temporal switching is actually blunted at bifurcations in the OZR[40, 41]. The cumulative outcome of increased perfusion heterogeneity across a microvascular network, along with simultaneous blunting of the temporal switching, will entrench the impairments to perfusion distribution and mass transport/exchange, ultimately contributing to negative outcomes for skeletal muscle performance. Our hypothesis, building on the above work, is that the Metabolic Syndrome entrenches alterations to blood flow distribution and negatively impacts erythrocyte distribution throughout the microvasculature. Specifically, we hypothesize that the alterations to perfusion distribution in the OZR, when iterated throughout the entire skeletal muscle network, will serve to lower average microvascular hematocrit and thus result in impaired oxygen delivery within the capillaries.

We predict that hematocrit in the skeletal muscle microcirculation of the OZR will be significantly lower across the whole organ compared to the LZR. This overall reduction of hematocrit would occur in the OZR due to a heterogeneous perfusion distribution that would skew the hematocrit disproportionally low compared to flow distribution. The primary goal of the experiment is to obtain microvascular hematocrit (H_{mv}) using the Overholser model, as previously described[42]. Additionally, capillary tube hematocrit will be obtained in a representative sample to determine the impact of an altered flow distribution on oxygen exchange vessels. The inability of the skeletal muscle microcirculation to

adequately regulate perfusion distribution becomes progressively more relevant as increased metabolic demand cannot be matched with increased perfusion. At rest, the lowered average hematocrit may have little impact on tissue oxygenation, but with increased metabolic demand this would result in an inadequate supply of oxygen to tissue. This would offer insight into the acceleration in fatigue resistance, and also into the increased inflammatory state often observed in the MetSyn, which may be due to the tissue hypoxia.

MATERIALS AND METHODS

Approximately 17 week old male lean and obese Zucker rats (Harlan) were used. All protocols have prior approval of the IACUC, the rats will be housed within the animal quarters of WVU, and provided with sterilized food and water *ad libitum*. All animals were anesthetized with sodium pentobarbital (390mg/mL), and a patent airway maintained with tracheal intubation. At the conclusion of the experiment, all animals are humanely euthanized with excess sodium pentobarbital and a bilateral pneumothoractomy.

Isolated Hind Limb preparation and Tracer Washout Curves - In a set of age matched animals, the self-perfused left hindlimb of each animal will be isolated in situ, as demonstrated previously[43]. The carotid artery will be cannulated for monitoring of mean arterial pressure and the jugular vein cannulated for infusion of heparin (500IU/kg) to prevent coagulation of the blood. An angiocatheter will be inserted into the femoral artery for insertion of each bolus tracer. A Transonic probe (0.5-0.7 PS) of the appropriate size will be placed on the femoral artery to monitor perfusion. A small shunt will be placed in the femoral vein of the gastrocnemius muscle to facilitate sampling of the venous effluent. The above referenced interventions, phentolamine (10 mg/kg), TEMPOL (50 mg/kg) and/or SQ-29548 (10 mg/kg), will be intravenously introduced to the animal and tested for efficacy using phenylephrine (10 μg/kg), methacholine (10 μg/kg) or U-46619 (10 μg/kg), respectively. Two radionuclides will be utilized, I^{125} labeled albumin and Cr^{51} bound to red blood cells. Upon bolus injection, the venous effluent will be

collected at a rate of 1/s for the subsequent 35 seconds. The subsequent injection, after each intervention, did not occur until 30 minutes of perfusion with an injection of homologous erythrocytes used to replace the lost hematocrit. They were examined for estimated microvascular hematocrit (H_{mv}). All were prepared using published protocols[42, 44-48].

Preparation of In Situ Cremaster Muscle: In a separate set of age matched animals the cremaster muscle was separated from surrounding tissues and isolated for viewing with intravital microscopy. During the entire experiment the cremaster was maintained at 35^{o}C, superfused with a physiological salt solution and bubbled with a 5% CO_2/balance N_2 gas. Capillaries with red blood cell flow were identified using on screen video microscopy and hematocrit was quantified at 10 vessels per animal. All procedures were performed under control conditions in LZR and OZR, and the following interventions were added to the superfusate; the anti-oxidant TEMPOL (10^{-3} M), the TxA_2 receptor antagonist SQ-29548 (10^{-4} M), and/or the $alpha_1$/$alpha_2$ adrenergic receptor antagonist phentolamine (10^{-5} M).

Data Analysis

For the tracer washout analysis, the following equations were used from Overholser et al. to obtain the hematocrit reduction ratio (h_r)[42]. The hematocrit reduction ratio is the ratio of the microvascular hematocrit to the large vessel hematocrit and is calculated from the equation below.

$C_{l.organ}(t\text{-}T) = h_r C_{R.organ}[(t\text{-}T)hr)$

where $C_{l.organ}$ is the albumin tracer curve, $C_{R.organ}$ is the red cell tracer curve, t is time, and T is the mean transit time. This will allow deduction of the microvascular hematocrit reduction ratio. The h_r can be entered into the following equation to calculate microvascular hematocrit.

$H_r = H_{mv}/ H_{lv}$ where H_{mv} is microvascular hematocrit and H_{lv} is large vessel hematocrit.

Capillary tube hematocrit was calculated from video stills utilizing the *in situ* cremaster preparation, as described previously[40, 41]. It was calculated by counting the number of red blood cells in a

known length and diameter of vasculature. All data is presented as mean ± SEM with statistically significant differences represented by $p<0.05$. Student's t-test or analysis of variance (ANOVA) with Student-Newman-Keuls post-hoc test was used as needed.

RESULTS

Table 1 contains baseline characteristics of the lean and obese Zucker rats used in the indicator dilution washout study. Compared to the LZR controls, at ≈17 weeks of age the OZR model exhibits significantly increased mass, moderate increases in mean arterial pressure, insulin resistance, dyslipidemia, and elevated plasma glucose levels.

Table 1: Indicator Dilution Washout	LZR	OZR
Mass (grams)	361 ± 9	688 ± 12
MAP	102 ± 4	138 ± 10

Figure 1 is a representative figure containing the washout data for I^{-125} labeled albumin and Cr^{-51} labeled RBCs in both the OZR and LZR. The solid red and black lines are the LZR albumin and RBC tracers respectively. The dotted red and black lines are the OZR albumin and RBC tracers respectively. It is evident that the OZR RBC's initially washout more rapidly than the LZR RBC's, but then slow at the end of the time period. The OZR albumin curve has a smaller height but a much higher tail than the LZR control.

Figure 2 presents the microvascular hematocrit as calculated from the ratio between the animal's respective albumin and RBC tracer washout curves. It shows that the LZR (n=5) microvascular hematocrit remains similar to the average large vessel hematocrit of 45. The OZR (n=8) microvascular hematocrit is significantly lower than the LZR control. The microvascular hematocrits of the OZR with interventions of phentolamine or TEMPOL/SQ-29548 appear lower but have very large SEM. The microvascular hematocrit of the OZR with all treatments is significantly elevated above the OZR baseline. * $p < 0.05$ vs. LZR. † $p < 0.05$ vs. OZR.

Figure 3 is the capillary tube hematocrit as calculated from video microscopy. There were no significant differences between LZR, OZR, and OZR with treatments. * $p < 0.05$ vs. LZR. † < 0.05 OZR.

Discussion

The culmination of recent work has shown that alterations within the skeletal muscle microcirculation of the obese Zucker rat result in increasingly heterogeneous perfusion distributions at bifurcations. Specifically, there is an increased perfusion distribution in the OZR with spatially distinct mechanisms that is unable to be compensated for temporally. This results in a 'low flow" and "high flow" pathway at bifurcations that is iterated across the microcirculatory network. This inability to adequately distribute blood flow will have a negative impact on erythrocyte distribution, with the bulk of RBC's flowing down the "high flow" pathway and being unable to redistribute to the "low flow" pathway with increased metabolic demand. The importance of distribution of erythrocytes lies within three basic concepts of erythrocyte distribution within blood flow. The first is the Fahraeus effect, which is a lowered tube hematocrit caused by the differential velocities of RBC's and plasma. The second is the Fahraeus network effect, which describes how an unequal hematocrit distribution at a proximal bifurcation will lead to increasingly heterogeneous hematocrit distribution further downstream and result in an averaged lower hematocrit. The final concept is phase separation, which describes how low flow branches or side branches may "skim" the RBC poor areas of the blood, again leading to lowered hematocrit in those side branches relative to the high flow[49]. The integration of all three concepts, when combined with the evidence of increased perfusion distribution heterogeneity in the OZR, suggests that this will lead to an overall reduction in microvascular hematocrit as well as capillary tube hematocrit.

The results of the indicator dilution tracer washout experiment show that there is a reduction in OZR microvascular hematocrit compared to the LZR. The treatments of phentolamine and TEMPOL/SQ-29548 by themselves demonstrate not necessarily a significant increase in hematocrit distribution, but certainly a large increase in the variance that removes any significance compared to the

LZR. However, treatment with all of the interventions in the OZR does significantly improve microvascular hematocrit compared to the LZR.

The capillary tube hematocrit does not show a significant difference between the LZR and OZR, or with any of the OZR interventional groups. However, what is readily apparent is the large variance observed in the OZR compared to any other group, LZR, OZR, or OZR + intervention. This indicates that there is indeed significant high and low hematocrit levels within the gas exchange vessels of the OZR, heterogeneity not observed in the LZR. The inability of this technique to obtain the lower hematocrit levels hypothesized may in fact be a limitation of the preparation itself, whereby vessels are chosen that have steady visible RBC flow, resulting in an inadequate sample size representative of the population.

The conclusion of the above research is that there is a lowered average hematocrit within the OZR microcirculation. It is a result of the entrenched heterogeneous perfusion distribution observed at bifurcations within the OZR, and not only serves as a significant contributor to the impaired performance of skeletal muscle, but most likely would result in development of ischemic or pro-inflammatory regions of tissue where the low distribution of erythrocytes exists. While the hematocrit within the capillaries does not initially show the differences hypothesized, the increased variance would indicate areas of significantly elevated and lowered hematocrit compared to the LZR, suggesting that perhaps our sample population is not representative of the whole tissue bed.

Taken together with our previous research, the outcome of this lowered microvascular hematocrit and increase in variance within the capillaries allows for a better understanding of the progressive decay of skeletal muscle function within MetSyn. Increasing evidence points toward altered regulation of microvascular control, largely influenced by alpha adrenergic dysfunction and oxidant stress based increases in thromboxane A_2, as a significant contributor to this dysfunction. This results in an inability of the peripheral vascular system to adequately deliver oxygen to the appropriate local tissue region. Speculatively, this has tremendous impact on the human population of MetSyn, including those already

diagnosed with PVD. Those diagnosed with PVD will be best served with not just exercise, but also treatment of the underlying microvascular problems. Further, as the epidemic of MetSyn and PVD increases within developed countries, the subpopulation of subject presenting without atherosclerotic plagues and lesions will require alternative diagnostic exams, as well as treatment of the microvascular disease.

ACKNOWLEDGEMENTS

This study was supported by grants from the National Institutes of Health (NIH DK R01 64668, T32 HL 90610 and RR 2865AR) and the American Heart Association (AHA EIA 0740129N). The authors also wish to express their gratitude for the expert technical assistance from Ms. Milinda James from the Department of Physiology and Pharmacology at West Virginia University and for support provided through the Translational Research Facility in the Center for Cardiovascular and Respiratory Sciences at the West Virginia University HSC.

Reference List

(1) **Ouriel K. Detection of peripheral arterial disease in primary care. *JAMA* 2001 September 19;286(11):1380-1.**

(2) **Mahoney EM, Wang K, Keo HH et al. Vascular hospitalization rates and costs in patients with peripheral artery disease in the United States. *Circ Cardiovasc Qual Outcomes* 2010 November;3(6):642-51.**

(3) **Ouriel K. Peripheral arterial disease. *Lancet* 2001 October 13;358(9289):1257-64.**

(4) **Allison MA, Ho E, Denenberg JO et al. Ethnic-specific prevalence of peripheral arterial disease in the United States. *Am J Prev Med* 2007 April;32(4):328-33.**

(5) **Lloyd-Jones D, Adams RJ, Brown TM et al. Heart disease and stroke statistics--2010 update: a report from the American Heart Association. *Circulation* 2010 February 23;121(7):e46-e215.**

(6) **Hamburg NM, Balady GJ. Exercise rehabilitation in peripheral artery disease: functional impact and mechanisms of benefits. *Circulation* 2011 January 4;123(1):87-97.**

(7) **Long J, Modrall JG, Parker BJ, Swann A, Welborn MB, III, Anthony T. Correlation between ankle-brachial index, symptoms, and health-related quality of life in patients with peripheral vascular disease. *J Vasc Surg* 2004 April;39(4):723-7.**

(8) **Frisbee JC, Goodwill AG, Butcher JT, Olfert IM. Divergence between arterial perfusion and fatigue resistance in skeletal muscle in the metabolic syndrome. *Exp Physiol* 2011 March;96(3):369-83.**

(9) **Goodwill AG, Frisbee SJ, Stapleton PA, James ME, Frisbee JC. Impact of chronic anticholesterol therapy on development of microvascular rarefaction in the metabolic syndrome. *Microcirculation* 2009 November;16(8):667-84.**

(10) **Alberti KG, Zimmet P, Shaw J. The metabolic syndrome--a new worldwide definition. *Lancet* 2005 September 24;366(9491):1059-62.**

(11) **Misra A, Khurana L. Obesity and the metabolic syndrome in developing countries. *J Clin Endocrinol Metab* 2008 November;93(11 Suppl 1):S9-30.**

(12) **Flegal KM, Carroll MD, Kit BK, Ogden CL. Prevalence of obesity and trends in the distribution of body mass index among US adults, 1999-2010. *JAMA* 2012 February 1;307(5):491-7.**

(13) **Cali AM, Caprio S. Obesity in children and adolescents. *J Clin Endocrinol Metab* 2008 November;93(11 Suppl 1):S31-S36.**

(14) **Ford ES, Mokdad AH. Epidemiology of obesity in the Western Hemisphere. *J Clin Endocrinol Metab* 2008 November;93(11 Suppl 1):S1-S8.**

(15) Ogden CL, Carroll MD, Curtin LR, McDowell MA, Tabak CJ, Flegal KM. Prevalence of overweight and obesity in the United States, 1999-2004. *JAMA* 2006 April 5;295(13):1549-55.

(16) Esposito K, Marfella R, Ciotola M et al. Effect of a mediterranean-style diet on endothelial dysfunction and markers of vascular inflammation in the metabolic syndrome: a randomized trial. *JAMA* 2004 September 22;292(12):1440-6.

(17) Scuteri A, Najjar SS, Muller DC et al. Metabolic syndrome amplifies the age-associated increases in vascular thickness and stiffness. *J Am Coll Cardiol* 2004 April 21;43(8):1388-95.

(18) Hill MA, Davis MJ, Meininger GA, Potocnik SJ, Murphy TV. Arteriolar myogenic signalling mechanisms: Implications for local vascular function. *Clin Hemorheol Microcirc* 2006;34(1-2):67-79.

(19) Hill MA, Zou H, Potocnik SJ, Meininger GA, Davis MJ. Invited review: arteriolar smooth muscle mechanotransduction: Ca(2+) signaling pathways underlying myogenic reactivity. *J Appl Physiol (1985)* 2001 August;91(2):973-83.

(20) Kuo L, Chilian WM, Davis MJ. Coronary arteriolar myogenic response is independent of endothelium. *Circ Res* 1990 March;66(3):860-6.

(21) Kuo L, Chilian WM, Davis MJ. Coronary arteriolar myogenic response is independent of endothelium. *Circ Res* 1990 March;66(3):860-6.

(22) Stepp DW, Frisbee JC. Augmented adrenergic vasoconstriction in hypertensive diabetic obese Zucker rats. *Am J Physiol Heart Circ Physiol* 2002 March;282(3):H816-H820.

(23) Saltzman D, DeLano FA, Schmid-Schonbein GW. The microvasculature in skeletal muscle. VI. Adrenergic innervation of arterioles in normotensive and spontaneously hypertensive rats. *Microvasc Res* 1992 November;44(3):263-73.

(24) Frisbee JC. Enhanced arteriolar alpha-adrenergic constriction impairs dilator responses and skeletal muscle perfusion in obese Zucker rats. *J Appl Physiol* 2004 August;97(2):764-72.

(25) Limberg JK, Morgan BJ, Sebranek JJ et al. Altered neurovascular control of the resting circulation in human metabolic syndrome. *J Physiol* 2012 December 1;590(Pt 23):6109-19.

(26) Licht CM, de Geus EJ, Penninx BW. Dysregulation of the autonomic nervous system predicts the development of the metabolic syndrome. *J Clin Endocrinol Metab* 2013 June;98(6):2484-93.

(27) Roberts CK, Sindhu KK. Oxidative stress and metabolic syndrome. *Life Sci* 2009 May 22;84(21-22):705-12.

(28) Goodwill AG, Stapleton PA, James ME, d'Audiffret AC, Frisbee JC. Increased arachidonic acid-induced thromboxane generation impairs skeletal muscle arteriolar dilation with genetic dyslipidemia. *Microcirculation* 2008 October;15(7):621-31.

(29) Beckman JA, Creager MA, Libby P. Diabetes and atherosclerosis: epidemiology, pathophysiology, and management. *JAMA* 2002 May 15;287(19):2570-81.

(30) Holvoet P. Relations between metabolic syndrome, oxidative stress and inflammation and cardiovascular disease. *Verh K Acad Geneeskd Belg* 2008;70(3):193-219.

(31) Ogden CL, Carroll MD, Kit BK, Flegal KM. Prevalence of obesity in the United States, 2009-2010. *NCHS Data Brief* 2012 January;(82):1-8.

(32) Bray GA, Bellanger T. Epidemiology, trends, and morbidities of obesity and the metabolic syndrome. *Endocrine* 2006 February;29(1):109-17.

(33) Hirsch AT, Hartman L, Town RJ, Virnig BA. National health care costs of peripheral arterial disease in the Medicare population. *Vasc Med* 2008 August;13(3):209-15.

(34) Grundy SM, Brewer HB, Jr., Cleeman JI, Smith SC, Jr., Lenfant C. Definition of metabolic syndrome: Report of the National Heart, Lung, and Blood Institute/American Heart Association conference on scientific issues related to definition. *Circulation* 2004 January 27;109(3):433-8.

(35) Flegal KM, Carroll MD, Kit BK, Ogden CL. Prevalence of obesity and trends in the distribution of body mass index among US adults, 1999-2010. *JAMA* 2012 February 1;307(5):491-7.

(36) Bray GA. The Zucker-fatty rat: a review. *Fed Proc* 1977 February;36(2):148-53.

(37) Frisbee JC, Goodwill AG, Butcher JT, Olfert IM. Divergence between arterial perfusion and fatigue resistance in skeletal muscle in the metabolic syndrome. *Exp Physiol* 2011 March;96(3):369-83.

(38) Frisbee JC, Hollander JM, Brock RW, Yu HG, Boegehold MA. Integration of skeletal muscle resistance arteriolar reactivity for perfusion responses in the metabolic syndrome. *Am J Physiol Regul Integr Comp Physiol* 2009 June;296(6):R1771-R1782.

(39) Xiang L, Naik JS, Hodnett BL, Hester RL. Altered arachidonic acid metabolism impairs functional vasodilation in metabolic syndrome. *Am J Physiol Regul Integr Comp Physiol* 2006 January;290(1):R134-R138.

(40) Butcher JT, Goodwill AG, Stanley SC, Frisbee JC. Blunted temporal activity of microvascular perfusion heterogeneity in metabolic syndrome: a new attractor for peripheral vascular disease? *Am J Physiol Heart Circ Physiol* 2013 February 15;304(4):H547-H558.

(41) Frisbee JC, Wu F, Goodwill AG, Butcher JT, Beard DA. Spatial heterogeneity in skeletal muscle microvascular blood flow distribution is increased in the metabolic syndrome. *Am J Physiol Regul Integr Comp Physiol* 2011 October;301(4):R975-R986.

(42) Overholser KA, Lomangino NA, Harris TR, Bradley JD, Bosan S. Deduction of pulmonary microvascular hematocrit from indicator dilution curves. *Bull Math Biol* 1994 March;56(2):225-47.

(43) Wu F, Beard DA, Frisbee JC. Computational analyses of intravascular tracer washout reveal altered capillary-level flow distributions in obese Zucker rats. *J Physiol* 2011 September 15;589(Pt 18):4527-43.

(44) Brigham KL, Faulkner SL, Fisher RD, Bender HW, Jr. Lung water and urea indicator dilution studies in cardiac surgery patients. Comparisons of measurements in aortocoronary bypass and mitral valve replacement. *Circulation* 1976 February;53(2):369-76.

(45) Frisbee JC, Barclay JK. Microvascular hematocrit and permeability-surface area product in contracting canine skeletal muscle in situ. *Microvasc Res* 1998 March;55(2):153-64.

(46) Frisbee JC, Barclay JK. Microvascular hematocrit and permeability-surface area product of in situ canine skeletal muscle during fatigue. *Microvasc Res* 1999 March;57(2):203-7.

(47) Goresky CA, Bach GC, Nadeau BE. On the uptake of materials by the intact liver. The concentrative transport of rubidium-86. *J Clin Invest* 1973 May;52(5):975-90.

(48) Goresky CA, Simard A, Schwab AJ. Increased hepatocyte permeability surface area product for 86Rb with increase in blood flow. *Circ Res* 1997 May;80(5):645-54.

(49) Pries AR, Secomb TW, Gaehtgens P. Biophysical aspects of blood flow in the microvasculature. *Cardiovasc Res* 1996 October;32(4):654-67.

Figure Legends

Figure 1: Representative figure of tracer washout curves. Presented are the I^{-125} labeled albumin (red lines) and the Cr^{-51} red blood cells (black lines). The LZR lines are solid and the OZR lines are dashed. The microvascular hematocrit is calculated as the ratio between the two lines using Overholser et al.

Figure 2: Bar chart showing the microvascular hematocrit as calculated from tracer washout curves of LZR, OZR, and OZR + interventions. Data is resented as mean ± SEM. * $p < 0.05$ vs. LZR. † $p < 0.05$ vs. OZR.

Figure 3: Bar chart showing capillary tube hematocrit as calculated from video stills for the LZR, OZR, and OZR ± interventions. Data is presented as mean ± SEM. * $p < 0.05$ vs. LZR. † $p < 0.05$ vs. OZR.

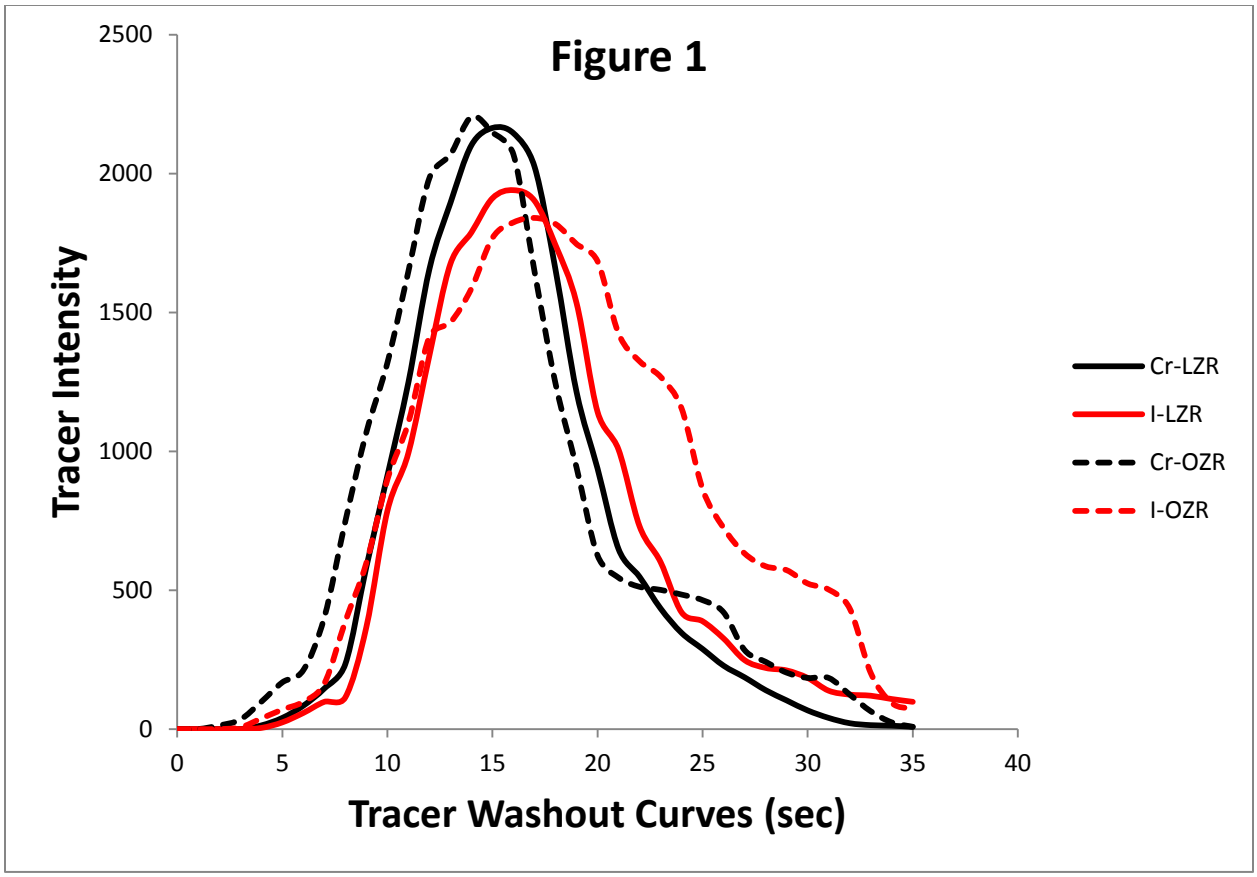
Figure 1
Tracer Intensity
2500
2000
1500
1000
500
0
0
5
10
15
20
25
30
35
40
Tracer Washout Curves (sec)
Cr-LZR
I-LZR
Cr-OZR
I-OZR

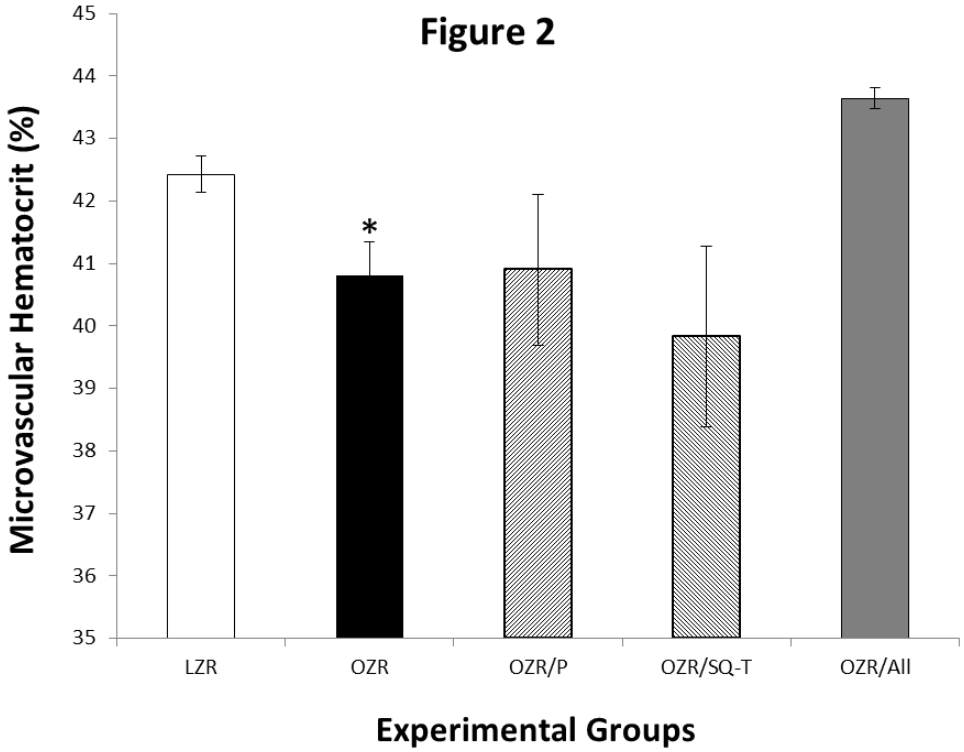
Figure 2
Microvascular Hematocrit (%)
45
44
43
42
41
40
39
38
37
36
35
*
LZR
OZR
OZR/P
OZR/SQ-T
OZR/All
Experimental Groups

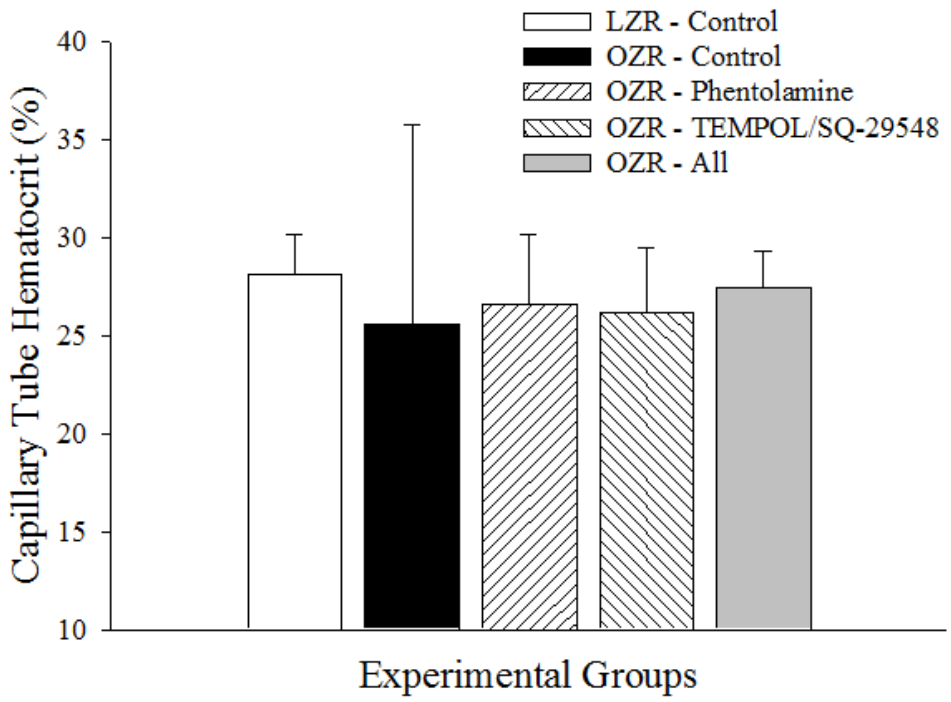
LZR - Control
OZR - Control
OZR - Phentolamine
OZR - TEMPOL/SQ-29548
OZR - All
Capillary Tube Hematocrit (%)
40
35
30
25
20
15
10
Experimental Groups

Conceptual Framework

The fifth and final chapter focused on the hemodynamics within a microvasculature network, and whether the spatial and temporal alterations to vascular tone in the Obese Zucker rat have an impact on microvascular hematocrit. It sought to integrate the previous work and determine whether there is an altered erythrocyte distribution throughout the microvascular and capillary networks. We found a significantly lowered microvascular hematocrit in the OZR and a large variation in capillary hematocrit compared to the healthy LZR. These results suggest that MetSyn induced alterations to vascular tone ultimately lead to a lowered erythrocyte distribution, and provide insight into the perfusion:demand mismatch and lowered performance outcomes observed in the OZR.

Discussion

The purpose of this dissertation is to investigate network control of blood flow to determine the extent to which Metabolic Syndrome-induced microvascular dysfunction alters hemodynamics within skeletal muscle. We first sought to determine if MetSyn impacts the ability of isolated microvessels to integrate multiple inputs and subsequently change overall diameter compared to a healthy animal. Myogenic activity is a significant contributor to vascular tone and significantly elevated vasoconstriction in response to elevated intraluminal pressure is observed in the OZR in compared to the LZR. The first chapter emphasized that MetSyn alters myogenic activity largely through increases in oxidant stress, which has the combined effect of reducing nitric oxide bioavailability and altering AA metabolism to increase production of vascular TxA_2. The data demonstrated that the oxidant stress derived changes to myogenic activation has a significant effect in blunting the responses of dilator stimuli. The blunted dilator response occurs in hypoxia, a dilation derived from endothelial dependent NO production, and dilation to a mimic of metabolic stimulation. Interestingly, the skeletal muscle microvasculature in the OZR shows an equal impact of an antioxidant or TxA_2 receptor antagonist at alleviating the blunted dilator response to hypoxia. In contrast, while there is a comparable blunted dilator response to acetylcholine, TEMPOL proved to be a far more effective intervention than SQ-29548. While treatment with adenosine (mimic for metabolic demand) showed a less severe blunting of dilation when integrated with pressure induced constriction, it still was lower, suggesting that the increased myogenic activation could play a role in altering blood flow despite increases in metabolic demand. Taken together, these data implicate oxidant stress and vascular production of TxA_2 as significant contributors to the increased myogenic activation seen in the OZR and serves to alter basal vascular tone and hemodynamics within the confines of MetSyn. This is part of the foundational work that illustrates *ex vivo* that MetSyn does not just alter point sources for reactivity in blood vessels, but fundamentally alters the ability of the network to appropriately integrate dilator and constrictor signals.

Building on this work, the second chapter demonstrates a functional performance inhibition within the OZR skeletal muscle. The OZR has significantly blunted blood flow, higher resistance, decreased oxygen

uptake, and decreased oxygen exchange compared to the LZR. These combined factors serve to significantly impair the OZR's ability to resist fatigue development at all levels of metabolic stimulus and are present even at rest. It was determined that the restricted bulk blood flow and increased resistance present in the OZR are alleviated with treatment of phentolamine, an alpha-adrenergic antagonist. The blunted oxygen extraction and oxygen uptake were alleviated with TEMPOL or SQ-29548. There were two key observations about these data. The first is that no treatment by itself improved tension development in the OZR compared to the LZR. This suggests a dual component of dysfunction that will equally serve to limit OZR skeletal muscle performance, and both components must be addressed for an effective outcome in terms of functional performance. The second observation is the decreased oxygen extraction and oxygen uptake in the OZR skeletal muscle. Classically it would be expected that by repairing the blunted bulk blood flow delivery within the muscle this would allow for adequate oxygen delivery throughout the skeletal muscle. Additionally, it would be expected that there would be an increased oxygen extraction as a compensatory mechanism for the decreased blood flow and previously identified rarefaction present in the OZR. This implies two spatially distinct mechanisms within the vasculature, an alpha-adrenergic constraint prohibiting bulk blood flow and dysfunction in the gas exchange regions of the vasculature dominated by increasing oxidant stress. This would provide the impetus for Chapter 3, where we begin to examine the perfusion distributions throughout the microvascular network.

Chapter 3 begins by changing the preparation to the *in situ* cremaster preparation, a preparation that allows us to examine an intact skeletal muscle microvascular network. The preparation allowed us to combine video microscopy with an optical Doppler velocimeter, thus enabling calculation of the blood flow distribution at bifurcations of varying sizes. A heterogeneous blood flow distribution was observed in the OZR microvascular network, meaning that a "high flow" and "low flow" pathway at each bifurcation was iterated throughout the entire network. Interestingly, the data revealed spatially distinct mechanisms, with alpha-adrenergic dysfunction dominating the proximal microcirculation and oxidant stress based increases in vascular TxA_2 playing a greater role in the distal microcirculation. The

respective interventions were able to restore perfusion distributions back to levels of control at each spatially distinct location. This was further supported by an I^{125} labeled albumin washout curve, which utilized the isolated gastrocnemius preparation. It is representative of whole network flow distribution, and the OZR washout kinetics clearly revealed altered intravascular flow patterns compared to the LZR, which was further confirmed with a computation model demonstrating the expected heterogeneous flow distribution throughout the OZR microvasculature and predicting a large number of very low flow ischemic pathways with only a few high throughput pathways.

The results of the previous study indicating a heterogeneous perfusion distribution with spatially distinct mechanisms in the skeletal muscle microvasculature of the OZR lead us to ask how the body would normally compensate for such dysfunction. When one examines the functional impact of a "high/low" flow pathway in microvascular skeletal muscle, one would expect to a see buildup of waste products and ischemic metabolites downstream of the low flow pathway, as predicted computationally. This would occur naturally even in health, as even the LZR does not have a perfect 50/50 flow distribution pattern. Due to the increase in perfusion distribution heterogeneity in the OZR, one would expect a more severe ischemia within the low flow pathway, thus providing an elevated rate of buildup of metabolically active waste products that would have a dilatory effect upon the low flow pathway. Thus the "high/low" flow pathway would switch, and we hypothesized that in the OZR there would be a significantly increased temporal switching compared to the LZR. However, the temporal switching was blunted in the OZR in both the proximal and distal microcirculation. The importance of blunted temporal switching cannot be understated. Not only is there no temporal compensation for the perfusion heterogeneity in skeletal muscle, but it is actually blunted. This implies that it will exacerbate the perfusion heterogeneity, locking in a high and low flow pathway, resulting in chronic ischemic regions of tissue at rest and permanently inhibiting blood flow regulation. Additionally, the temporal aspect of the data allowed for the generation of an attractor for the OZR and LZR. An attractor is a set of conditions that a dynamic system will adhere to over time. In the LZR, attractor centers on 0.5, but has a broad and

diverse range. This illustrates the constant flux that persists at homeostasis. Systems must be perturbed at multiple levels to alter attractors, and this is clearly illustrated in the OZR. The attractor for the OZR was elevated and reduced in range compared to the LZR. This suggests a limited ability of the OZR microvascular network to respond adequately to perturbations. The cumulative outcome of spatial and temporal alterations to skeletal muscle microvasculature is to produce an inability of the system to adequately regulate blood flow. This evidence, combined with previously referenced papers, suggest that this altered perfusion distribution will have an effect on erythrocyte distribution throughout the system, and brought us to Chapter 5.

Chapter 5 hypothesizes that the altered perfusion distribution iterated across the microvascular network, combined with an inability to temporally compensate, will result in a lowered microvascular hematocrit as well as a lowered capillary hematocrit. It utilizes indicator dilution washout curves to obtain a "snapshot" of microvascular hematocrit as well as video microscopy to obtain a representative sample of capillary hematocrit. The results showed that the OZR showed a significant decrease in microvascular hematocrit. Treatment with either an alpha-adrenergic blocker, antioxidant, or TxA_2 receptor antagonist improved the variance of the OZR, but only with all three was there a significant improvement of hematocrit with equal variance to even above levels of control. The capillary hematocrit proved slightly troublesome, as it indicated no significant differences between any groups, LZR or OZR. However, the variance of the OZR indicates very high and low flow hematocrits, which when averaged are not significantly different. This would indicate that our hypothesis is correct, and perhaps our sample is not representative of the true population.

To summarize the above dissertation, the evidence presented suggests that MetSyn contributes to dysfunctional vascular control through increased myogenic activation, which is brought on by oxidant stress based increases in vascular production of TxA_2. This, combined with adrenergic dysfunction, results in significant impairments to the ability of skeletal muscle to resist fatigue. Subsequent research demonstrates that a primary consequence of alterations to vascular tone is increased perfusion

heterogeneity at bifurcations, and that this perfusion heterogeneity exists at both the proximal and distal microcirculation. The mechanisms of this dysfunction are spatially distinct, with adrenergic dysfunction dominating at the proximal microcirculation and increases in oxidant stress and alterations to arachidonic acid metabolism dominating in the distal microcirculation. Further, MetSyn blunts the temporal switching that potentially could alleviate the increased perfusion distribution. The cumulative outcome of spatial and temporal alterations to vascular tone is a lower microvascular hematocrit, which could serve as a influential contributor to the inability of the OZR skeletal muscle to resist fatigue development.

MetSyn entrenches a pathological condition whereby the skeletal muscle circulation is limited not only in matching perfusion with demand, but also restricts the logical compensation through temporal switching. This inevitably leads to the condition whereby a subject is unable to reverse the decreased performance outcome, and we argue that it is at this point where PVD, CVD, and the other pathologies intrinsically indicated by MetSyn begin to present. Further studies are needed to examine the impact of common interventions on microvascular function. These include but are not limited to exercise, weight loss, surgery, lifestyle alterations, and pharmaceutical drugs. Each needs to be evaluated for its impact on the underlying microvascular dysfunction. Taken together, this dissertation hopefully sheds light on the mechanisms within the microcirculation that MetSyn and PVD impact, and allows for novel and relevant treatment for the human population.